CHEMOENZYMATIC SYNTHESIS OF HEPARAN SULFATES, AND INVESTIGATIONS OF THEIR ROLE IN CELL SIGNALING, HUMAN HEALTH AND DISEASE

Matt Suflita

Submitted in Partial Fulfillment of the Requirements
for the Degree of

DOCTOR OF PHILOSOPHY

Approved by:
Dr. Robert J. Linhardt, Chair
Dr. Lee Ligon
Dr. Mattheos Koffas
Dr. Jon Dordick

Department of Biology
Rensselaer Polytechnic Institute
Troy, New York

[May 2018]

Submitted April 2018

By

Matt Suflita

Table of Contents

List of Tables

List of Figures

Acknowledgements

I owe a lot of thanks to a lot of people, too many to list here. Firstly, I'd like to thank my thesis advisor, Dr. Robert J. Linhardt. You were understanding and accommodating throughout one of the most difficult times in my life, and kept me going even when I thought it was hopeless. I'd also like to thank my thesis committee members: Dr. Lee Ligon, who gave me the final push I needed to get across the finish line, Dr. Matheos Koffas, and Dr. Jon Dordick. Thanks also to Fuming Zhang and Karen Coonrad, who were incredibly kind and helpful throughout my time in the Linhardt lab.

I'd like to thank those I had the opportunity to collaborate with, Dr. Jian Liu and the rest of his lab at the University of North Carolina; Dr. Eric Schmidt and Sarah Haeger at the University of Colorado. I was incredibly fortunate to be able to visit your labs to learn about your research as you helped me with mine.

I also want to thank my colleagues. One of the benefits of a large lab like ours is that it affords plenty of opportunities to work on a diverse set of research projects, and to learn from people with different skill sets and backgrounds. Special thanks to: Ujjwal Bhaskar, Li Fu, Victor Schultz, Jianhua Zhang, Chao Cai, So-Young Kim, Paiyz Mikael, Greg Neirode, Dylan Bruckner, Jake Englaender, Deepika Vaidyanthan, Joel Janke, Ranodhi Udangawa, Lei Lin, Xinyue Liu, Brady Cress, and many more.

Lastly, I'd like to thank my family and friends. Mom, you taught me how to write well and pushed me to excel in school. Dad, you raised me to be curious about the world and taught me about all the strange and wonderful creatures in it. You're the best parents a son could possibly ask for, and without your support and tough love I would not have made it this far. Thanks to my brother and sister, who are always there when I need help or advice, you are both such unique and caring people. And finally, to my wonderful, beautiful, special girlfriend, who supported me throughout this long six year period, without your love I would not have had the strength to continue.

Abstract

Heparan sulfate and heparin are linear polysaccharides, called glycosaminoglycans, which possess many important biological and pharmacological activities. While heparin has historically received most of the scientific attention for its anticoagulant activity, interest has steadily grown in the multi-faceted role heparan sulfate plays in normal and pathophysiology. Cell surface heparan sulfate binds signaling proteins such as fibroblast growth factors and promotes the formation of signaling complexes. In endothelial cells, heparan sulfate in the glycocalyx forms a physical barrier critical for endothelial function, and its degradation in response to direct injury or septic shock leads to tissue damaging inflammation.

Heparin is a critically important drug, with an accordingly high demand. The heparin contamination crisis of 2008 caused over 200 deaths worldwide, and illustrated the problems associated with animal sourced heparin. Chemical synthesis of glycosaminoglycans is largely precluded by their structural complexity, which led our lab to develop methods for the chemoenzymatic synthesis of heparan sulfates toward a bioengineered heparin replacement for current animal source heparin.

This thesis will explore methods for chemoenzymatic synthesis of heparan sulfates, and their role in fibroblast growth factor signaling and sepsis pathology. We first present the scalable production of recombinant heparin biosynthetic enzymes used in chemoenzymatic synthesis of heparan sulfates. Next, we demonstrate the successful application of fluorous-tagged sugars in an iterative chemoenzymatic synthesis of heparan sulfate oligosaccharides, and a one-pot chemoenzymatic synthesis of anticoagulant heparin. We then applied chemoenzymatic methods to synthesize a library of structurally defined heparan sulfate oligosaccharides with domain structure, which were used in combination with a cell-based signaling assay to investigate the structure-activity relationship of heparan sulfate domains in fibroblast growth factor signaling *in vitro*. We found clear differences in

signaling requirements for fibroblast growth factors 1 and 2, which suggests the possibility of defined heparan sulfate therapeutics targeted to specific fibroblast growth factor signaling pathways.

The last chapter details two *in vivo* studies of the role of heparan sulfate in disease. We first examined the reconstitution of heparan sulfate in the endothelial glycocalyx following sepsis-induced degradation. Homeostatic pulmonary endothelial glycocalyx reconstitution occurred rapidly after non-septic degradation and was associated with induction of the heparan sulfate biosynthetic enzyme exostosin-1. In contrast, sepsis was characterized by loss of pulmonary exostosin-1 expression and delayed glycocalyx reconstitution. Rapid glycocalyx recovery after non-septic degradation was dependent upon induction of fibroblast growth factor receptor 1 expression and was augmented by fibroblast growth factor-promoting effects of circulating heparan sulfate fragments released during glycocalyx degradation. While sepsis-released heparan sulfate fragments maintained this ability to activate fibroblast growth factor receptor 1, sepsis was associated with the downstream absence of reparative pulmonary endothelial fibroblast growth factor receptor 1 induction.

We next sought to determine if urinary indices of GAG fragmentation are associated with outcomes in patients with critical illnesses such as septic shock or acute respiratory distress syndrome. Indices of GAG fragmentation correlated with both the development of renal dysfunction over the 72 hours after urine collection and with hospital mortality. This association remained after controlling for severity of illness and was similarly observed using the inexpensive dimethylmethylene blue assay. These predictive findings were corroborated using urine samples previously collected at three consecutive time points from patients with acute respiratory distress syndrome.

1. INTRODUCTION

1.1. Structure and biosynthesis of heparan sulfate, heparin, and related glycosaminoglycans

Heparan sulfate (HS) and heparin (HP) are anionic, linear polysaccharides, called glycosaminoglycans (GAGs), which are abundant in all animal species. These GAGs are biosynthesized as proteoglycans (PGs), consisting of an elongated core protein and one or more GAG chains covalently attached to core protein serine residues[3]. The structurally related HS and heparin GAGs are composed of a repeating disaccharide unit, comprised of β-D-glucuronic acid (GlcA) or α-L-iduronic acid (IdoA) 1, 4-glycososidically linked to D-glucosamine (GlcN) (Fig. 1.1A). This disaccharide unit can be modified in various ways. The uronic acid residues can be modified with a 2-*O*-sulfo group (IdoA2S and rarely GlcA2S). The GlcN residue can contain an *N*-acetyl or *N*-sulfo group (GlcNAc or GlcNS), as well as modified with 6-*O*-sulfo group and 3-*O*-sulfo groups (GlcNAc6S and GlcNS6S, or rarely GlcNAc3S and GlcNS3S or GlcNAc3S6S and GlcNS3S6S[4]). With 32 (2^6) possible modifications for each disaccharide unit (although not all possible disaccharide units have been detected in natural HS/HP), the structures of HS and heparin are extremely complex and information dense. Heparin has a relatively uniform high level of sulfation (2.5-3 sulfo groups/disaccharide). In contrast, HS has an overall lower level of sulfation (0.5-1.5 sulfo groups/disaccharide) and a domain structure, which is determined by the presence or absence of GlcNS residues. Long stretches of GlcNAc-containing disaccharides correspond to the largely unsulfated NA domain, while shorter clusters of GlcNS-containing disaccharides correspond to the more highly sulfated NS domains, which are rich in IdoA, IdoA2S and GlcNS6S residues[5,6]. Heparin, a widely used anticoagulant drug, is essentially an extended NS

Portions of this chapter previously appeared as: Suflita, M., Fu, L., He, W., Koffas, M. & Linhardt, R. J. Heparin and related polysaccharides: synthesis using recombinant enzymes and metabolic engineering. *Appl. Microbiol. Biotechnol.* **99,** 7465–7479 (2015)., and Fu, L., Suflita, M. & Linhardt, R. J. Bioengineered heparins and heparan sulfates. *Adv. Drug Deliv. Rev.* **97,** 237–249 (2016).

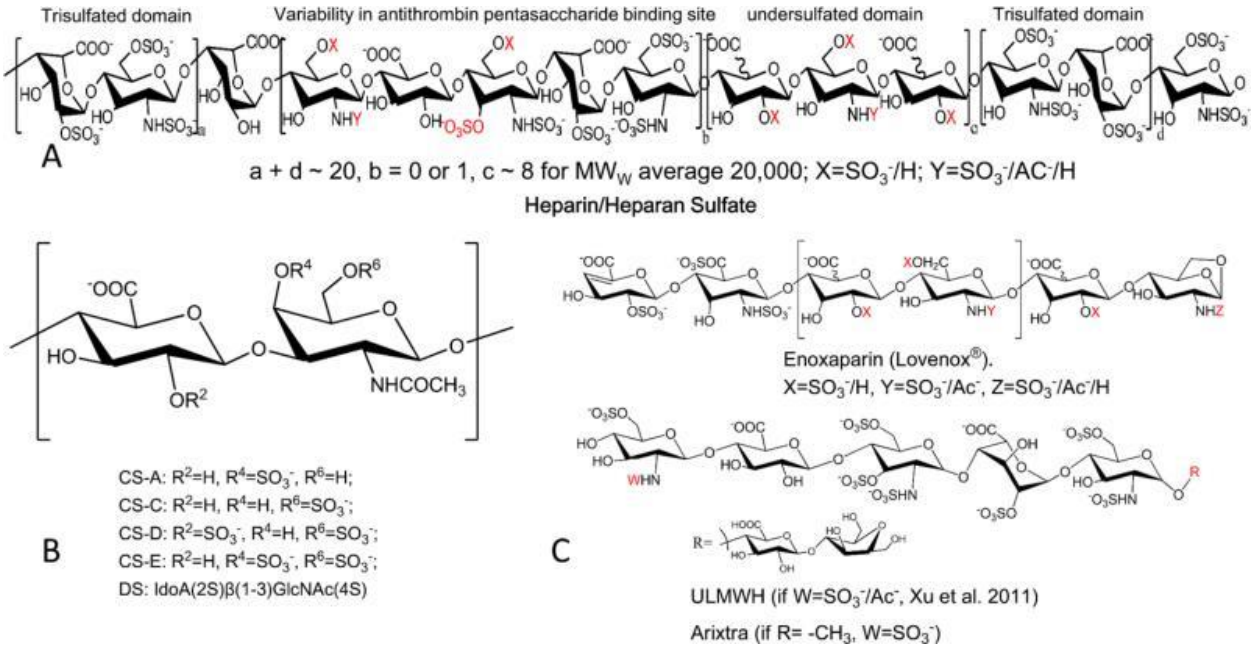

Figure 1.1. Structures of glycosaminoglycans and their oligosaccharides. A. Structure and common domains of heparin (if b = 1) or heparan sulfate (if b = 0). B. common chondroitin sulfates. C. Low molecular weight heparins (Lovenox) and ultra-low molecular weight heparins (ULMWH and Arixtra).

domain with a very high level of sulfation, and rich in trisulfated disaccharides of the structure GlcNS6S-IdoA2S. The rare 3-sulfo group found in both heparin and HS is an essential component of the antithrombin III (AT) binding site, a pentasaccharide sequence that activates AT and which is responsible for anticoagulant activity[4]. Chondroitin sulfate (CS) is a sulfated glycosaminoglycan similar to HS, with the repeating disaccharide unit of GlcA linked to *N*-acetyl-D-galactosamine (GalNAc). The GalNAc residue can have sulfo groups substituted at the 4- and 6-hydroxyls of the GalNAc (Figure 1.1B). The GlcA residue in CS can also be epimerized to IdoA, present in dermatan sulfate (DS, also known as chondroitin sulfate B), and both the GlcA and IdoA residues can contain sulfo groups at their 2-positions. CS-GAGs also have domain structures, similar to HS-GAGs[7].

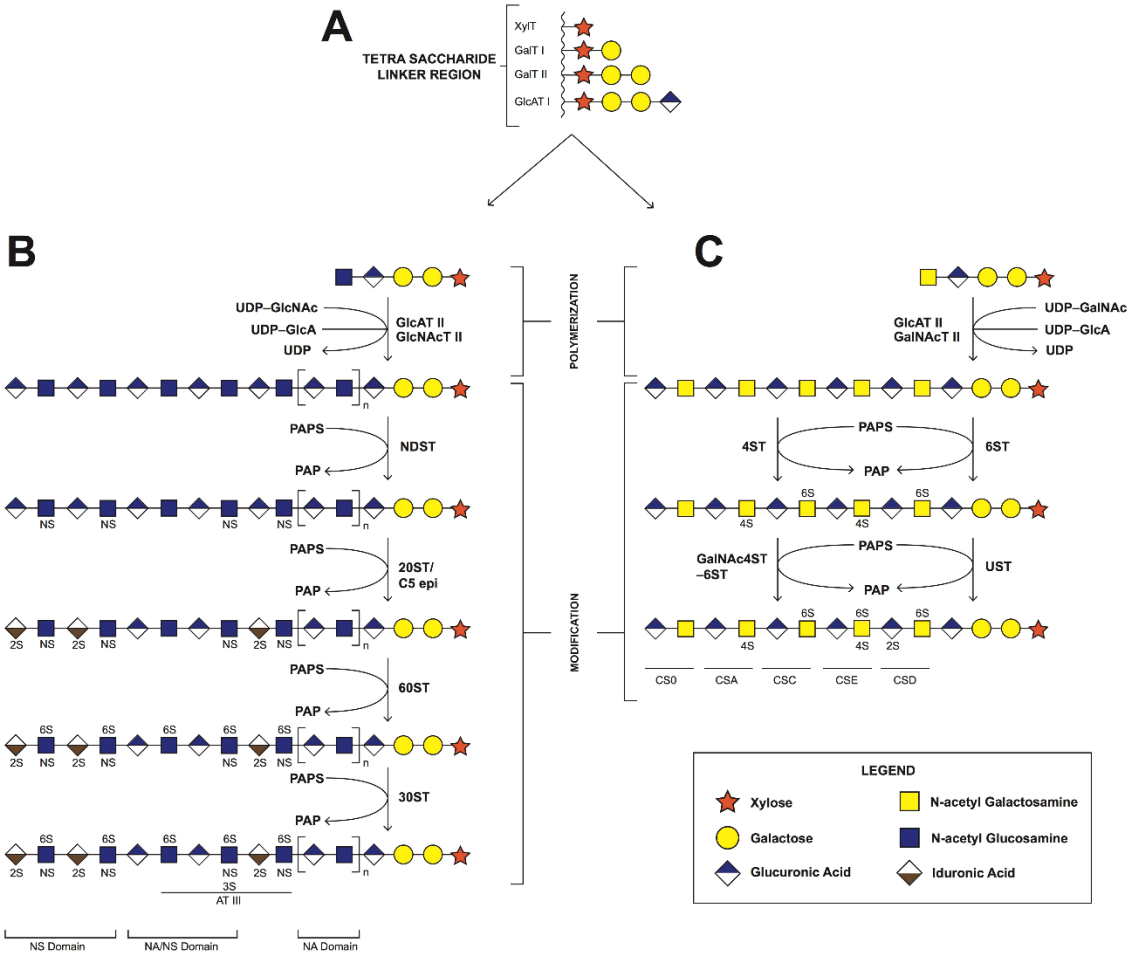

Figure 1.2. Biosynthesis of heparin/heparan sulfate and chondroitin sulfates. A. Synthesis of the tetrasaccharide linker region. B. Polymerization and modification pathway of heparin/heparan sulfates. C. Polymerization and modification pathway of chondroitin sulfates.

HS and heparin are biosynthesized in the endoplasmic reticulum (ER) and the Golgi compartments. Biosynthesis begins in the ER with the stepwise addition of four monosaccharides (xylose-galactose-galactose-GlcA) to a serine residue in the core protein, which form the tetrasaccharide linker region[8] (Fig. 1.2A). Heparin is biosynthesized exclusively on the serglycin core, while HS is can be biosynthesized on a variety of different core proteins, including members of the syndecan and glypican families[9,10]. Glycosyltransferase enzymes catalyze the alternating addition of UDP-activated GlcA and GlcNAc residues to polymerize the chain, which is then modified by *N*-deacetylase, C_5-epimerase and

sulfotransferase enzymes[9]. *N*-deacetylase/*N*-sulfotransferases (NDST) are bifunctional enzymes (multiple isoforms) that replace the *N*-acetyl group with an *N*-sulfo group, a critical step for formation of domain structures[5]. Subsequent modifications by C_5-epimerase (C_5-Epi) and *O*-sulfotransferases (OSTs) are dependent on the presence of GlcNS residues (NS domains), while NA domains remain largely unmodified[5,11]. Iduronic acid residues are produced by C5-epimerase, which converts GlcA into IdoA, working in concert with 2-*O*-sulfotransferase (2OST) to give IdoA2S. In rare cases, 2OST modifies GlcA to form GlcA2S. GlcNS residues are then modified by 6-*O*-sulfotransferases (6OSTs), followed by 3-*O*-sulfotransferases (3OSTs). There are multiple isoforms of both 6OST and 3OST that display different specificity in their recognition sites. Tissue specific expression of different enzyme isoforms fine-tunes the synthesis of HP and HS to produce different structures, allowing adaptation of function to the local cellular environment. HS isolated from different tissues have different ratios of component disaccharides, which can be thought of as a kind of "glyco-fingerprint," and can show distinctive changes in certain cancers[12-14].

1.2. Biological activities of HS/HP

The combinatorial complexity of HS structure and biosynthesis translates into an equally complex set of biological activities. The most well-known and established pharmacological activity of the heparin GAG is its anticoagulant activity. Heparin has been widely used as an anticoagulant drug since the 1930s[4], and today is an essential drug for treating thrombosis and related conditions. Interestingly, the biological function of endogenous heparin is not as an anticoagulant. Heparin is biosynthesized in mast cells and stored intracellularly and does not normally come into contact with blood. While the precise biological function of heparin is still unknown, it might be related to mast cell response to parasitic infections[4,15]. The anticoagulant activity of heparin is mediated by its binding to antithrombin III (AT),

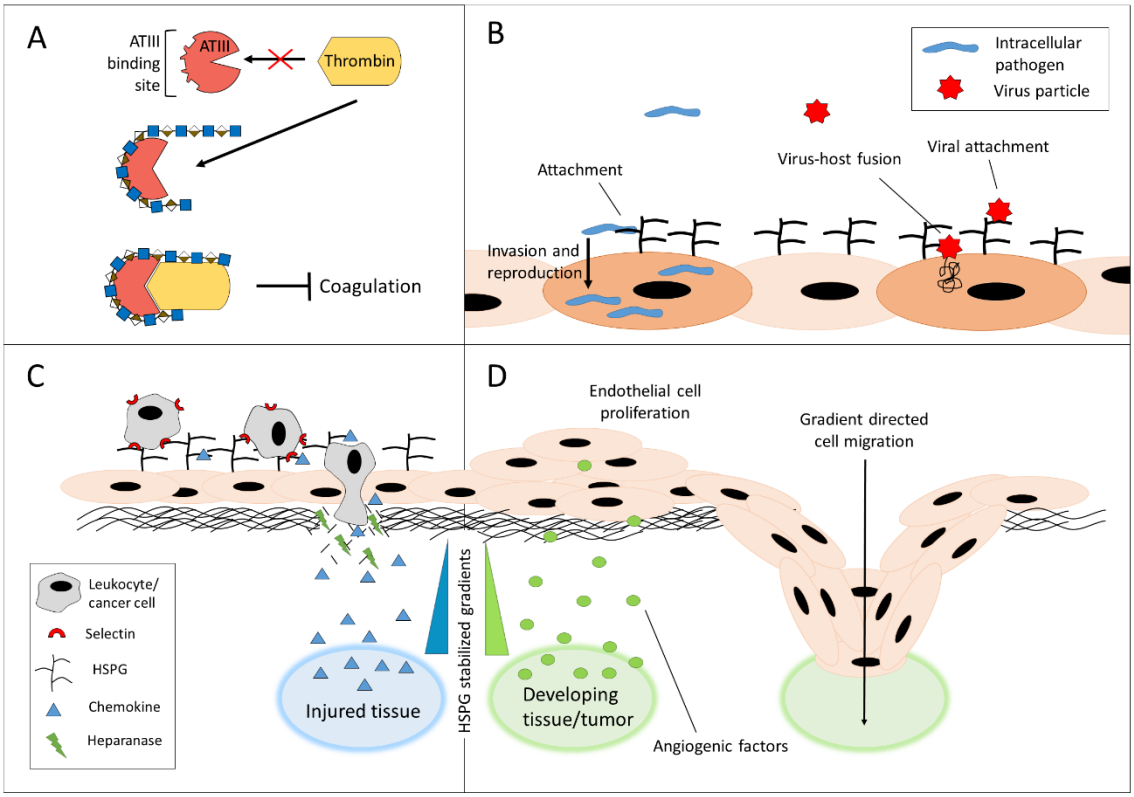

Figure 1.3. Bioactivities of heparin/HS. A. Anticoagulant activity of heparin- a pentasaccharide sequence in heparin induces a conformational shift in ATIII upon binding, which irreversibly binds thrombin, which also binds to heparin at an adjacent site, to inhibit coagulation. B. Role of heparan sulfate proteoglycans (HSPGs) in infectious disease- Intracellular pathogens and viruses bind cell surface HSPGs to facilitate invasion or viral fusion. C. Role of HSPGs in leukocyte extravasation/metastasis- rolling along endothelial surface is mediated by selectin-HS binding, and chemokines bound to endothelial HSPGs attract the leukocyte to damaged tissue. Invasion requires heparanase activity to degrade HSPGs in the basement membrane. D. Role of HSPGs in angiogenesis-HSPGs stabilizes gradients of angiogenic factors (VEGF, PDGF, FGF2) to direct blood vessel formation.

an inhibitor of serine proteases, including thrombin and factor Xa, involved in the coagulation cascade[4] (Fig. 1.3A). On binding heparin, AT undergoes a conformational change that amplifies its inhibitory activity by several orders of magnitude. The interaction between AT and heparin is mediated through a specific pentasaccharide sequence with a central 3-*O*-sulfo group, termed the AT-binding site (Fig. 1.1). This binding site is also found in endothelial HS and may provide a basal level of anticoagulant activity responsible for the blood compatibility of the endothelium[16]. Interestingly, inhibition of thrombin (anti-FIIa activity) requires more than a pentasaccharide AT binding site, a chain of 16-18 saccharides is required for irreversible binding of thrombin by the HP-AT in a ternary complex. However, the AT pentasaccharide

sequence bound to AT is only sufficient for the direct inhibition of factor Xa making it a specific anti-FXa agent. This discovery led to the development of low molecular weight heparins (LMWHs) as selective for factor Xa inhibitors (anti-FXa/anti-FIIa activity of ~ 5-10), which was believed would reduce bleeding complications and heparin-induced thrombocytopenia[16-18].

A much more complex biological activity of HS-GAGs is their role in developmental biology and cell signaling. Cell surface and extracellular matrix (ECM) HSPGs exhibit complex pleiotropic effects, playing roles in cell differentiation, migration, angiogenesis, and regulation of cell signaling[19]. HS is essential for proper development, and mutations in HS biosynthetic genes are known to cause a range of conditions resulting in abnormal bone and organ formation[20]. As a major component of the ECM, HSPGs exhibit binding affinities for major ECM proteins including fibronectin, collagen and laminin, which are critical in cell adhesion and provide spatial context for cell signaling[19,21,22]. With a diverse array of sub-structures, HS acts as a binding platform for a host of extracellular signaling molecules such as growth factors, chemokines and morphogens, regulating their diffusion and distribution in the ECM[19,21,22]. HS can also signal directly as a co-receptor, as in the case of fibroblast growth factor (FGF) signaling[23,24]. The FGF family is responsible for directing a wide range of developmental processes. Formation of an FGF-FGF receptor (FGFR) signaling complex requires HS, whose role is to coordinate specific pairings of FGFs and FGFRs by binding to each, which have different preferences in HS structure[24,25]. However, the precise nature and specificity of these interactions is still being investigated. It is more difficult to say exactly how HSPGs modulate the response to other extracellular signaling molecules. In addition to FGFs, HS binds a number of other growth factors (GFs) (vascular endothelial (VE) GF, platelet derived GF, glial cell-derived neurotrophic factor, and hepatocyte GF) and cytokines (interleukin (IL)-12, midkine, pleiotrophin, platelet factor 4)[21,22,26]. How this binding affects the complex spatial biology of the ECM is poorly understood, especially given the diverse array of differentially expressed HSPGs, and the variable composition of their HS chains[23]. One mechanism by which HSPGs

modulate signaling pathways is by stabilizing gradients of signaling molecules, which provide spatial information to cells during development[27]. In angiogenesis, HSPGs establish a gradient of VEGF, which provides spatial context for the migrating endothelial cells which will form the blood vessel (Fig. 1.3D)[28]. HSPGs can also facilitate the internalization of signaling molecules or act as storage, to be released by heparanase, a mammalian endoglucuronidase that cleaves HS chains[26,29,30]. In wound healing, heparanase accelerates repair through the release of these bound signaling molecules[31]. Moreover, increased syndecan expression is seen in migrating and proliferating cells at the injury site, which likely act to regulate ECM organization and growth factor response[32,33].

HSPGs are also a very common cellular receptor for viral and bacterial pathogens, which bind the HS chain to facilitate attachment and invasion of specific host tissues (Fig. 1.3B)[15]. Papillomavirus infection requires binding to either syndecan or glypican HS, and ectopic expression of these HSPGs has been shown to enhance infectivity[34]. Some viruses recognize specific sequences in HS, as seen in herpes simplex virus type-1, whose glycoprotein D binds a 3-*O*-sulfo group containing octasaccharide to trigger fusion of the host cell and virus[35]. Many intracellular bacterial pathogens such as those in the genus *Chlamydia* and *B. burgdorferi*, the causative agent of Lyme disease, invade host cells through similar mechanisms. The malarial protozoan *P. falciparum* infects liver tissue by binding to hepatocyte-associated HS chains, allowing remarkable specificity in host cell infection[36]. HSPGs can also play a key role in the virulence of many bacterial infections. *H. pylori* and *P. aeruginosa* stimulate the shedding of syndecan-1, which can inhibit neutrophil-mediated bacterial killing, and exacerbate inflammatory damage to tissues[37,38].

HSPGs are intimately involved in inflammatory processes, primarily for their role in regulating leukocyte extravasation (Fig. 1.3C). Leukocytes in the blood first weakly bind to the endothelial surface and roll along it, caused by the interaction between endothelial HS and L-selectin and P-selectins on the leukocyte[39,40]. Interleukins and chemokines bound to endothelial HS attract the leukocyte to the site of injury[19], where it activates integrins to produce a stronger adhesion in preparation for extravasation.

HSPGs are major structural components of basement membranes, along with laminin and collagen, and provide a physical barrier to invading cells. Leukocytes extravasating to injury sites break down this barrier through the action of heparanase and various proteases, releasing biologically active HS fragments and their bound signaling molecules in the process[39]. Heparanase expression in many cancers can correlate with poor prognosis and higher metastatic potential as a result of co-opting this extravasation mechanism[41,42]. Remarkably, metastatic potential can be acquired by non-metastatic T-lymphoma cells on transfection with heparanase[43]. The breakdown of the basement membrane during metastasis also drives tumor angiogenesis by increasing the availability of angiogenic growth factors such as vascular endothelial growth factor, and HS fragments which can drive FGF signaling[44]. Heparanase causes increased expression of these growth factors, as well as syndecan-1, which is shed from the cell surface at a higher rate. This shed syndecan-1 concentrates growth factors in the tumor microenvironment, accelerating proliferation and angiogenesis[45].

In addition to its anticoagulant activity, heparin has been shown to have anti-inflammatory and anti-metastatic properties, primarily through binding L-selectin and P-selectin, which inhibit the ability of invading cells to bind to the endothelial surface[40,46,47]. Heparin has shown positive effects in acute inflammatory conditions such as bronchial asthma, ulcerative colitis and burns, and LMWH was found to afford a survival benefit (independent of its anticoagulant activity) to cancer patients[31,40,48–50]. However, complications associated with the anticoagulant properties of heparin may limit its use in these applications. Heparin and LMWH may have additional anti-cancer and anti-inflammatory effects due to its ability to competitively inhibit heparanase, but evidence remains scant. However, heparanase inhibiting heparin mimetics such as PI-88 and PG545, have shown potent anti-metastatic and anti-angiogenic effects, and are currently in clinical trials[49,51].

A key element of the multifaceted biological activity of HS-GAGs is their complex structure and regulation. Detailed knowledge of structure-activity relationships will be essential for developing new

therapeutics, which target HS-GAG associated processes. One major roadblock has been the inability to synthesize GAGs with defined structures. The complexity of HS largely precludes its chemical synthesis. However, new approaches, such as chemoenzymatic synthesis and bioengineering, offer promising results.

1.3. Preparation of animal sourced GAGs and low molecular weight heparins

Current heparins and CSs are derived from a variety of animal tissues. Animal source materials present serious concerns for the possibility of transmission of viral and prion diseases, and the susceptibility of animal populations to infectious disease or overharvesting has potential to drastically reduce supply. Moreover, seasonal, geographical and subspecies variations may alter the product obtained from a given animal species. The process of preparing pharmaceutical grade heparin has been altered somewhat over time as the primary tissue source has changed from dog liver to beef lung and finally to porcine intestine[52]. The preparation of heparin from ruminant tissues obtained at slaughterhouses present a special concern particularly following the appearance of bovine spongiform encephalopathy (BSE, "mad cow disease") in both humans and cattle[53] and scrapies prion in sheep[54]. Thus, the use of bovine and ovine tissue products as injectable pharmaceuticals has declined and these tissues are now rarely used in heparin production.

The methods used today for the commercial preparation of heparin have changed from that used early in the 20th century and involve five basic steps (Figure 1.4): 1) preparation of tissue; 2) extraction of heparin from tissue; 3) recovery of raw heparin; 4) purification of heparin; and 5) recovery of purified heparin[55-61]. However, to minimize the environmental impact of high-ash, high-biochemical oxygen demand hydrolyzed protein, raw heparin extraction typically takes place at the hog slaughtering facility

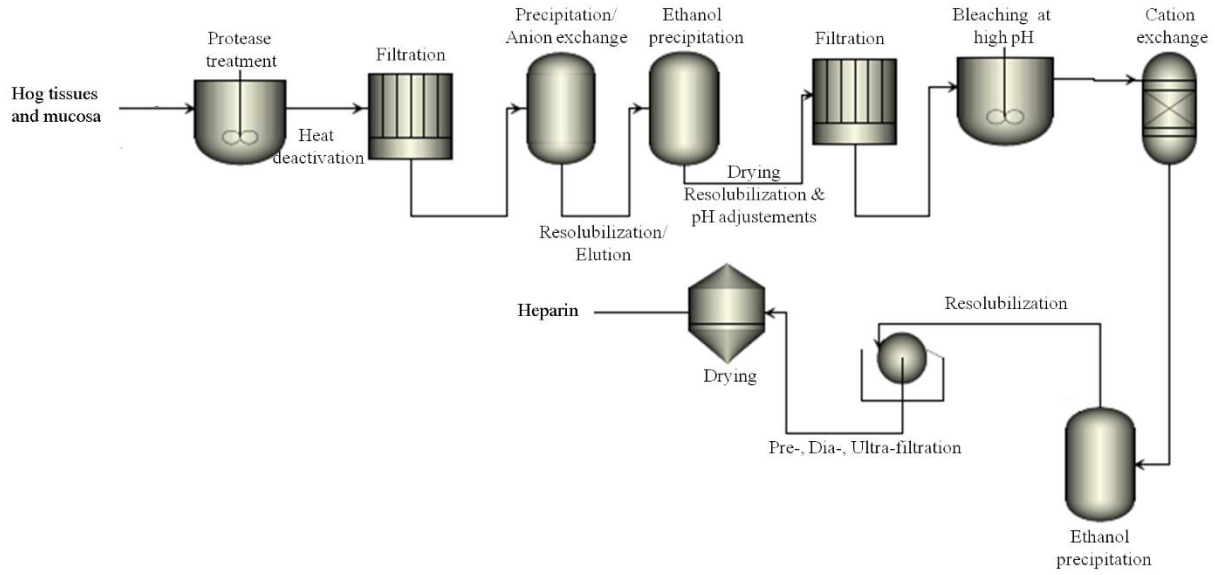

Figure 1.4. Extractive preparation of heparin. Process flow chart of heparin purification beginning with porcine tissue.

itself (not under current good manufacturing practices (cGMP) conditions). Additional high potency heparin may be recovered by saving the waste brine solution of the hog casings operation[58]. There are growing concerns about porcine tissue nowadays, especially after the heparin crisis that took place in 2008. This crisis involved the introduction of an oversulfated chondroitin sulfate into heparin produced from hogs in China leading to the death of nearly 100 Americans[62]. Poor oversight and lack of cGMP in slaughterhouses leaves the heparin supply chain open to this kind of adulteration, which can be difficult to detect. Bovine lung heparin can be distinguished from porcine intestinal heparin because it contains a different distribution of structural variants of the antithrombin pentasaccharide binding site as well as other differences in disaccharide composition[63,64]. It is somewhat more difficult to distinguish bovine intestinal heparin or ovine intestinal heparin[64]. Moreover, blends of pharmaceutical grade heparins prepared from different species might make the content of non-porcine heparin even more difficult to assess.

Low molecular weight heparins or fractionated heparins with a molecular weight of ~ 3–8 kDa are a group of heparin-derived anticoagulant/antithrombotic agents (Figure 1.1C), and their development began approximately 30 years ago[17]. Currently, the commercial preparation of LMWHs from unfractionated heparin includes the controlled chemical depolymerization of heparin by peroxidative cleavage, nitrous acid cleavage, and chemical β-elimination (Figure 1.5B). These chemically depolymerized LMWHs such as enoxaparin, Ardeparin sodium, Dalteparin sodium, Nadroparin calcium, Reviparin sodium and Certroparin sodium contain artifacts including 2,6-anhydromannitol, epoxide, 1,6-anhydroglucopyranose, and 1,6-anhydromannopyranose due to the harsh reaction conditions[65]. Potential side effects associated with these process artifacts still remain unknown, and what's more, the animal sourced unfractionated heparin starting material for LMWHs is still at risk.

However, Arixtra® (fondaparinux sodium), a synthetic heparin pentasaccharide drug, introduced by Sanofi in 2002[66] is an example of an ultra-LMWH. This ultra-LMWH (<3 kDa) drug was based on a simplification of the elegant synthesis of the heparin antithrombin pentasaccharide binding site, first reported by Choay and coworkers in the 1980s[67] (Figure 1.5A). Arixtra differs from heparin in that it is a specific anti-factor Xa agent, which lacks many of the important pharmacological properties of the polycomponent, polypharmacolgical drug heparin[68].

About 40% of all heparin used each day in US is unfractionated heparin. It is primarily used in dialysis and hospitalized patients as an intravenous drug. Approximately 55% of US heparin market is dominated by LMWHs, principally used subcutaneously for the treatment of deep vein thrombosis. The final 5% of the heparin market is comprised of the expensive synthetic ultra-LMWH, fondaparinux, which is used in select applications when a side effect, known as heparin-induced thrombocytopenia, is anticipated. The ultra-LMWH market share represents only ~ $0.5B of the total worldwide heparin market of around $4B[61]. Thus, the worldwide market is evenly split between the use of heparin and LMWHs with very little synthetic ultra-LMWH being used. The reasons for the low demand for

fondaparinux are: 1. Expense — fondaparinux is roughly 1000-fold more expensive than heparin and 50-fold more expensive than LMWHs; 2. Poorer pharmacological profile — heparin and LMWH are polycomponent, polypharmacolgical agents that show a better overall therapeutic profile in patients than fondaparinux; 3. Safety — fondaparinux and LMWHs are not reversible with protamine posing

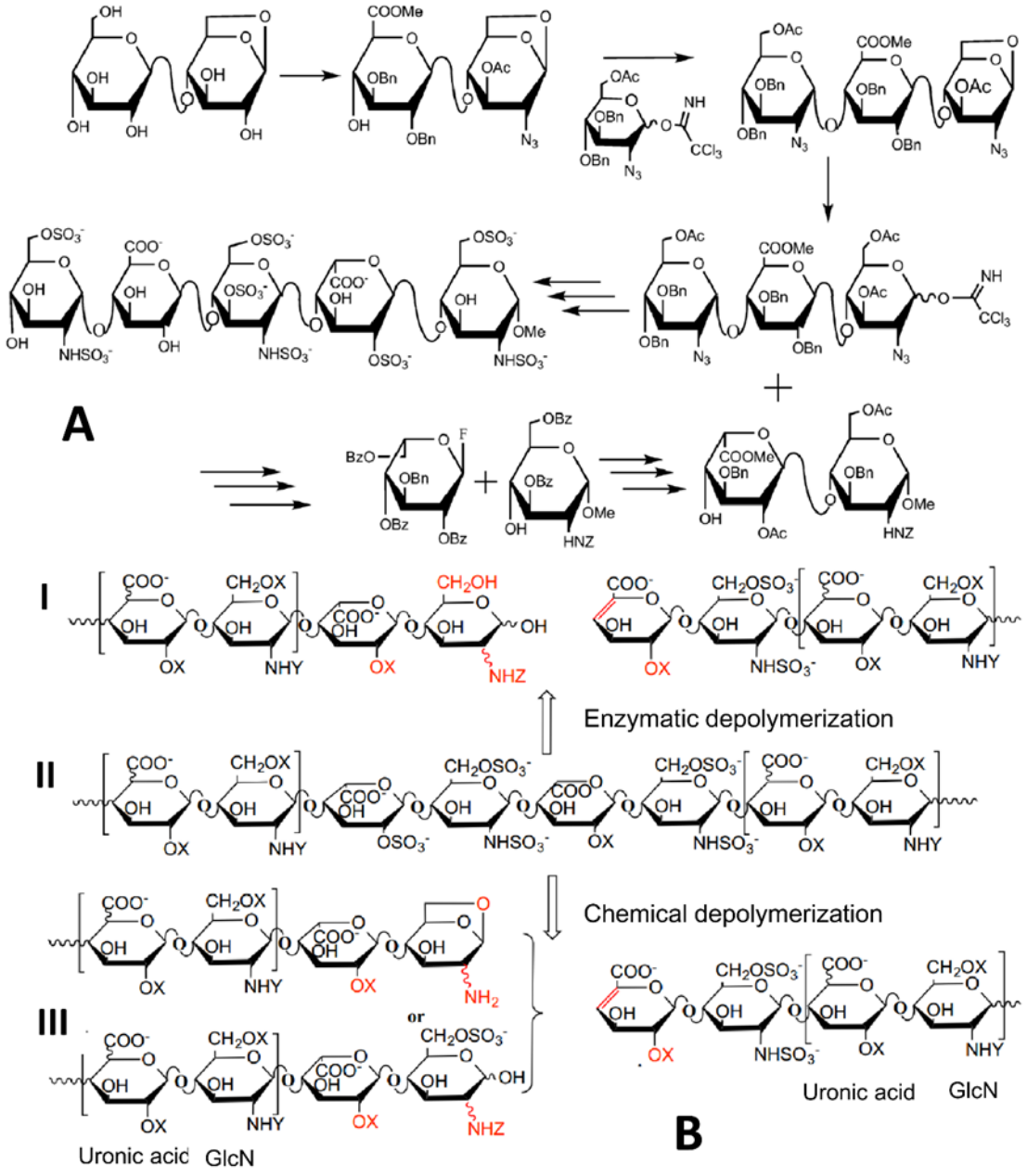

Figure 1.5. Chemical synthesis, depolymerization and enzymatic depolymerization of ultra-low molecular weight heparin and low molecular weight heparin. A. Convergent chemical synthesis of Arixtra from cellobiose. B. Enzymatic (I) and chemical (III) depolymerization toward low molecular heparins using unfractionated heparin (II).

safety concerns; and 4. Limitations — fondaparinux is ineffective in a number of applications where heparin and LMWHs are currently used. A new ultra-LMWH called semuloparin has recently been developed for the prevention of venous thromboembolism. It is a semisynthetic ultra-LMWH that is prepared by a selective and controlled depolymerization of heparin through a β-elimination reaction only at the less hindered regions using a phosphazene base[69]. Due to its bulky structure, the base cleaves the heparin chain, leaving the crowded AT-binding site intact. Studies in patients showed the antifactor Xa/antifactor IIa ratio of semuloparin to be above 30, indicating nearly pure anti-factor Xa activity[70]. Although the preparation cost is significantly lower than that of fondaparinux, it is neither homogeneous nor structurally defined and, since it is still derived from porcine intestinal heparin semuloparin, could be subject to contamination or adulteration.

1.4. Enzymatic tools for chemoenzymatic synthesis of GAGs

The chemical syntheses of heparin or heparin-like drugs typically involve numerous steps and result in low overall yields and high costs, which limits its clinical application. Chemists are starting to turn towards enzymatic or chemoenzymatic synthesis to circumvent these problems[71-73]. Unlike most chemical reactions, these enzymatic reactions are highly chemospecific, regiospecific and stereospecific. Using recombinant technology, glycosyltransferases and heparin biosynthetic enzymes have been cloned, expressed, and studied for the synthesis of heparin[74,75]. Initial efforts towards a chemoenzymatic preparation of heparin used C_5-Epi to convert the GlcA of the heparosan polysaccharide to IdoA, relying primarily on chemical modifications for the introduction of *N*- and *O*-sulfo groups, creating unwanted sulfation sites[76]. An enzymatic synthesis of an oligosaccharide based on the structure of HS has been accomplished using the heparin/HS modification enzymes[77] and glycosyltransferases[78].

Enzymatic synthesis of polysaccharides and oligosaccharides of defined lengths has recently become possible due to the availability of many recombinantly expressed glycosyltransferases. These

enzymes use UDP-activated sugars produced by uridyltransferases such as GlmU, which can be used to produce UDP-GlcNAc and UDP-GalNac in vitro, building blocks for HS and CS backbones respectively. GlmU is flexible in its substrate specificity, allowing the synthesis of some unnatural UDP-sugars. These unnatural sugars can then be tagged and polymerized into novel glycosaminoglycans[79]. This technique has been used to incorporate labile *N*-trifluoroacetyl groups into HS oligosaccharides, which can later be enzymatically sulfated[22,78,80]. Polymerizing enzymes can be processive, by addition of alternating UDP-sugars, or may catalyze the addition of a single sugar, as in KfiA, a UDP-GlcNAc transferase that has been used to build heparin oligosaccharides in a controlled, stepwise manner[78,80]. Processive glycosyltransferases such as heparosan synthases 1 and 2 (PmHS1 & PmHS2) from *Pasteurella multocida*, and chondroitin polymerase from *Escherichia coli* K4, have been used to synthesize HS and CS backbones of varying molecular weight[81,82]. Additionally, site-directed mutagenesis studies have been able to isolate two single-action *P. multocida* PmHS2 mutants, which can be used to build oligosaccharides in a step-wise manner[83].

Many sulfotransferases involved in GAG biosynthesis have been expressed and characterized *in vitro*. Unique to HS biosynthesis is the introduction of *N*-sulfo groups that is carried out by *N*-sulfotransferase/*N*-deacetylases (NDSTs), bifunctional enzymes with two active sites[84]. While the bacterial recombinant expression of active *N*-deacetylase domain has been difficult, the bacterially expressed *N*-sulfotransferase domain (NST) has been used in conjunction with *N*-trifluoroacetyl sugars to achieve precise the introduction of *N*-sulfo groups sites in heparin oligosaccharides[78,80]. The presence of *N*-sulfo groups are a prerequisite for the further introduction of *O*-sulfo groups and for C_5 epimerization, thus NDST specificity controls the formation (or absence, as in heparin) of domain structures in HS[85]. C_5-Epi, which produces critical IdoA residues in HS-GAGs, is thought to act irreversibly in vivo, likely due to concurrent introduction of 2-*O*-sulfo groups by GAG-modifying enzyme complex of C_5-Epi and 2-*O*-sufotransferase (2OST). The introduction of a 2-*O*-sulfo group blocks the reversible

activity of C_5-Epi in vitro possibly due to steric hindrance suggested from the recent crystallization of C_5-Epi in complex with a heparin oligosaccharide[86]. There is only one 2OST isoform identified in humans and it can act on both IdoA and GlcA residues adjacent to an *N*-sulfo glucosamine (GlcNS) residue without a 6-*O*-sulfo group, with a preference for IdoA. A crystallization study elucidated the molecular basis of this specificity, showing favorable interactions with the *N*-sulfo group, and suggesting steric hindrance with the 6-*O*-sulfo groups of the adjacent residue[87]. Three 6-*O*-sulfotransferase isoforms (6OST-1,2,3) have been identified in humans, and found to have slightly different specificities, 6OST-1 and 6OST-2 prefer to transfer a 6-*O*-sulfo groups to a GlcNS that is next to an GlcA residue and IdoA2S residue, respectively[61]. There are at least 6 different isoforms of 3-*O*-sulfotransferases (3OSTs) with distinct substrate specificities, two of which (3OST-1 & 3) have solved crystal structures[88,89]. Comparison of the two structures reveal distinct binding modes for the two isoforms, suggesting a mechanism for recognition of fine saccharide structure. It is thought that the presence of 3-*O*-sulfo groups can regulate many important HS functions. This is due to the modification being critical for protein binding of at least two specific saccharide sequences, the AT-binding site and the binding of the gD envelope protein of herpes simplex virus 1[35,90].

In addition to the HS sulfotransferases, there are several recombinant CS sulfotransferases with demonstrated in vitro activity, including chondroitin-4-sulfotransferase 1 (C4ST-1), chondroitin-6-sulfotransferase 1 (C6ST-1), *N*-acetylgalactosamine-4-sulfate 6-sulfotransferase (GalNAc4S-6ST), and uronosyl 2-sulfotransferase (UA2ST)[91]. Less is known about the CS sulfotransferases and the two CS C_5 epimerases[92-95], but it is likely that the activities, specificity and biosynthetic control parallels that of the HS biosynthetic enzymes. Moreover, specific CS structures seem to play prominent roles in nervous tissues and in brain development and function[96].

Finally, while not directly involved in GAG biosynthesis, arylsulfotransferase-IV (AST-IV), a mammalian liver detoxification enzyme involved in transferring sulfo groups to the hydroxyl groups of

phenols, has been indispensable for chemoenzymatic synthesis of sulfated GAGs. While normally catalyzing the transfer of a sulfo group from PAPS to a phenol, at high concentrations of p-nitrophenyl sulfate, AST-IV can be used to catalyze the reverse reaction transferring a sulfate group from p-nitrophenyl sulfate to PAP, thus, forming PAPS, the universal sulfate donor for sulfotransferases. This reverse reaction can be used as a cofactor regeneration system when coupled to HS or CS sulfotransferase reactions and overcomes strong product inhibition of these sulfotransferases by PAP[97]. This cofactor regeneration also produces p-nitrophenol, a yellow colored product which can be easily monitored at a 400 nm wavelength, forming the basis of a commonly used sulfotransferase assay[98,99]. Collectively, this cofactor regeneration system and colorimetric assay represents a valuable enzymatic toolbox for GAG synthesis.

Further structural elucidation of the GAG biosynthetic enzymes and enzymes for cofactor recycling may lead to new, engineered forms with novel specificities, further expanding the range of tools available. While protein engineering offers opportunities to improve the stability and activity of these recombinant enzyme catalysts, the lack of crystal structures for many of these enzymes poses a barrier to progress. Further efforts to scale-up the production of these enzymes in fed-batch fermenters are underway, and have been demonstrated for 4 out of 5 of the HS sulfotransferases including 2OST-1, C_5-Epi, 6OST-1 and 6OST-3[100-102]. This opens the way for the industrial scale production of GAGs.

1.5 Chemoenzymatic synthesis of HP/HS targets

Efforts to produce high-value oligosaccharide targets using this enzymatic toolbox are underway. Two fondaparinux-like ultra-LMWHs (Figures 1.1 & 1.6) that showed excellent *in vivo* and *in vitro* anticoagulant activity have been chemoenzymatically synthesized using heparin biosynthetic enzymes[103]. By using a chemoenzymatic approach, it is notable that these homogeneous heptasaccharides were synthesized through an approach biomimetic to heparin biosynthesis and within 12 steps at multi-milligram scale and in approximately 40% overall yield. Both heparin constructs were

synthesized initially on a heparosan-derived disaccharide acceptor containing a ring-contracted anhydromannitol residue. Using the *N*-acetyl glucosaminyltransferase (KfiA) and the heparosan synthase (pmHS2)[82], the acceptor was elongated stepwise from a disaccharide to a heptasaccharide, using the unnatural GlcN-trifluoroacetyl donor, which was later deprotected and *N*-sulfonated. KfiA transferred GlcN-trifluoroacetyl smoothly, demonstrating that uridine diphosphate sugar is a compatible unnatural substrate for KfiA. Compared with chemical glycosylation, enzymatic glycosylation proceeded with over 80% yield and in a stereospecific manner, giving the correct stereochemistry at each anomeric center.

The selective epimerization and sulfation of heparin oligosaccharide backbones are done using C_5-Epi and *O*-sulfotransferases, which converts GlcA into its C_5-epimer IdoA and transfers sulfo groups to desired positions, respectively. The selectivities of these modification enzymes provide excellent control over products but require careful reaction scheme design and careful selection of the appropriate isoforms to obtain the desired target structures. The most effective schemes are those that follow the

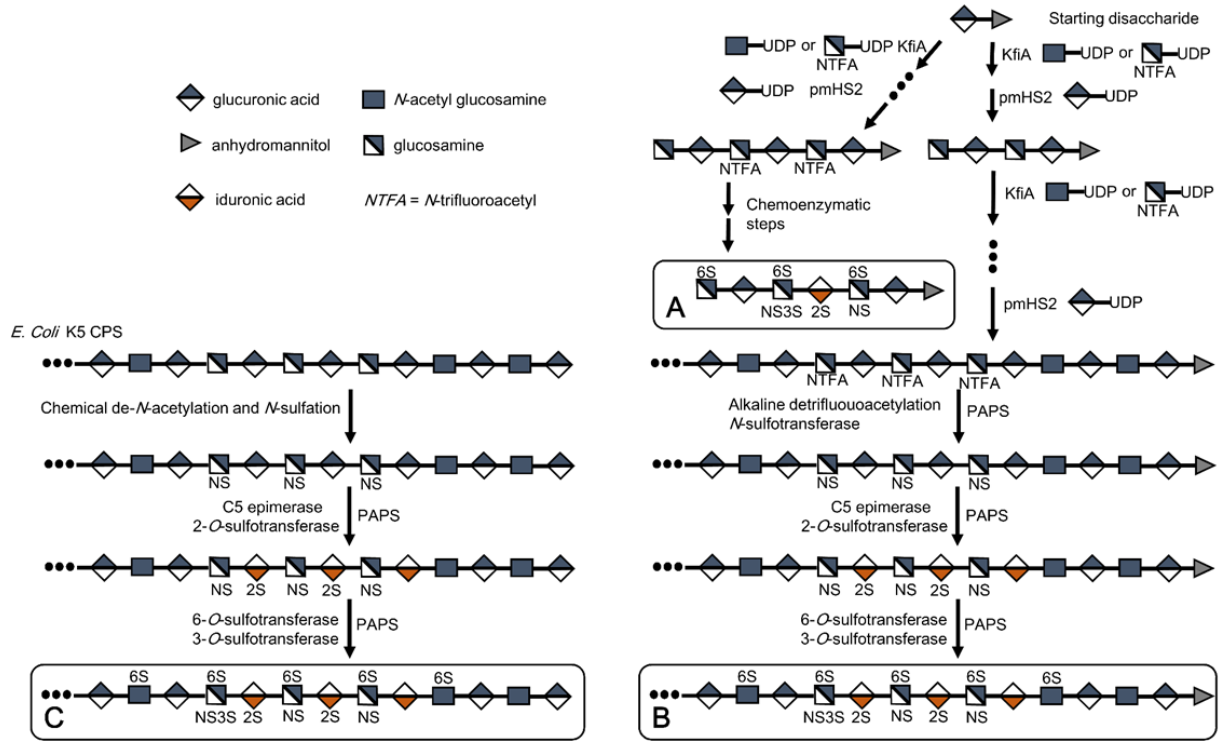

Figure 1.6. Chemoenzymatic synthesis of ultra-low molecular weight heparins (A), low molecular weight heparins (B), and bioengineered heparin (C).

reaction order found in natural heparin synthesis. Investigation of ideal reaction order and enzymatic activity, based on the heparin biosynthesis pathway, has shown that C_5-Epi only converts GlcA residues between two GlcNS residues[78] to IdoA and works best collaborating with 2OST, which locks the normally reversible epimerization into the IdoA conformation upon introduction of the 2-*O*-sulfo group. This specificity requires the NST pre-treatment before C_5-Epi and 2OST[104].

Recently, one-pot enzymatic synthesis has been explored for the preparation of certain heparin oligosaccharide targets[105]. Chemoenzymatic strategies appear to be the next step in the development of efficient syntheses of heparin oligosaccharides having up to 20 saccharide units.

Sugiura and coworkers have chemoenzymatically synthesized various CS species with defined lengths and defined sulfate compositions, using bacterial chondroitin polymerase and recombinant CS sulfotransferases, including chondroitin-4-sulfotransferase-1 (C4ST-1), chondroitin-6-sulfotransferase-1 (C6ST-1), *N*-acetylgalactosamine 4-sulfate 6-sulfotransferase (GalNAc4S-6ST), and uronosyl 2-sulfotransferase (UA2ST). Chemoenzymatic synthesis enables the generation of CS chains of the desired lengths, compositions, and distinct structures, and the resulting library will be a useful tool for studies of CS functions[91].

Another approach to oligosaccharide synthesis, used in preparing LMWHs involves the controlled enzymatic depolymerization of heparin using recombinant heparinases. In contrast to chemical depolymerization, enzymatic depolymerization using recombinant heparin lyases was proven to be a relatively artifact-free method[106]. Enzymatic depolymerization of heparin in scalable and potentially provides more access to LMWHs with specific in vivo biological and pharmacological activities. LMWHs, such as tinzaparin, prepared through controlled heparinase treatment have already been successfully commercialized.

A concerted effort is currently underway to chemoenzymatically synthesize a full length bioengineered heparin, based on the overexpression of the *E. coli* K5 capsular polysaccharide (CPS)

heparosan, and subsequent modification with recombinant HP biosynthetic enzymes[107]. Such a bioengineered heparin might one day be approved as a generic heparin and also used in the preparation of LMWHs, increasing the supply and eliminating the risks that come with drugs derived from animal tissues[61,62,108]. Small amounts of bioengineered heparin have been prepared from this *E. coli* heparosan in several laboratories[77,107,109]. Over the past 5 years, research has focused on developing a scalable process capable of producing sufficient quantities of a bioengineered heparin for pre-clinical and clinical evaluation. Even greater challenges are anticipated to meet global demand (over 100 tons/y) if a bioengineered, generic version of heparin, chemically and biologically equivalent to current USP heparin, is to be introduced in the future[62,108,110].

Unlike the chemoenzymatic synthesis of LMWHs and ULMWH oligosaccharides, the process for preparing bioengineered heparin begins with an *E. coli* fermentation to prepare the CPS, heparosan, followed by its chemical (or enzymatic) de-*N*-acetylation and *N*-sulfonation. Treatment of *N*-sulfo, *N*-acetyl heparosan with recombinant *O*-sulfotransferases and C_5-Epi in the presence of a PAPS cofactor recycling system results in a bioengineered heparin that closely resembles the chemical and biological properties of heparin. Key elements for the commercialization include: process control, scale-up, and a reduction in the costs of CPS, recombinantly expressed biosynthetic enzymes, and PAPS cofactor[97,111,112].

Recombinant heparin biosynthetic enzymes, C_5-Epi, 2OST, 6OST and 3OST, are expressed fused to maltose binding protein (MBP) or histidine $(His)_6$ tagged at their *N*-termini. This affords a handle that allows for the convenient purification of these enzymes and their immobilization onto beaded supports. Immobilization both stabilizes these enzymes and allows for their easy recovery and reuse, which simplifies product purification. A recent investigation showed that the enzymes maintain greater than 80% of activity after immobilization[113]. These recombinant enzymes have been immobilized on amino-linked agarose gel beads at a loading of 20 mg/ml of gel with enhanced thermo stability[114].

The control of number and weight average molecular weight of the final bioengineered heparin is another challenge for making a product that closely resembles porcine intestinal heparin. The heparosan CPS from *E. coli* K5 has a higher average molecular weight (75 KD) than heparin (~ 15 KD)[107]. Moreover, as sulfo groups are transferred to heparosan the molecular weight of a given chain increases by 1.60-fold to 1.75-fold. The average molecular weight of the CPS can be conveniently decreased in the base- catalyzed de-*N*-acetylation to between 8 KD to 10 KD, affording a precursor polysaccharide that will afford a bioengineered heparin of the same average molecular weight as porcine intestinal heparin. Process control, time, temperature, base and heparosan concentration can be optimized based on the starting CPS to afford an intermediate with desired molecular weight properties and *N*-acetyl content[108]. It might also be possible to control the molecular weight of heparosan through manipulation of culture conditions, chain termination and genetic manipulation[115]. Infection with phage carrying heparosan lyase has been examined as a means to control molecular weight[114]. Molecular weight can be rapidly estimated by polyacrylamide gel electrophoresis and analyzed by size-exclusion chromatography and comparison made to a USP heparin standard. The chemical *N*-sulfonation step also needs to be controlled to ensure all the amino groups in the glucosamine residues are either substituted with an *N*-sulfo or *N*-acetyl group[116].

Recently, a successful one-pot chemoenzymatic synthesis of complex full-length heparin/HS polysaccharides has been achieved beginning from *N*-sulfoheparosan in our laboratory. This approach of modulating enzymatic activity through use of an optimized enzyme/substrate ratio is suited for high throughput screening studies aimed at better understanding of heparin's structural heterogeneity and its impact on structure activity relationship. Diversity in 3OST family (7 different isoforms) is primarily responsible for wide array of biological functions attributed to heparin/HS glycosaminoglycans. One-pot chemoenzymatic synthesis of heparin/HS chains provides a way to decipher the substrate specificity of various 3OST isoforms with easy availability of polysaccharide/oligosaccharide substrates[117].

2. PRODUCTION OF RECOMBINANT HEPARIN/HEPARAN SULFATE BIOSYNTHETIC ENZYMES

2.1. Introduction

Heparin is a critically important anticoagulant drug that is derived from animal tissue[4]. The heparin contamination crisis of 2008[62] led our laboratory to research the preparation of a bioengineered heparin to replace this animal-sourced drug[108]. Bioengineered heparin is prepared from heparosan, →4) *N*-acetyl-α-D-glucosamine (1→4) ß-D glucuronic acid (1→ (→4) GlcNAc (1→4) GlcA(1→), the capsular polysaccharide of *E. coli* K5[118], which is chemically converted to *N*-sulfo-heparosan (NSH) and then enzymatically modified in a three-step process to obtain anticoagulant heparin[108] (Fig. 2.1). Truncated Golgi proteins, missing their transmembrane domain, are expressed from *E. coli* as maltose binding protein (MBP)-fusion proteins[119]. The first enzymatic step uses 2-*O*-sulfotransferase (2-OST) and C_5-epimerase (C_5-Epi), to convert *N*-sulfo heparosan into an intermediate polysaccharide rich in →4)GlcNS(1→4) IdoA2S(1→ disaccharides (where S is sulfo and IdoA is α-L-iduronic acid). The second step uses 6-*O*-sulfotransferase isoforms 1 and 3 (6OST-1, 6OST-3) to produce a polysaccharide rich in →4)GlcNS6S(1→4) IdoA2S(1→ sequences, also known as tri-sulfated disaccharides, the main component of heparin[4]. Both of these critical steps in bioengineered heparin preparation relies on the use of recombinant arylsulfotransferase IV (AST-IV) to regenerate 3'-phosphoadenosine-5'-phosphosulfate (PAPS) using *p*-nitrophenylsulfate as a sacrificial sulfo donor[97,99,120].

The generation of small quantities of bioengineered heparin, closely resembling animal-sourced heparin has been demonstrated[118]. However, substantial quantities of *E. coli* expressed recombinant 2-OST and C_5-Epi are required to scale-up this process. It is essential to produce the enzymes in a high yield

---

Portions of this chapter previously appeared as: Zhang, J., *et al*. High cell density cultivation of a recombinant *Escherichia coli* strain expressing a 6-O-sulfotransferase for the production of bioengineered heparin. *Appl. Microbiol.* **97,** 3893–3900 (2014)., and Zhang, J., *et al*. High cell density cultivation of recombinant *Escherichia coli* strains expressing 2-*O*-sulfotransferase and C5-epimerase for the production of bioengineered heparin. *Appl. Biochem. Biotechnol.* **175,** 2986–2995 (2015).

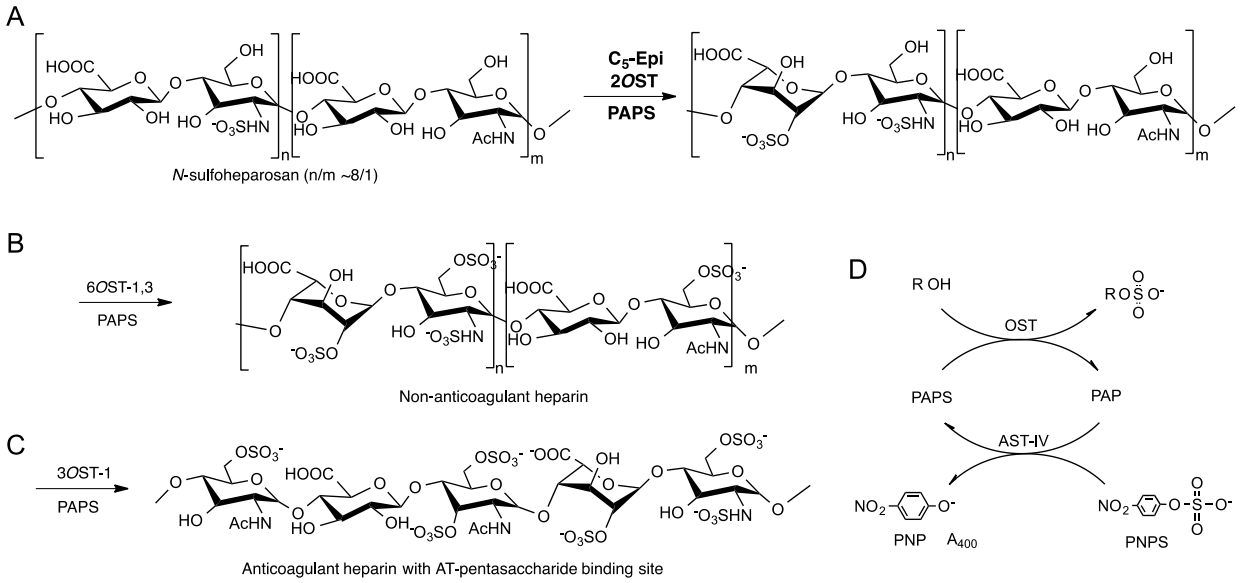

Figure 2.1. Three-step enzymatic synthesis of heparin from *N*-sulfoheparosan. A. In the first step *N*-sulfoheparosan is treated with 2-OST and C_5-Epi. B. In the second step 6-*O*-sulfotransferase isoforms 1 and 3 are used to prepare non-anticoagulant heparin. C. In the third enzymatic step 3-*O*-sulfotransferase isoform 1 is used to introduce the antithrombin (AT) pentasaccharide-binding site affording anticoagulant heparin. D. PAPS, used as the sulfo donor in each step, forms PAP, which is recycled using aryl sulfotransferase IV (AST-IV) and p-nitrophenyl sulfate (PNPS) as a sacrificial sulfo donor, forming p-nitrophenol (PNP) which can be detected by its absorbance at 400 nm. The R at the top of panel D corresponds to the polysaccharide substrate.

stirred tank fermentor for bioengineered heparin to become commercially viable. The following studies describe the production scale-up of three enzymes, C_5-Epi, 2-OST, and 6-OST-3 from shake-flask to stirred tank fermenter.

2.2. Results

2.2.1. Shake flask preparation of C_5-Epi and 2-OST

One-liter shake flask experiments were performed to investigate the medium, culture and induction conditions that are suitable for fed-batch expression. The batch cultures of recombinant *E. coli* were carried out in LB medium[119,121]. To identify medium conditions suitable for batch fed batch fermentation, we investigated the effect of different media components on the expression of 2-OST and

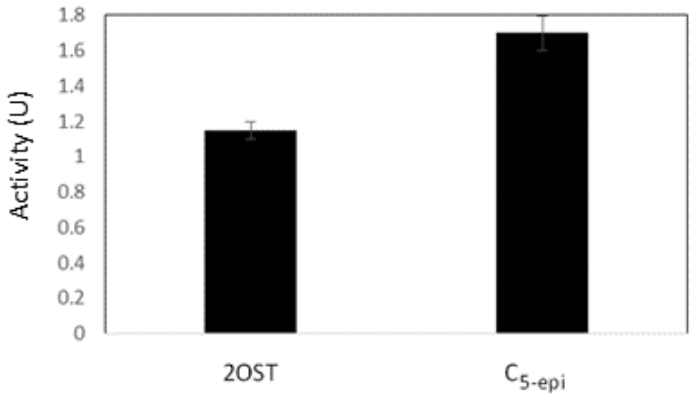

Figure 2.2. Activity of 2-OST and C_5-Epi expressed in shake flask fermentation.

C_5-Epi. A new M9 salt and glucose containing medium was identified that can be used to express both enzymes. The cultures were grown to an OD_{600} of 0.6, and induced using Isopropyl β-D-1-thiogalactopyranoside (IPTG) at 0.2 mM for 2-OST, and IPTG plus 200 mg/ml of arabinose for C_5-Epi. The results showed that the activities of 2-OST and C_5-Epi were 1.7 ± 0.1 U and 1.15 ± 0.05 U, respectively (Fig. 2.2).

2.2.2. Fed batch reactor system preparation of C_5-Epi and 2-OST

The fed-batch fermentation of 2-OST produced a maximum cell density of 5.5 g_{cdw}/l, and a productivity of 6.0 mg/l-h (Table 2.1.). A 20 g portion of cell biomass yielded a highly concentrated elution of 167 mg/l 2-OST enzyme upon purification, with a specific activity of 0.54 ± 0.01 nmol/min mg. After a 20-hour incubation of fed batch 2-OST with *N*-sulfo-heparosan (NSH) and control C_5-Epi (from shake flask), the conversion of GlcNS-GlcA disaccharides to GlcNS-IdoA2S reached 63.4% of total disaccharides. Acetic acid, which was produced as a by-product during batch mode, is generally produced at a high specific growth rate when there is excess carbon source or oxygen-limited conditions[122]. In this experiment, acetic acid accumulated up to 15.1 g/l in the cell-free culture medium; therefore, a constant feeding rate did not meet the demand of exponential cell growth, and the glucose concentration varied over a wide range. (Fig. 2.3). Fed-batch fermentation of C_5-Epi reached a maximum cell density of 5.9 g_{cdw}/l, with a

Table 2.1. Fed batch fermentor produced 2-OST and C_5-Epi enzyme results.

	2-OST	C_5-Epi
Induction time (h)	17	16
Total hours of induction (h)	11	14
Feeding start time (h)	6	5
Fermentation time (h)	28	30
Maximum cell density (g_{cdw}/l)	5.5	5.9
Purified enzyme concentration (mg/l)	167	65
Enzyme yield /biomass (mg/g_{cdw})	30.3	11.1
Productivity (mg/l h)	6.0	2.2
Final specific activity (nmol/min mg)	0.54 ± 0.01	1.78 ± 0.05
Heparin disaccharide (ΔUA2S – GlcNS)(%)	63 ± 0.3	70 ± 1.1

productivity of 2.2 mg/l-h. The concentration of purified enzyme from a 20 g portion of cell biomass was 65.3 mg/l, and the final specific activity was 1.78 ± 0.05 nmol/ min mg (Table 2.1, Fig. 2.4). The 20 h reaction of fed batch C_5-Epi and control 2-OST (from shake flask) produced 70% GlcNS-IdoA2S disaccharides, reaching a very high conversion rate. As mentioned above, the acetic acid concentration was quite high, which suggests that the feeding model should be optimized for higher cell density and/or higher enzyme production.

The 2-OST and C_5-Epi were purified using an amylose column. There were four bands observed for each enzyme in SDS-PAGE analysis; the highest molecular weight (MW) band corresponded with the highest intensity and the expected molecular weights for each enzyme (107.3 & 79.2 kD for C_5-Epi and 2OST respectively) (Fig. 2.3).

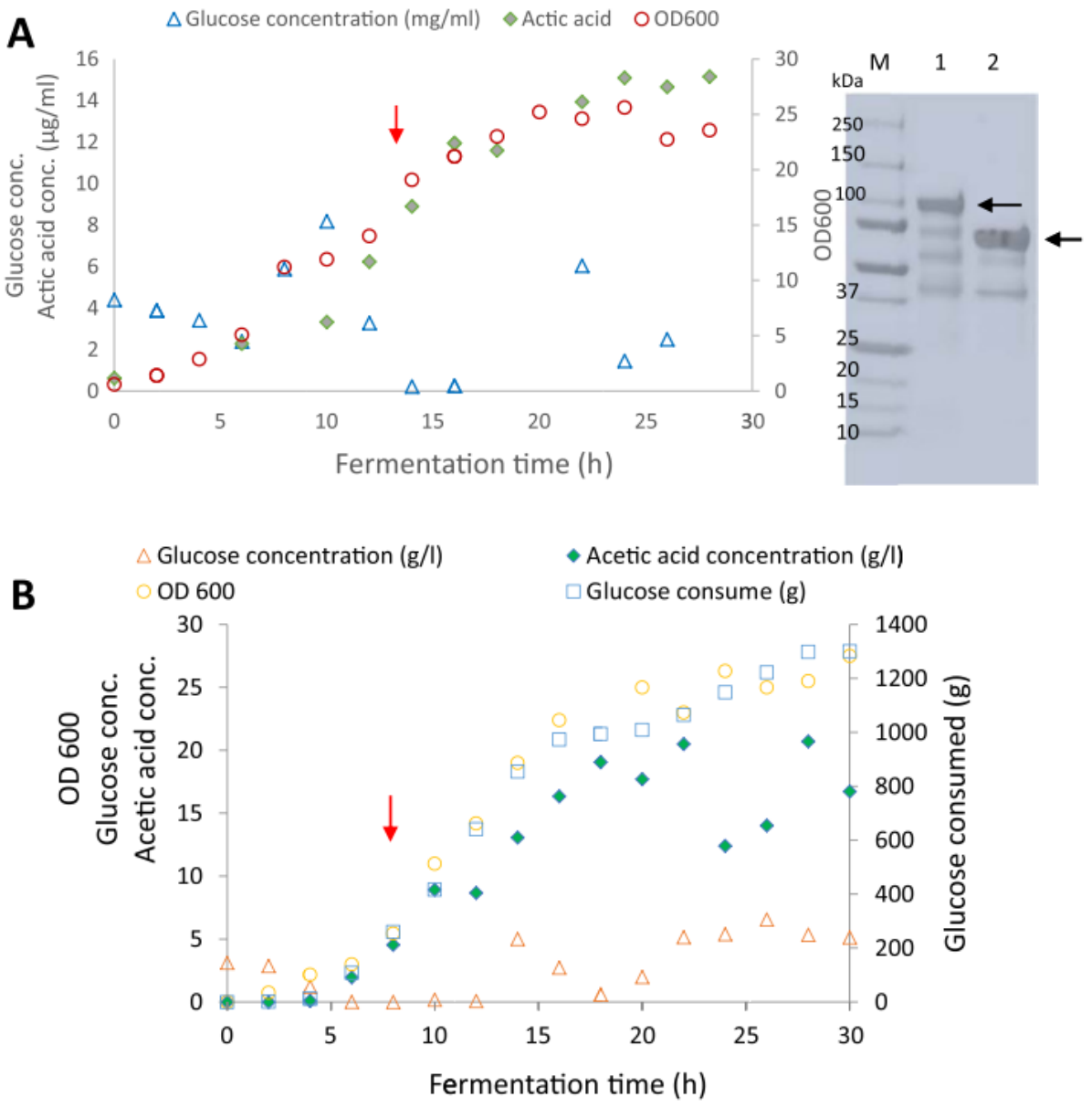

Figure 2.3. ***E. coli*** **2-OST and C_5-Epi fed-batch fermentation. A. 2-OST fermentation and B. C_5-Epi fermentation: bacterial growth (open circles), glucose concentration (open triangles), acetic acid concentration (filled diamonds), and glucose consumed (open squares). Induction times for 2-OST and C_5-Epi were indicated by red arrows. C. SDS-PAGE analysis of purified enzyme; lanes 1, 250–10 kDa ladder; 2, purified C_5-Epi; 3, purified 2- OST. The specific enzyme bands are indicated by black arrows.**

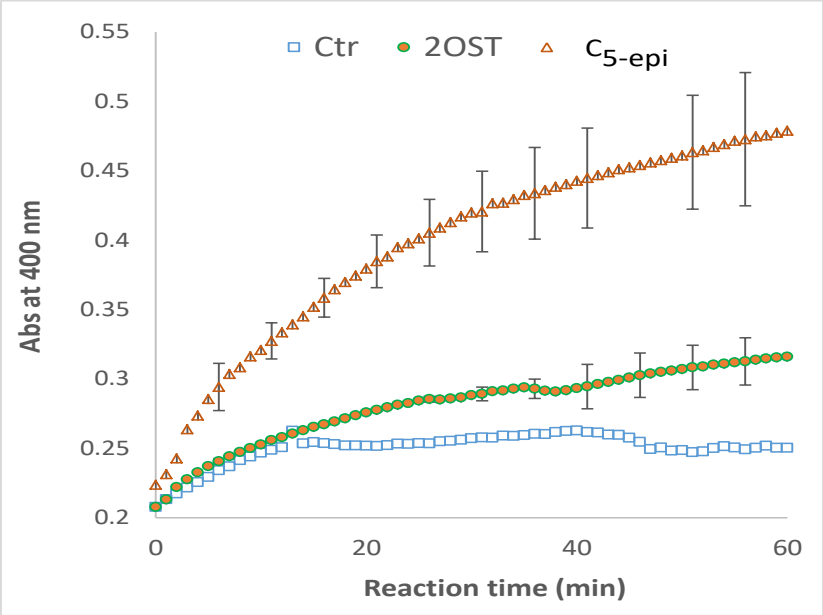

Figure 2.4. Measurement of specific activity during a 1-h reaction catalyzed by 2-OST and C_5-Epi purified from fed-batch fermentations. Control, without substrate (open squares), 2-OST (filled circles), 2-OST and C_5-Epi (open triangle).

2.2.3. Shake flask preparation of 6-OST-3

As with C_5-Epi and 2-OST, shake flask experiments were performed to investigate the medium composition, induction, and culture conditions that would be suitable for fed-batch expression of 6-OST-3. For 6-OST-3 expression, fructose (22.2 mM), glucose (22.2 mM) and glycerol (43.5 mM) were selected as carbon sources for the media. Based on the growth rate, enzyme production and enzyme specific activity, glycerol was selected over the other sugars, although both the enzyme amount (1.56 mg/l) and specific activity (1.21 U/mg) were lower than the values obtained with growth on LB media, 1.98 mg/l and 1.43 U/mg, respectively (Fig 2.5.).

LB medium with a 2% inoculum is generally used to produce 6-OST-3 at small scale. In such cases we have observed that induction conditions have a significant influence on the activity of 6-OST-3.

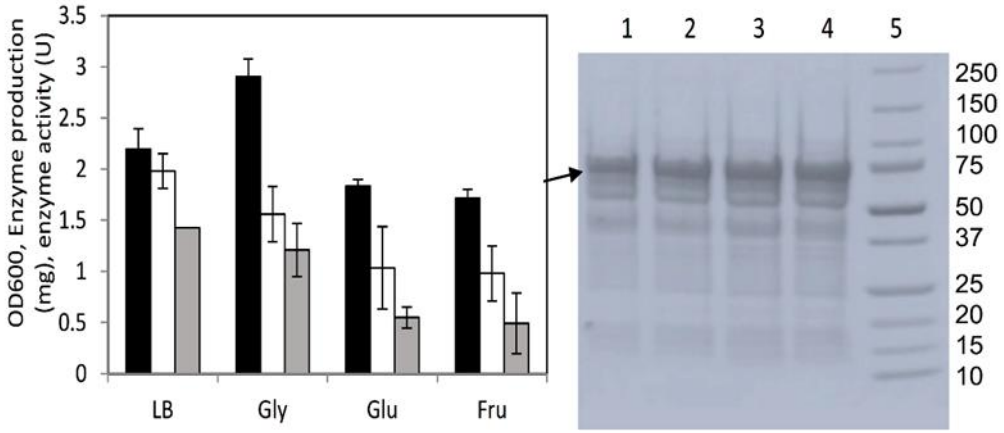

Figure 2.5. Expression of 6-OST-3 with LB and LB plus 0.4% of different carbon sources. Left panel: OD600, enzyme production and activity of 6-OST-3 expressed from LB media, LB plus 43.5 mM glycerol, LB plus 22.2 mM glucose and LB plus 22.2 mM fructose. Black columns: OD600, White columns: enzyme protein production, Gray columns: enzyme activity. Right panel: SDS-PAGE analysis of purified protein solution; lane 1, LB plus 22.2 mM fructose; 2, LB plus 22.2 mM glucose; 3, LB plus 43.5 mM glycerol; 4, LB; 5, 250–10 kDa molecular weight ladder. The 6-OST-3 bands are indicated by arrows

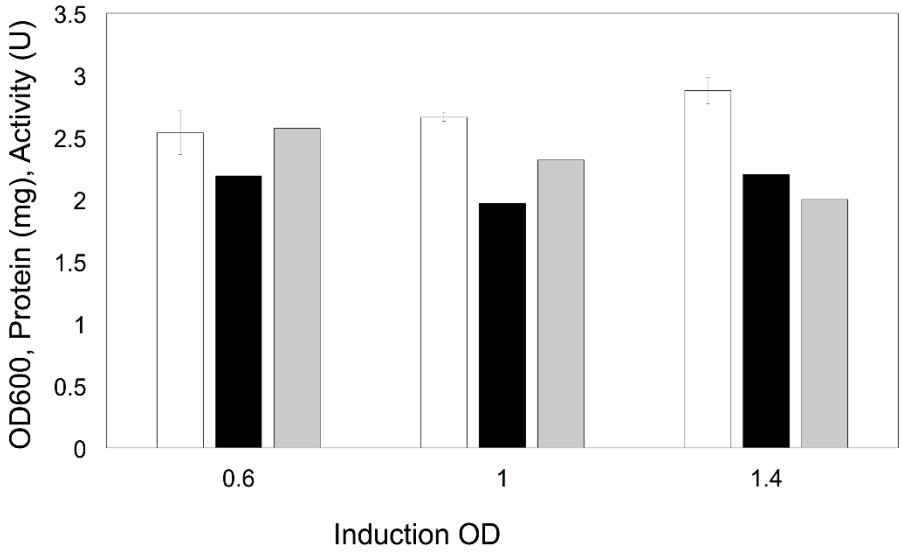

Figure 2.6. Expression of 6-OST-3 at different induction ODs. Cultures were induced at OD_{600} values of 0.6, 1.0 and 1.4 in LB plus 43.5 mM glycerol. Black columns: OD_{600}, White columns: enzyme protein production, Gray columns: enzyme activity.

Therefore, we investigated the effect of inducing at different OD_{600} on the resulting 6-OST-3 activity (Fig.2.6.). The results showed that although the activities were decreased slightly when induction takes place at higher OD_{600} values, there was no significant difference in induced protein production.

2.2.4. Fed batch production of 6-OST-3

The high cell density culture of recombinant *E. coli* was used to obtain recombinant proteins with high yield and high productivities. This is required to meet the high demand for enzymes in the large-scale production of bioengineered heparin. High cell density culture also has the advantage of increasing the effectiveness of the process, reducing culture and wastewater volumes, production costs, and upfront investment for fermentation equipment.

Table 2.2. Comparison of shake flask 6-OST-3 expression with fed-batch. Expression parameters for fermentations A, B, C, and shake flask LB media control.

	FB A	FB B	FB C	LB
OD_{600} at induction time	7.5	9.5	3.5	0.6
Cell density at induction (gcdw/l)	2.6	3.5	0.8	
Feeding start time (h)	6	10	4	
Fermentation time (h)	26	26	24	
Maximum cell density (g_{cdw} /l)	7.6	10.5	5.7	
Purified 6-OST-3 concentration (mg/l)	61.5	52.9	120.7	6.1
Yield 6-OST-3/biomass (mg/g_{cdw})	8.1	5.0	21.2	
Productivity 6-OST-3 (mg/l/ h)	2.4	2.0	5.0	0.29
Final specific activity (nmol/min/mg)	1.36 ± 0.185	1.55 ± 0.144	1.67 ± 0.172	2.55
Productivity 6-OST-3 (U/l/h)	3.26	3.10	8.35	0.74
NS6S content (% ± SD)	79.93 ± 2.45	82.94 ± 0.58	83.18 ± 3.07	93.68

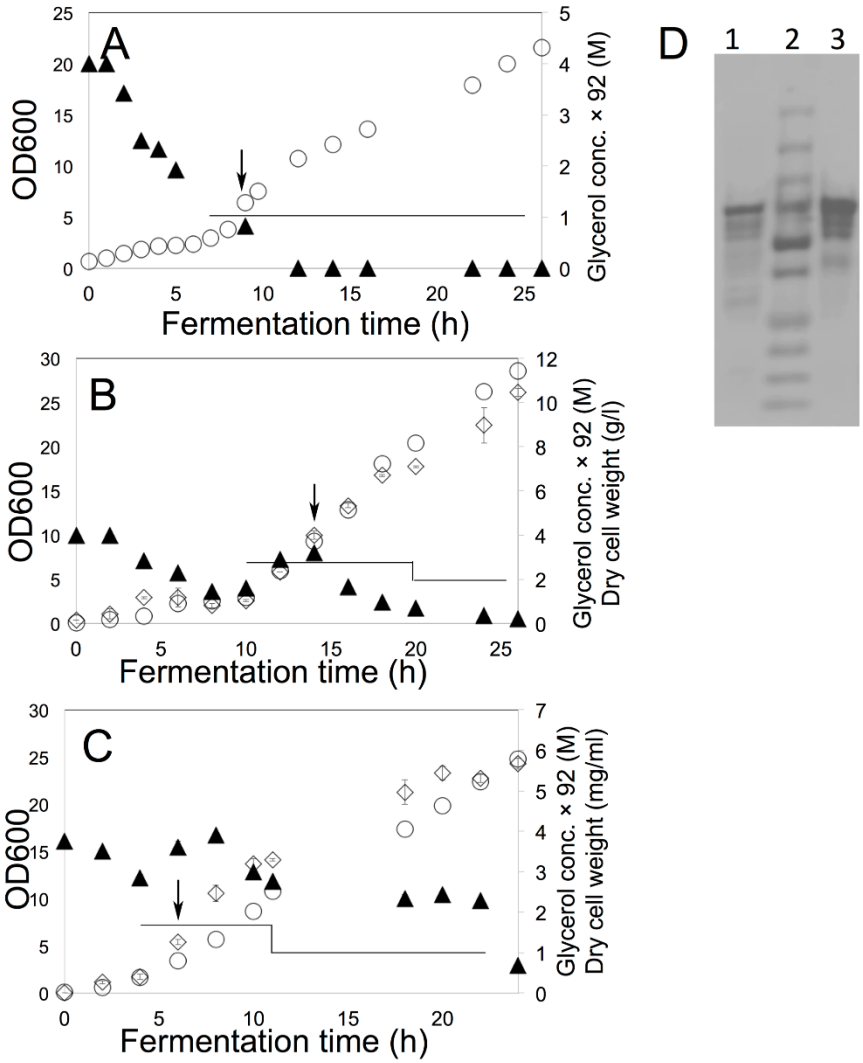

Figure 2.7. Three fed batch fermentations of 6-OST-3. Panels A, B and C show fed batch fermentation profiles from batch A, B and C, respectively. Bacterial growth (empty circles), glycerol concentration (filled triangles), and dry weight of biomass (empty diamonds), feeding profile (lines). Induction was performed with 0.1 mM IPTG at 7.5, 9.5 and 3.5 OD_{600}, respectively, as indicated by the arrows. D: SDS PAGE analysis of purified enzyme; lane 1, purified enzyme from batch A; lane 2, molecular weight standards 250-10 kDa; lane 3, purified enzyme from batch C.

Three experiments were performed to examine the effect of feeding time, feeding rate, and induction time on the yield and activity of 6-OST-3. The results of these studies are presented in Figures 2.7 and 2.8 and Table 2.2.

For the first batch, we controlled the feeding rate at 0.6 ml/min from 6 h, so that the glycerol concentration was almost zero (Fig. 2.7.). This kept the growth rate relatively slow, though the maximum

cell density still reached 7.6 g_{cdw}/l. The productivity of 6-OST-3 was 2.4 mg/l/h), and the final specific activity was 1.36 ± 0.185 nmol/min/mg.

For the second batch, expression was induced when the OD_{600} reached 9.3 (Fig. 2.7.), and the feeding rates were 3 ml/min from 9 h and 1 ml/min after induction at 14 h. During the expression period, the glycerol concentration again got quite low suggesting a more robust feeding strategy was needed. Despite this it reached a high maximum cell density of 10.5 g_{cdw}/L, and a 6-OST-3 productivity of 2.0 mg/l/h, The final specific activity was 1.55 ± 0.144 nmol/min/mg.

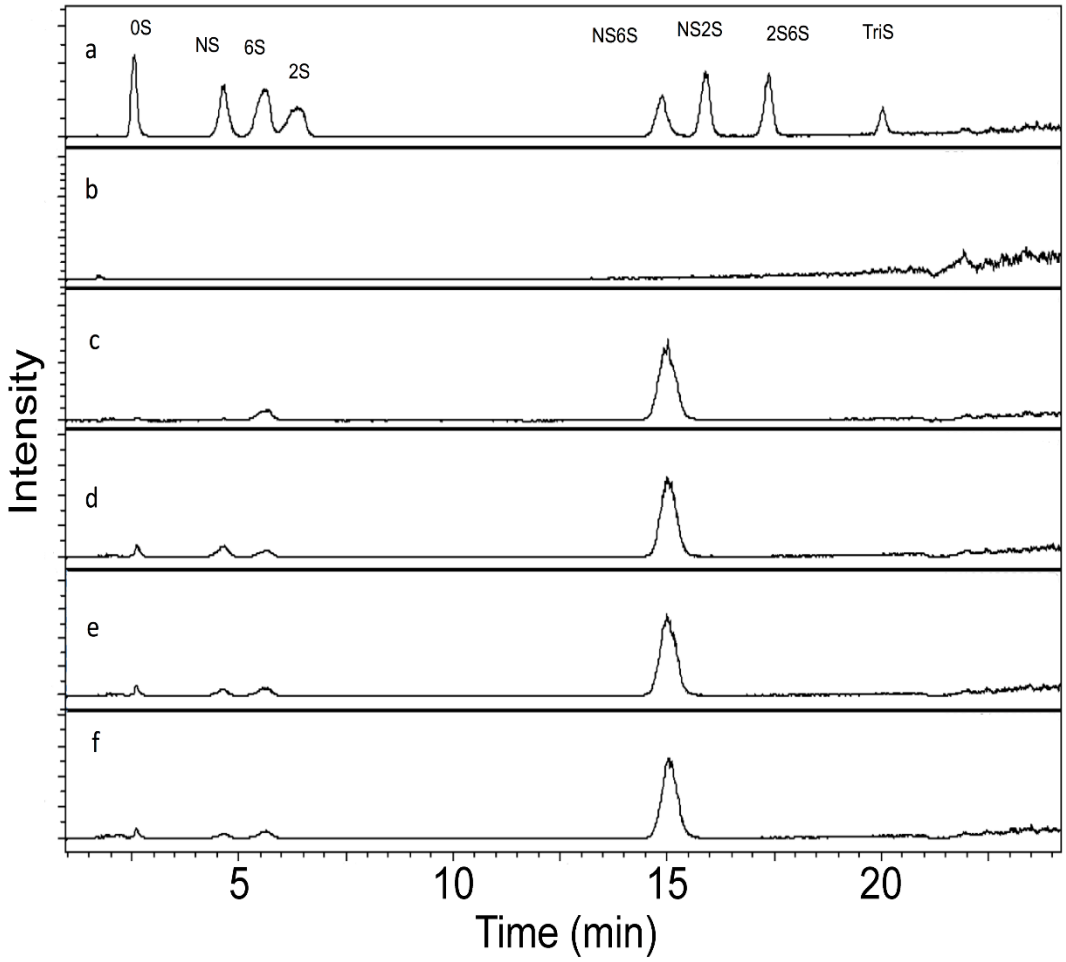

Figure 2.8. LC-MS extracted ion chromatographs (EIC) of 6-OST-3 treated NSH products. a. 8 HP/HS disaccharide standards; b. control; c. product from LB shake flask 6OST treatment; d. product from batch A 6OST treatment; e. product from batch B 6OST treatment; f. product from batch C 6OST treatment. Unsaturated disaccharide standards of heparan sulfate (0S, ΔUA-GlcNAc; NS, ΔUA-GlcNS; 6S, ΔUA-GlcNAc6S; 2S, ΔUA2S-GlcNAc; 2SNS, ΔUA2S-GlcNS; NS6S, ΔUA-GlcNS6S; 2S6S, ΔUA2S-GlcNAc6S; and TriS, ΔUA2S-GlcNS6S, where GlcNAc is *N*-acetyl-D-glucosamine and ΔUA 4-deoxy-α-L-*threo*-hexenopyranosyluronic acid).

For the third batch, the expression was induced at an OD_{600} of 3.46 (Fig. 2.7.), with feeding rates of 1.8 ml/min from 4 h and 1 ml/min after 8 h. An early induction time led to a low maximum cell density of 5.7 g_{cdw}/l (Table 2.1). However, 6-OST-3 productivity was 5.0 mg/l/h, more than double either of the previous batches. The final specific activity was 1.67 ± 0.172 nmol/min/mg.

To test enzyme performance in a chemoenzymatic synthesis, 50 μg of each fed batch 6-OST-3, shake flask and control 6-OST-3 were incubated overnight with an NSH substrate containing 89% GlcNS residues and 11% GlcNAc residues. The control and shake flask 6-OST-3 produced up to 89% GlcNS6S product. Liquid chromatography-mass spectral analysis showed that the NS6S percent conversion of 6-OST-3 from batches A B and C were 79.9% ± 2.5, 82.9% ± 0.6 and 83.2% ± 3.1, respectively.

2.3. Discussion

The chemoenzymatic preparation of a bioengineered heparin relies on three enzymatic steps, the first and most difficult step requires the extensive epimerization of GlcA to IdoA by C_5-Epi and its subsequent sulfation with 2-OST to afford IdoA2S. Since the epimerization reaction catalyzed by C_5-Epi is reversible, 2-OST must be present to quickly trap IdoA as IdoA2S, which is present in 80–90% of heparin disaccharides. The main heparin disaccharide, IdoA2S-GlcNS6S, requires the action of 6-OST-1 and -3. Thus, there is a need for large quantities of heparin biosynthetic enzymes, especially C_5-Epi and 2-OST, that can only be satisfied by large volume fed batch fermentations. Initial attempts to prepare these critical enzymes resulted in either low levels of these enzymes or inactive enzymes. Preventing the accumulation of toxic levels of acetic acid is a major task to achieve high cell concentrations in the bioreactor. The accumulation of acetic acid in the media may have toxicity effects on the cells in the culture, the primary factor being its ability to diffuse across *E. coli* cellular membranes. Diffusing acetic acid or other organic acids entering into the cytoplasm will disrupt the pH and anion pool of the cytoplasm, and the resulting increase in acidity can affect the integrity of purine bases. The pH change can also denature essential enzymes inside the cell, negatively affecting cell viability and enzyme

expression[122]. The specific growth rate of *E. coli* K12 batch cultured in the fermenter decreased from 15 to 5 g/l as the acetic acid concentration increased. Growth-inhibiting acidic byproducts of incomplete substrate oxidation, such as acetic acid, are produced in response to oxygen limitation or excess carbon. The formation of acetic acid and subsequent growth inhibition can be avoided by limiting the amount of carbon source in the culture media via an exponential feeding strategy[123] or by controlling the dissolved oxygen level[124]. Although active 2-OST and C_5-Epi were obtained, the fed-batch fermentations were not optimized, cell densities achieved were not sufficiently high, and the relationship between the growth rate and enzyme expression is unclear. Additional work remains to be performed before this process step can be taken to pilot-scale production.

In addition to controlling acetate accumulation in the culture medium, a serious problem with expressing 6-OST-3 in fed batch systems is the tendency to form inclusion bodies. The lack of chaperone folding proteins and a post-translational modification system in *E. coli* often causes aggregation and low productivity of recombinant eukaryotic proteins[125]. Being a truncated, transmembrane protein expressed as a maltose binding protein fusion, 6-OST-3 is likely to mis-fold in the absence of chaperones and may form soluble aggregates. The cell targets these soluble but inactive enzyme aggregates for incorporation into inclusion bodies, thereby decreasing productivity[126].

Out of the different feeding strategies and induction times, Batch C gave the highest productivity levels, at 8.35 U/l/h, with the trade-off of a lower maximum cell density. Batch C also had the highest specific activity, though it was lower than shake flask produced 6-OST-3. Batch B reached the highest maximum cell density by delaying induction, which unexpectedly did not increase productivity, in fact decreasing it relative to A and C. Assuming there is a degree of leaky expression, a higher induction OD, as in batch B, could mean more pre- existing inclusion bodies or soluble aggregates before induction, leading to easier incorporation of the enzyme into these inactive forms after induction. This may be the reason that there is a correlation between high induction OD and low enzyme productivity.

2.4. Conclusions and future directions

Despite significant obstacles, successful fed batch fermentations were carried out for each of the three enzymes. Additional optimization is needed before attempting to meet the needs of a large scale bioengineered heparin process. However, it has been demonstrated that nearly all of the enzymes needed can be produced in a fed batch system, 2-OST, C_5-Epi, and 6-OST-3 in the above studies, and 6-OST-1 in an earlier study from the Linhardt lab[100]. 3-*O*-sulfotransferase (3OST) is the last enzymatic step in making a bioengineered heparin, and is currently produced in shake flasks with LB. The relative scarcity of the 3-*O*-sulfo group modification diminishes the need for large quantities of enzyme.

A successful future optimization will require careful tuning of feeding and culture parameters, and a strategy to minimize enzyme aggregation, inclusion bodies, and toxic metabolite buildup. The transformation of the 6-OST-3 strain with a chaperone protein plasmid could decrease aggregation. It may be worth pursuing other eukaryotic expression systems, given the presence of post-translational modifications and glycosylation, which would likely improve stability and activity. Chinese Hamster Ovary (CHO) cells are a eukaryotic system currently used for industrial scale enzyme production, and therefore may be a good fit.

2.5. Materials and methods

2.5.1. Bacterial strain, plasmid, and enzyme constructs

The recombinant *E. coli* Rosetta-gami B (DE3) strain (Novagen, Cambridge MA, USA) strain with the plasmid pMalc2x was used to express all enzymes. The enzyme constructs were as follows: the catalytic domain of Chinese hamster ovary 2-*O*-sulfotransferase (Arg^{51}–Asn^{356}) -MBP fusion product[119], the human C_5-epimerase (Glu^{53}-Asn^{609}) -MBP fusion product[127], and the catalytic domain of mouse 6-OST-3 (Pro^{121}–Pro^{450}) -MBP fusion product[119].

2.5.2. Media composition and shake flask expression

Shake flask experiments for C_5-Epi and 2-OST were performed in either LB media, or a glucose and M9 minimal salts (64 g Na_2HPO_4-$7H_2O$, 15 g KH_2PO_4, 2.5 g NaCl, 5.0 g NH_4Cl)-based medium, with 200 ml/l of M9 salts, 2 ml/l of 1M $MgSO_4$, 20 ml/l of 20% glucose, 100 µl/l of 1 M $CaCl_2$, 20 g/l yeast extract and 1 ml/l of a trace metal solution. Trace metal solution was made according to Matsui[12] with the following modification in composition (g/l): $FeSO_4 \cdot 7H_2O$, 10.0; $CaCl_2$, 2.0; $ZnSO_4 \cdot 7H_2O$, 2.2; $MnSO_4 \cdot 4H_2O$, 0.5; $CuSO_4 \cdot 5H_2O$, 1.0; $(NH_4)_6MoO_{24} \cdot 4H_2O$, 0.1 and $Na_2B_4O_7 \cdot 10H_2O$ (dissolved in 5 M HCl), 0.02. Shake flask experiments for 6-OST-3 were performed in LB medium and LB with 43.5 mM glycerol, 22.2 mM glucose, or 22.2 mM fructose.

Antibiotics were added to the media to select for the plasmid and prevent the growth of contaminating microbes, after being filtered with a syringe through a 0.22-µm membrane. Ampicillin (50 mg/l), tetracycline (12.5 mg/l), and kanamycin (50 mg/l) were added for 2-OST and 6-OST-3 expression. For C_5-Epi expression, 50 mg/ml chloramphenicol was added along with the other three antibiotics.

Transformed cells were incubated at 37^{o}C on shaker at 220 rpm overnight to prepare cultures from stock bacteria. A 1-l media flask was inoculated with 10% (v/v) of overnight culture. When the fermentation reached an optical density at 600 nm (OD_{600}) of 0.6-0.8, the temperature was decreased to 22ºC for 30 min. A 200 µL aliquot of 1 M isopropyl-thiogalactopyranoside (IPTG) was added to each liter of fermentation media for induction. The culture was shaken for 16-18 h at 220 rpm at the reduced temperature of 22˚C.

2.5.3. Fed batch reactor setup

A 20-l bioreactor (Bio-Flo 4500, New Brunswick Scientific, Enfield, CT, USA), *in situ* sterilizable and equipped with pH and pO_2 probes (Mettler, Toledo, Switzerland) was used for fed-batch experiments.

During growth the fermentation parameters were controlled by Biocommand A4 software (Eppendorf, Inc., Enfield, CT, USA).

For the 5-l fed-batch fermentation, 200 µL of glycerol stock bacteria were inoculated into a 250 ml shake flask containing 50 ml LB medium. After 12 h of cultivation in a shaker incubator (220 rpm) at 37°C, the entire pre-culture was aseptically transferred into a 2.5 l shake flask containing 500 ml LB medium and incubated under the same condition for 10 h. This was used to inoculate the 5-l fed-batch fermentation that took place in the 20-l bioreactor. Fed-batch experiments were performed at 37°C and pH of 7.0 in 5-l LB containing 43.5 mM glycerol. The DO was set to 20% and cascade controlled by inlet airflow rate and agitation speed. The pH was set to 7.0 and cascade controlled by acid pump for hydrochloric acid and base pump for ammonia water.

In 2-OST fed-batch experiment, the culture was fed from 6 h to 10 h at a constant feeding rate of 5 ml/ min, from 12 h to 22 h at a constant feeding rate of 3 ml/min, from 24 h to 26 h at a constantly feeding rate of 1 ml/min. IPTG was added to a final concentration of 0.2 mM as soon as the OD_{600} value reached 22.5. In the C_5-Epi fed-batch experiment, the culture was also constantly fed after 5 h with a feeding rate of 3 ml/min until 15 h and then from 19 h to 25.5 h at a rate of 1.5 ml/min. C_5-Epi fed-batch experiment was induced at an OD_{600} value of 22.4 at final concentrations of 0.2 mM IPTG and 1 mg/ml arabinose.

For the 6-OST-3 fermentations, after 4–10 h of batch phase, the culture was fed with a concentrated solution (435 mM glycerol, 150 g/l yeast extract, and 48.7 mM $MgSO_4 \cdot 7H_2O$). In a first fed-batch experiment (FB A), the culture was fed after 6 h at a constant feeding rate of 1 ml/min. IPTG was added to a final concentration of 1 mM as soon as the OD_{600} value reached about 7.5. In the second fed-batch experiment (FB B), the culture was constantly fed after 10 h with a feeding rate of 3 ml min^{-1} over the first 4 h and then at 1.7 ml/min until the end of fermentation. FB B was induced at an OD_{600} value of 9.5. In a third fed-batch experiment (FB C), the culture was fed after 4 h at a constant feeding rate of 1.8

ml/min over the first 8 h and then at a constant feeding rate of 1.0 ml/min until 22 h into the fermentation. FB C was induced at an OD_{600} value of 3.5.

Bacterial growth was monitored at different time points by measuring the optical density at 600 nm (OD600) with a UVmini-1240 spectrophotometer (Shimadzu, Japan). The culture was diluted to the linear range. The cell pellet was collected by centrifugation at 3501 × *g* for 20 min at 4°C and frozen.

2.5.4. Biomass extraction and enzyme purification

The pellet (20 g) was suspended in 100 ml of ice-cold loading buffer A (25 mM Tris-HCl, pH 7.4, containing 500 mM NaCl) by vortexing, and cells were lysed on ice using a Q700 sonicator (Qsonica, Newtown, CT, USA) at power level 4.5 for 1 min (30 strokes, 1s on and 1s off). Sonication of the re-suspended cells was performed 3-times according to the program, taking 30 s breaks between each cycle. Cell debris was spun down at 20 000 × *g* at 4°C for 30 min, and the supernatant was filtered through a 0.22 µm filter by using vacuum system into 50 ml tube cooled in an ice bath. The sample containing the expressed enzyme was maintained on ice briefly prior to fast performance liquid chromatography (FPLC) purification.

The FPLC system was manually washed, without an attached column, for 5 min at a flow rate 5 ml/min with eluting buffer B (25 mM Tris-HCl, pH 7.5, containing 500 mM NaCl and 40 mM maltose monohydrate) and then washed for 5 min at flow rate 5 ml/min with loading buffer A. The amylose column was connected to the FPLC system and washed with buffer A for at least 3 column volumes. The sample was then loaded onto the column at a reduced flow rate of 1 ml/min, and washed with buffer A for 10-15 min at a flow rate 2 ml/min. The enzyme was eluted with buffer B at a flow rate 2 ml/min for 5 min by manual operation. Purified enzyme was collected on a fraction collector with UV_{280} detection and fractions containing the 6-OST peak were pooled together in a 50 ml tube. Glycerol 10 vol% was added to the enzyme before it was stored at -80°C.

2.5.5. Protein concentration and SDS-PAGE

Protein concentration was determined with Nanodrop 3300 (Thermo Fisher Scientific Inc., Wilmington, DE, USA). SDS-PAGE protein analysis was performed in a Mini-Protean Tetra system (BIORAD, Hercules, CA, USA), by loading 30 µl of 1:1 (v:v) boiled protein solution and dye buffer on a 4–20% precast gel (Mini protean TGX gels, BIORAD) and running in a Tris, glycine and SDS buffer (10x Tris/glycine/SDS buffer, BIORAD) at 100 V for 45 min. A 250 kDa to 10 kDa protein standard (Precision Plus Protein Kaleidoscope, BIORAD) was used as ladder. Gels were washed with tap water for 30 min and then stained by soaking for 5 h in Coomassie blue solution (Gel Code Blue Safe Protein Stain, Thermo Fisher Scientific).

2.5.6. Activity assay

The 2-OST activity assay was performed as previously described with some modification[120,127,128]. The activity was analyzed by incubating 50 µg of purified 2-OST with 25 µg of *N*-sulfoheparosan, 25 µg of AST-IV, 0.5 µM *para*-nitrophenylsulfate (PNPS) and 2 µg 3'-phosphoadenosine-5'-phosphosulfate (PAPS) in 250 µl system with supplement of 50 mM MES buffer pH 7.0. 10 mM $MnCl_2$, 5 mM $MgCl_2$, and 1% Triton X-100 (pH 7). For assaying the activity of C_5-Epi, in addition to 50 µg purified C_5-Epi, 50 µg purified 2-OST was also added to the assay system mentioned above[121].

The 6-OST activity assay was performed as previously described with some modification[100]. The activity was analyzed by incubating 50 µg (0.6 nmoles) of purified 6-OST-3 with 25 µg (~25 nmoles) of *N*-sulfo-heparosan decasaccharide, 25 µg (0.7 nmoles) of aryl-sulfotransferase, 0.5 µM *para*-nitrophenylsulfate (PNPS) and 4 nmoles of 3'-phosphoadenosine-5'-phosphosulfate (PAPS) in 250 µl system with supplement of 50 mM MES buffer pH 7.0.

The assays were conducted in transparent, 96-well plates purchased from Greiner Bio-One (Monroe, NC, USA). The plates were incubated at 37°C in SpectraMax plate reader (Molecular Devices, Sunnyvale, CA, USA). A kinetic model was used to measure the absorbance at 400 nm/min over 1 h. The enzyme activity was calculated using the following equation:

$$\text{Specific activity} = \frac{\text{Abs}_{t2}\text{-Abs}_{t1}}{\varepsilon_0} * \frac{1}{\text{RT}} * \frac{1}{1000} * 1 * \frac{1}{[\text{Enz}]_{1/10}} * 1000 \quad (2.1)$$

Abs_{t2} and Abs_{t1} are the absorbance at 400 nm at t_2 min and t_1 min, respectively. The time range was chosen between a linear segment of the plot. ε_0 is the extinction coefficient (10.5×10^{-3}), RT is the reaction time (min), $[\text{Enz}]_{1/10}$ is the concentration of the assayed enzyme divided by ten. One unit of the activity equals to per mg enzyme produce 1 nmol PNP/min.

2.5.7. Disaccharide mass analysis

The disaccharide analysis was carried out as reported previously[128]. Heparin lyases 1, 2, and 3 (10 mU each) in 5 µl of 25 mM Tris, 500 mM NaCl, 300 mM imidazole buffer (pH 7.4) were added to 10 µg of 2-OST, C_5-Epi, or 6-OST-3 treated sample in 100 µl of distilled water and incubated at 35 °C for 10 h to degrade the hydrolyzed sample completely. The products were recovered by centrifugal filtration using an YM-10 micro-concentrator, and the disaccharides were recovered in the flow-through and freeze-dried. The digested disaccharides were dissolved in water to concentration of 50-100 ng/2 µl for liquid chromatography (LC)-mass spectrometric (MS) analysis.

LC-MS analyses were performed on an Agilent 1200 LC/MSD instrument (Agilent Technologies, Inc. Wilmington, DE) equipped with a 6300 ion trap and a binary pump followed by a UV detector equipped with a high-pressure cell. The column used was a Poroshell 120 C18 column (2.1 × 100 mm, 2.7 µm, Agilent, USA). Eluent A was water/acetonitrile (85:15) v/v, and eluent B was water/acetonitrile (35:65) v/v. Both eluents contained 12 mM tributylamine (TrBA) and 38 mM ammonium acetate with pH adjusted to 6.5 with acetic acid. The gradient of solution A for 5 min followed by a linear gradient from 5 to 15 min (0-40% solution B) was used at flow rate of 150 µl/min.

3. CHEMOENZYMATIC SYNTHESIS OF HEPARIN AND HEPARAN SULFATES

3.1. Introduction

Of all the classes of GAGs, the heparan sulfate (HS) and heparin family of GAGs are the most attractive therapeutic targets[127] as they are known to regulate a wide range of physiological processes[131-133] through their interactions with biologically important proteins, such as growth factors[21,134]. However, even with recent advances in synthetic carbohydrate chemistry,[72] the preparation of HS and heparin oligosaccharides remains a major challenge due to their structural complexity and heterogeneity. Therefore, chemoenzymatic approaches, relying on biosynthetic enzymes for the synthesis of highly sulfated GAG oligosaccharides, represent powerful and efficient alternatives to traditional methods[103,135,136]. This chapter will detail two studies of chemoenzymatic synthesis of heparin and heparan sulfates; the fluorous assisted synthesis of heparan sulfate oligosaccharides[137], and a one-pot combinatorial synthesis of heparin[117].

Fluorous chemistry emerged as a new tool for solution-phase high-throughput organic synthesis in the late 1990s[138]. Fluorous separation techniques rely on the high affinity of perfluoroalkyl chains toward fluorous surfaces and solvents. Fluorous tag- facilitated chemical synthesis has been developed extensively by Curran[139] over the past decade and applied to proteomics[140], peptide synthesis[141], and carbohydrate microarrays[142]. In contrast to the streptavidin−biotin system, fluorous tags bind to a fluorous surface through fluorous solid-phase extraction (FSPE) and can be easily released through fluorophilic elution. Reversible binding, ease of purification, broad reaction scope, and an ability to be automated all make fluorous tagging especially suitable for high-throughput combinatorial synthesis[143]. In recent years, fluorous techniques have been applied to oligosaccharide synthesis and

---

Portions of this chapter previously appeared as: Cai, C., *et al*. Fluorous-assisted chemoenzymatic synthesis of heparan sulfate oligosaccharides. *Org. Lett.* **16,** 2240–3 (2014)., and Bhaskar, U., *et al*. Combinatorial one-pot chemoenzymatic synthesis of heparin. *Carbohydr. Polym.* **122,** 399–407 (2014).

have significantly facilitated purification. In their automated solid-phase oligosaccharide synthesis, Seeberger and co-workers used a TIPS-like fluorous linker to “cap” unreacted sugar residues and to remove unwanted deletion sequences from the glycosylation mixture[144]. Huang and co-workers reported a similar strategy, where the fluorous “cap” is applied to the product, and used to synthesize linear and branched oligosaccharides in a one-pot manner[145]. Pohl and co-workers attached a fluorous linker at the reducing end of a mannoside to prepare linear and branched mannose oligosaccharides[146]. Boons and co-workers reported a modular synthesis of heparan sulfate tetrasaccharide with a fluorous tagged aminopentyl linker at the reducing end of glucosamine substrates[147]. Although recent advances in chemoenzymatic synthesis of heparan sulfate oligosaccharides have included one-pot synthesis and the synthesis at the hundreds of milligram scale, development of more efficient and less time-consuming methodology is still necessary to speed up the purification process. The application of fluorous techniques in enzymatic reactions is still not well developed. In the first study, we report a fluorous-assisted chemoenzymatic synthesis of heparan sulfate oligosaccharides from a chemically synthesized disaccharide acceptor, with a fluorous Boc (FBoc)[19] on the glucosamine nitrogen at the reducing end. Liu and co-workers synthesized a similar heparan sulfate oligosaccharide with a fluorous linker but with an unnatural anhydromannitol residue at the reducing end[78]. The newly designed disaccharide acceptor in this study has an α-configured *O*-methyl glycoside at the reducing end, which can serve as a potential starting point for chemo- enzymatic synthesis of the heparin pentasaccharide anticoagulant drug Arixtra (fondaparinux).

Heparin, the first biopolymeric drug, possesses a wide range of structural heterogeneity owing to its biosynthesis[61]. Heparin’s diverse fine structure is further complicated by an animal-sourced, tissue-based recovery, leading to considerable structural differences within commercial heparin active pharmaceutical ingredients (APIs)[148]. Serious concerns about control of livestock, the primary source of heparin, have been raised since the 1990s following a series of incidents involving bovine spongiform

encephalopathy, viral infections and prion contamination[149]. A lack of quality control during initial recovery stages led to adulteration of the pharmaceutical heparin supply with over- sulfated chondroitin sulfate (OSCS), resulting in an international crisis in 2008 associated with over 100 deaths reported in the US alone[53,62]. The inherent problems with animal tissue-based heparin production have motivated us to develop a commercially feasible chemoenzymatic heparin preparation process[107]. This is based on bacterial fermentation of *Escherichia coli* K5 to generate a capsular polysaccharide heparin precursor, which is then chemically *N*-deacetylated and *N*-sulfonated[108,150]. The *N*-sulfated product is then sequentially treated with recombinant enzymes (derived from the heparin biosynthetic pathway and expressed in *E. coli*) to epimerize uronic acid residues and sulfate C2, C3 and C6 positions[108,150]. Each enzymatic reaction step utilizes a cofactor regeneration system to regenerate the critical sulfo-donor PAPS[97]. First, C_5-epimerase (C_5-Epi) converts uronic acid to iduronic acid, and 2-*O*-sulfotransferase (2-OST) sulfates the C2 position[104,107,151]. This is followed by sulfation at the C6 position by two isoforms of 6-*O*-sulfotransferase (6-OST-1 & -3), which produces a non-anticoagulant heparin structure[100,107,119]. 3-*O*-sulfotransferase-1 (3-OST-1) then sulfates the C3 position, to generate anticoagulant heparin[107,152]. A similar sequential approach led to another version of bioengineered heparin derived from partially *N*-deacteylated/*N*-sulfonated heparosan as substrate[108]. This chemoenzymatic approach has also been employed to generate an analogue of ultra-low molecular weight heparin (ULMWH), Arixtra[103]. The total synthesis of full length heparin polysaccharides is considered infeasible owing to large number of modest yield steps and side product formation[61,73]. One-pot chemical synthesis in organic chemistry is frequently employed for simplified synthesis of glycoconjugates and sugar building blocks. One-pot chemical synthesis of heparin oligosaccharides from sugar building blocks with low to moderate overall yield has been previously described[118,153]. This one step synthesis enables high speed processing of analogues with increased overall process yield. Combinatorial one-pot synthesis can potentially be used toward preparation of heparin mimetic microarrays for deciphering the effect of structural

heterogeneity on structure activity relationship (SAR) and heparin–protein interactions[21,118,154]. As an alternative to the sequential process design, we developed a one-pot chemoenzymatic synthesis of heparin from *N*-sulfo heparosan leading to generation of biologically active bioengineered heparin products.

This chapter will present the results of two studies on chemoenzymatic synthesis of HS/HP targets, a fluorous-assisted chemoenzymatic synthesis of HS oligosaccharides[137], and the one-pot chemoenzymatic synthesis of heparin[117].

3.2. Results

3.2.1. Synthesis of a fluorous-tagged disaccharide acceptor

Our retrosynthetic analysis of the heparan sulfate oligosaccharides (**3.1** and **3.2**) with fluorous-assisted methodology is shown in Figure 3.1. These would be prepared from the fluorous acceptor **3.3** through a repetition of enzymatic backbone elongation followed by *N*-sulfation, 6-*O*-sulfation, and deprotection of the FBoc tag. Fluorous disaccharide **3.3** would be chemically synthesized through introduction of the FBoc tag to the free amino group on the reducing end of disaccharide **3.4**, which would be obtained through a chemical glycosylation of acceptor **3.7** with donor **3.6** and global deprotection and hydrogenation of the fully protected disaccharide **3.5**. The synthesis of donor **3.6** and acceptor **7** followed a conventional synthetic route described in the Supporting Information (Schemes SI1 and SI2). As shown in Figure 3.2., the glycosylation of **3.6** with **3.7** afforded disaccharide **3.8** in moderate yield. With the fully protected disaccharide in hand, the TBDPS group was removed initially by treatment with HF· Py21 to afford disaccharide **3.9**. The unprotected C6-hydroxyl group was then oxidized to a carboxylic acid using TEMPO- BAIB22 to afford **3.5**. The Bz groups were removed by strong base treatment followed by hydrogenation for 3 d using Pd/C as the catalyst. All deprotection steps proceeded smoothly to give the disaccharide **3.4** in high yields (Fig 3.2).

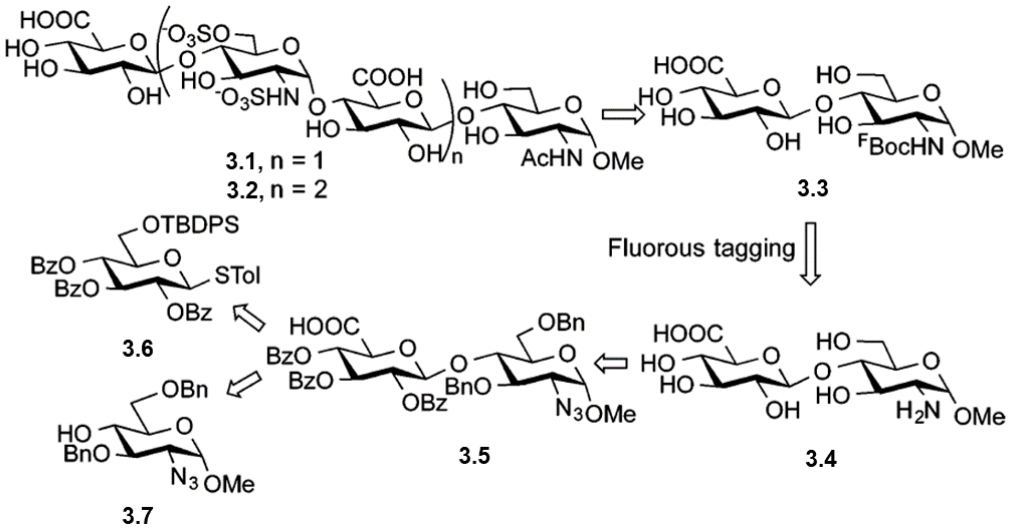

Figure 3.1. Retrosynthetic analysis of heparan sulfate tetrasaccharide (3.1) and hexasaccharide (3.2).

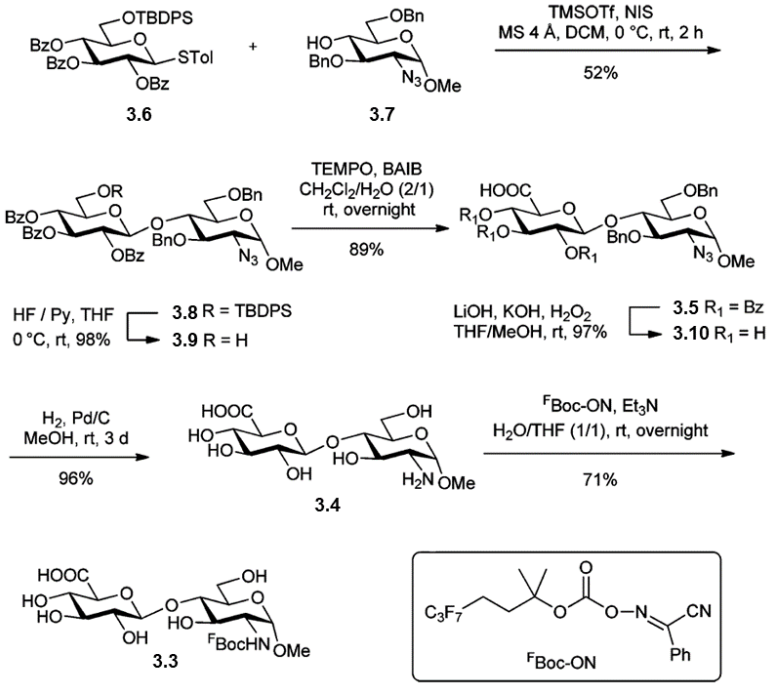

Figure 3.2. Synthesis scheme for fluorous tagged disaccharide 3.3.

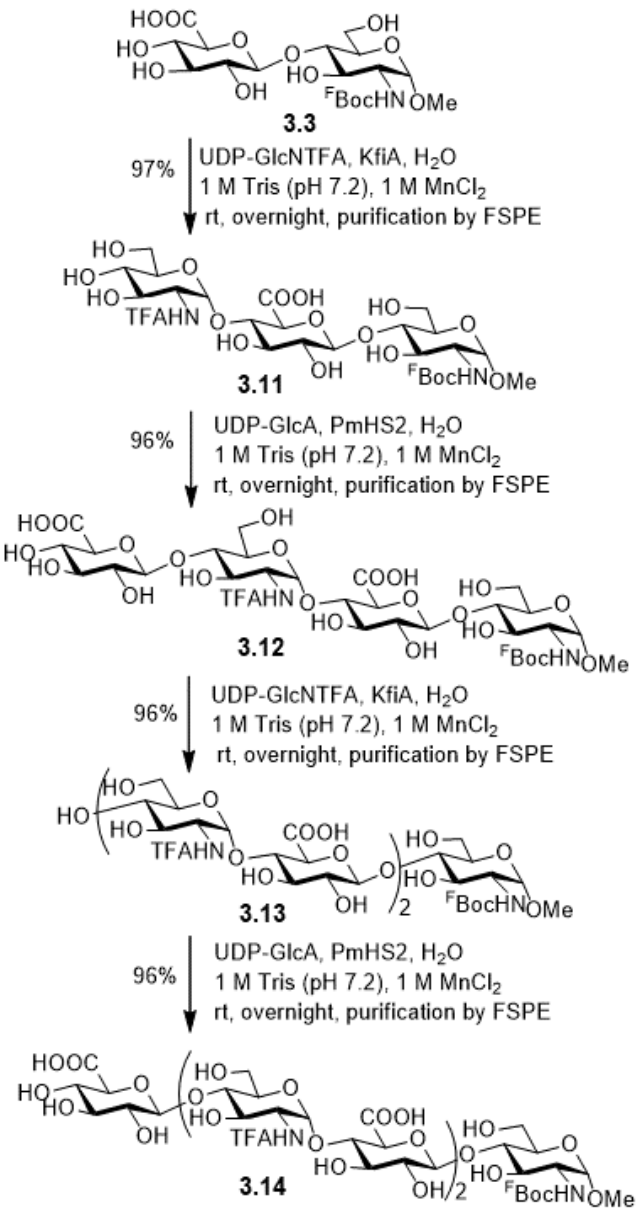

Figure 3.3. Enzymatic elongation of the disaccharide heparosan analog.

3.2.2. Enzymatic backbone elongation and sulfation

Fluorous-tagged disaccharide acceptor **3.3** was next elongated with *Escherichia coli* glycosyltransferase KfiA and uracil diphosphate-*N*-trifluoroacetylglucosamine (UDP-GlcNTFA) to construct trisaccharide **3.11** (figure 3.3). After flash elution through FSPE with water and methanol, respectively, the pure trisaccharide **3.11** was collected in methanol and identified by LC−MS and NMR

spectroscopy. One cycle of fluorous-assisted purification generally takes < 0.5 h and affords a relatively pure product. The GlcNTFA residue is an unnatural analogue of GlcNAc and should allow the selective introduction of *N*-sulfo groups in the future synthesis of HS oligosaccharides. Following the same protocol as above, *Pasteurella multocida* heparan synthase (PmHS2) and uracil diphosphate−glucuronic acid (UDP−GlcA) were employed to construct the tetrasaccharide (**3.12**). These steps were repeated one more time to afford the pentasaccharide (**3.13**) and hexasaccharide (**3.14**) with the GlcA−GlcNTFA repeating unit. With the HS backbone constructed and in hand, we subsequently sulfated these substrates to check their performance with FSPE separation. Base-catalyzed ($MeOH/NEt_3/H_2O$, 2/1/2) deprotection of the trifluoroacetamide group was followed by the chemical *N*-sulfation with $SO3{\cdot}MeN_3$ and Na_2CO_3 to form *N*-sulfated tetrasaccharide (**3.15**) (Figure 3.4). A high-field shift of 0.5 ppm for H-2 was observed in the ^1H and 2D correlation spectroscopy (COSY) NMR (^2H_2O, 600 MHz) in the glucosamine residue that had been *N*-sulfated (data not shown). The heparan sulfate 6-*O*-sulfotransferase isoforms -1 and -3 (6-OST-1 and 6-OST-3) were incubated together with **3.15** and PAPS to obtain the 6-*O*-sulfo group containing tetrasaccharide **3.17**, and excess PAPS and buffer salts were easily removed by fluorous solid phase extraction (FSPE). ^1H NMR (^2H_2O, 600 MHz) showed that the peaks at 3.67 and 3.78 ppm, corresponding to the protons on the C6 of the internal glucosamine residue in **3.15**, shifted to 4.09 and 4.37 ppm in the product **3.17**. 2D COSY and heteronuclear multiple-quantum correlation (HMQC) NMR spectroscopy also confirmed the formation of **3.17** (data not shown). The glucosamine residue at the reducing end of **3.15** was not 6-*O*-sulfated, suggesting that additional studies are required to more fully understand the specificity of the 6-*O*-sulfotransferases. Subsequently, hexasaccharide **3.18** was obtained using the same protocol, including *N*-sulfation, 6-*O*-sulfation, and FSPE steps. We found that some product was retained on the FSPE column after four sulfate groups had been added on the HS chain, but it could be easily released by employing trifluoroethanol as a cosolvent. Deprotection of FBoc was initially attempted, based on a literature method, **3.19** using either

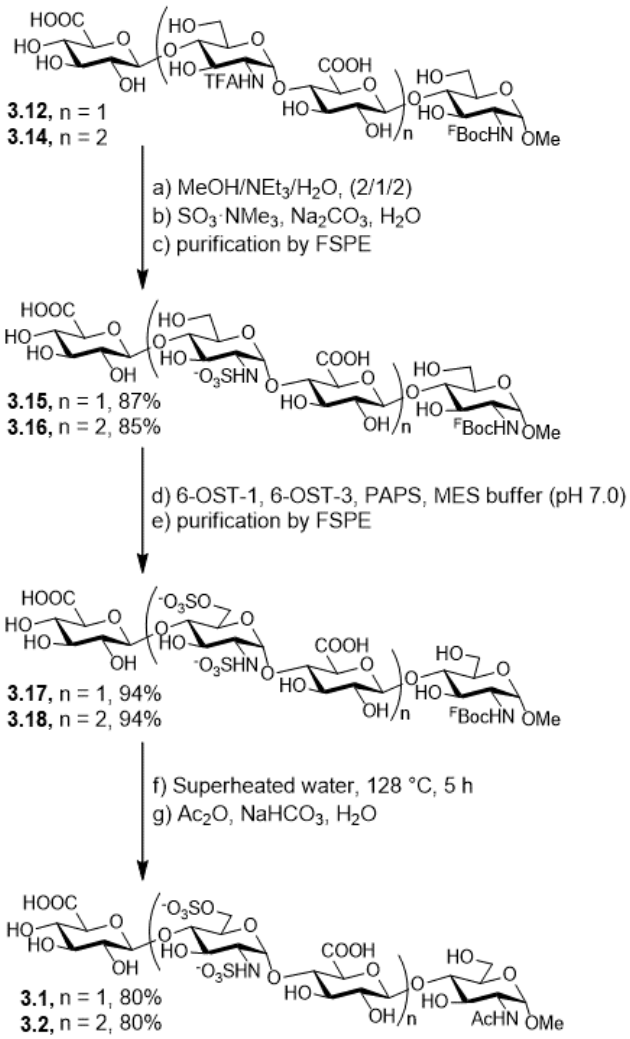

Figure 3.4. Enzymatic sulfation and deprotection of the heparan sulfate oligosaccharides.

50% aqueous TFA at room temperature or 3 N aqueous HCl at 60 °C for 2 h. We observed that while 3 N HCl removed the fluorous tag from tetrasaccharide (**3.17**), it also resulted in complete sulfate loss. Treatment of the model substrate **3.3** with 50% aqueous TFA only afforded a 10% yield even for 24 h. Finally, superheated water (liquid water between 100 and 374 °C), a green solvent, was successfully employed to remove FBoc tag from substrates **3.17** and **3.18**, and the HS tetrasaccharide (**3.1**) and hexasaccharide (**3.2**) were obtained after N-acetylation.

3.2.3. Effect of C_5-Epi and 2OST on non-anticoagulant heparin composition in one pot synthesis

On treatment with a mixture of heparin lyase 1, 2, and 3, heparin is degraded into unsaturated disaccharides along with a small quantity of lyase resistant 3-*O*-sulfo group-containing tetrasaccharide, associated with the AT binding site. The trisulfated (TriS) disaccharide comprising of IdoA2S and GlcNS6S is the major disaccharide sequence (66–85%) in porcine heparins[107]. The microheterogeneity of the saccharides in bioengineered heparin is critical for chemical and biological equivalence to porcine heparin and the TriS disaccharide content equivalence is an important prerequisite for the regulatory approval of any generic product. Our chemoenzymatic process begins with partial chemical *N*-deacetylation/*N*-sulfonation of heparosan, as an alternative to enzymatic modification by the *N*-deacetylase/*N*-sulfotransferase (NDST) family of enzymes in vivo. C_5-Epi catalyzes the isomerization of GlcA residue to an IdoA residue in NSH flanked by GlcNS or GlcN. The reversible biphasic catalytic mechanism of C_5-Epi adds further complexity[104]. Addition of a sulfo group derived from PAPS at the C2 position of IdoA by 2-OST renders the isomerization irreversible and drives the overall equilibrium toward an IdoA rich 2-*O*-sulfo group-containing product. The wide variation in potential substrates with regards to sulfation levels (0–3 sulfo groups/disaccharide) and polymer chain lengths, coupled with lack of reliable real time assays, further complicate our understanding of this C5-epimerization/2-*O*-sulfotransferase step. Often, additional enzymatic modifications are required to achieve a high level of 2-*O*-sulfo groups and a high content of IdoA, comparable to that observed in porcine heparin[113]. Based on these considerations, we focused on combinatorial modulation of C_5-Epi/2-OST activity while maintaining the other required biosynthetic enzymes (except 3-OST-1) at control levels. The control reaction (1) was designed with a 1:1 enzyme to substrate (E:S) ratio by mass, similar to previous work[107,108]. The C_5-Epi and 2OST E:S ratio was increased by either 2-fold or 10-fold, individually and together, with respect to the control. The disaccharide composition (mass percentages) of the digested products, as determined by LC–MS quantification, are presented in Table 3.1. Reaction 1 contained a

Table 3.1. Effect of C_5-Epi and 2OST on disaccharide composition of heparin products generated using combinatorial one-pot enzymatic preparation. The numbers depict mass percentage of each disaccharide in the digested product. (OS=ΔUA-GlcNAc, NS= ΔUA-GlcNS, 6S= ΔUA-GlcNAc6S, 2S= ΔUA2S-GlcNAc, NS6S= ΔUA-GlcNS6S, NS2S= ΔUA2S-GlcNS, 2S6S= ΔUA2S-GlcNAc6S, Tris= ΔUA2S-GlcNS6S). ΔUA corresponds to 4-deoxy-α-L-threo-hex-4-eno-pyranosyluronic acid.

Sample (ID)	OS (%)	NS (%)	6S (%)	2S (%)	NS6S (%)	NS2S (%)	2S6S (%)	TriS (%)
Control (1)	12.9±1.2	9.7±0.3	0.0±0.0	0.3±0.0	17.5±0.4	24.6±0.5	0.0±0.0	35.1±1.6
2-fold C5 (2)	13.7±0.9	9.5±0.6	0.0±0.0	0.1±0.2	14.0±3.1	31.9±1.8	0.8±1.2	29.9±0.0
10-fold C5 (3)	11.9±3.0	5.7±0.2	0.0±0.0	0.3±0.4	17.3±0.7	24.2±0.4	0.0±0.0	40.5±2.0
2-fold 2OST (4)	10.5±2.0	5.0±1.1	0.0±0.0	0.8±0.5	13.7±1.4	29.9±1.8	0.0±0.0	40.9±0.1
10-fold 2OST (5)	5.4±0.8	1.7±0.2	0.0±0.0	0.0±0.0	11.1±2.7	22.1±1.2	0.0±0.0	58.9±3.8
2- fold C5 & 2OST (6)	10.7±1.4	5.7±0.2	0.0±0.0	0.8±0.1	10.1±0.1	35.1±1.1	0.0±0.0	38.4±2.6
10-fold C5 & 2OST (7)	6.1±1.2	1.6±0.6	0.0±0.0	0.0±0.0	7.8±0.7	15.7±0.9	0.0±0.0	67.9±2.1

moderate level of TriS disaccharide (~35.1%) with significant formation of NS2S (~24.6%) and NS6S (~17.5%) disaccharides. Variation of C_5-Epi alone (Reactions 2 and 3) had relatively little impact on the overall structure and resulted in similar composition of TriS, NS2S and NS6S. However, a similar variation in 2-OST had a profound effect on the resulting disaccharide composition. Use of a 10-fold higher E:S ratio for 2-OST alone (Reaction 5) led to the formation of a product with high TriS disaccharide content (~58.9%). Use of 10- fold higher E:S ratio for C_5-Epi and 2OST (Reaction 7) led to further improved TriS content (~67.9%) with significant NS2S (~15.7%) and NS6S (~7.8%) disaccharide formation. The low NS content (~1.6%) of Reaction 7 signifies near complete conversion of available substrate sites into NS2S, NS6S and TriS disaccharides in one single step. Use of excess 2-OST, in Reactions 5 and 7, led to products with similar core structure as porcine heparins. This is indicative of the action of 2-OST being the rate-limiting step and makes 2-OST an ideal target for protein engineering to improve its activity. Although better results were achieved with 10-fold higher C_5-Epi and 2-OST compared to the 10-fold higher 2-OST

alone, NMR spectroscopy is clearly required to accurately assess the role of C_5-Epi on the chemical composition of the heparin product. The formation of minor disaccharides particularly 6S, 2S and 2S6S in all combinatorial one-pot syntheses suggests the complexity introduced by substrate sites tied to the acetylated regions of the polysaccharide chains toward enzymatic action. It should be noted that the molar enzyme to substrate ratio is still highly favorable for a one-pot synthesis owing to large number of available substrate sites (~20 per chain) and high molar mass of enzymes. 10-fold higher E:S ratio of 2-OST alone or with C_5-Epi were chosen for incorporation of 3-*O*-sulfo groups to obtain heparin with anticoagulant activity.

3.2.4. Effect of 6-OST-1 & 6-OST-3 on non-anticoagulant heparin composition in one-pot synthesis

The 6-*O*-sulfotransfrase enzyme family in vivo contains three different isoforms, and sulfates the C6 position on GlcNS or GlcNAc, particularly those in GlcNS-IdoA2S domains. The three different isoforms possess similar substrate specificity and can introduce 6-*O*-sulfo groups into polysaccharide chains with various levels of *N*-sulfo and 2-*O*-sulfo group substitution, however, the 6-OST- 1 prefers the absence of 2-*O*-sulfo group[61,99]. The iterative bioengineered heparin chemoenzymatic process developed in our laboratory[108] utilizes 6-OST- 1 & 3 isoforms. Thus, in the combinatorial experiments, the E:S mass ratio for 6-OST-1 & -3 was varied 2-fold and 10-fold, alone or in combination, with respect to the control. The resulting product disaccharide compositions are presented in Table 3.2. A 2-fold increase in E:S ratio for 6-OST-1 (Reaction 8) or 6-OST-3 (Reaction 10) resulted in an increase in the formation of TriS disaccharide content. In contrast, a 10-fold increase of 6-OST-1 (Reaction 9) or 6-OST-3 (Reaction 11) E:S ratio led to a decrease in TriS content. The impact of altered 6-OST-1 E:S ratio was more evident on the minor disaccharide composition and can be explained by the relative rates of *O*-sulfation and substrate specificity. The total 6-OST, sum of 6-OST-1 & -3 masses, in reaction mixtures 8 and 10 is 1.5-fold higher than Reaction 1, without any change in the amount of 2-OST. With the C_5-Epi/2-OST composition unchanged and comparable to 6-OSTs, the rate of 2-O-sulfonation is similar to 6-O-

Table 3.2. Effect of 6-O-Sulftransferase-1 & 3 on disaccharide composition of heparin products generated using combinatorial one-pot enzymatic preparation. The numbers depict mass percentage of each disaccharide in the digested product. (0S=ΔUA-GlcNAc, NS= ΔUA-GlcNS, 6S= ΔUA-GlcNAc6S, 2S= ΔUA2S-GlcNAc, NS6S= ΔUA-GlcNS6S, NS2S= ΔUA2S-GlcNS, 2S6S= ΔUA2S-GlcNAc6S, Tris= ΔUA2S-GlcNS6S). ΔUA corresponds to 4-deoxy-α-L-*threo*-hex-4-eno-pyranosyluronic acid.

Sample (ID)	OS (%)	NS (%)	6S (%)	2S (%)	NS6S (%)	NS2S (%)	2S6S (%)	TriS (%)
Control (1)	12.9±1.2	9.7±0.3	0.0±0.0	0.3±0.0	17.5±0.4	24.6±0.5	0.0±0.0	35.1±1.6
2-fold 6OST1 (8)	9.9±1.3	5.1±09	0.0±0.0	0.0±0.0	24.6±0.8	13.7±0.9	0.0±0.0	46.7±2.1
10-fold 6OST1 (9)	5.3±0.0	2.1±0.7	0.2±0.0	0.0±0.0	64.9±0.7	2.6±0.2	0.0±0.0	24.9±0.2
2-fold 6OST3 (10)	9.5±3.5	5.4±0.2	0.0±0.0	0.0±0.0	27.8±0.9	11.4±0.7	0.0±0.0	46.0±2.7
10-fold 6OST3 (11)	3.9±0.5	0.6±0.9	0.2±0.0	0.0±0.0	84.0±0.6	0.5±0.8	0.0±0.0	10.7±1.6
2-fold 6OST1&3 (12)	8.5±0.5	3.7±0.8	0.0±0.0	0.0±0.0	38.5±1.0	10.6±0.3	0.0±0.0	38.8±0.5
10-fold 6OST1&3 (13)	3.2±1.2	0.0±0.0	0.2±0.0	0.0±0.0	89.6±1.0	0.0±0.0	0.0±0.0	7.1±0.2

sulfation and results in products qualitatively similar to Reaction 1. The percentage of 2-*O*-sulfation, the sum of NS2S and TriS, remains the same in Reactions 8 and 10, while a small increase in TriS and NS6S content indicates greater extent of 6-O-sulfation with respect to Reaction 1. Both Reactions 9 and 11 have 5.5-times higher amounts of 6-OSTs, compared to Reaction 1, and display remarkably different disaccharide compositions. The NS6S disaccharide was the most abundant disaccharide (>64%) while TriS disaccharide was lower than Reaction 1. Enhanced 6-*O*-sulfation rapidly catalyzes the formation NS6S in place of the desired TriS, as the formation of latter is limited by NS2S generation from its relatively slower 2-*O*-sulfation. The NS6S disaccharide, thus formed, may be an unsuitable substrate for C_5-Epi/2-OST, blocking the generation of TriS disaccharide. The disaccharide composition follows similar trend for Reactions 12 and 13 wherein both 6-OST-1 & -3 are simultaneously varied by either 2-fold or 10-fold. In Reaction 12, with 2-fold higher 6-OST-1 & -3, a composition similar to Reactions 8 and 10 is observed, while use of 10-fold higher 6-OST-1 & -3 leads to NS6S as the most abundant disaccharide in Reaction 13. The blocking of potential epimerization/2-*O*-sulfonation sites due to enhanced 6-*O*-

sulfonation rate is evident, as negligible proportion (~ 7.1%) of 2-*O*-sulfo groups is present in Reaction 13. The use of higher E:S ratio of 6-OSTs failed to achieve products structurally similar to porcine heparins and resulted in a low TriS content. These results support the presumed order of sulfation in the heparin/HS biosynthesis as followed in our iterative process and suggest epimerization/2-*O*-sulfation takes place prior to 6-*O*-sulfation.

3.2.5. Effect of enhanced cofactor recycling on non-anticoagulant heparin composition in one-pot synthesis

The consumption of PAPS, a critical sulfo group donor, by sulfotransferases leads to generation of 3'-adenosine 5'-phosphate (PAP). AST-IV reversibly catalyzes the transfer of a sulfo group from PNPS to PAP and converts it into PAPS, thereby establishing an efficient in vitro cofactor recycling system[97]. This cofactor recycling system is essential to overcome the prohibitively high cost of commercially available PAPS for improved process economics and allows for use of catalytic amount of PAPS. The results for a two level combinatorial variation of AST IV E:S mass ratio are presented in Table 3.3. Use of 10-fold higher AST IV (Reaction 15) showed an elevated TriS disaccharide content compared to 2-fold higher AST IV (Reaction 14) and Reaction 1. These results are in agreement with the observed rapid

Table 3.3. Disaccharide composition of heparin products generated using enhanced PAPS regeneration. The numbers depict mass percentage of each disaccharide in the digested product. (OS=ΔUA-GlcNAc, NS= ΔUA-GlcNS, 6S= ΔUA-GlcNAc6S, 2S= ΔUA2S-GlcNAc, NS6S= ΔUA-GlcNS6S, NS2S= ΔUA2S-GlcNS, 2S6S= ΔUA2S-GlcNAc6S, Tris= ΔUA2S-GlcNS6S). ΔUA corresponds to 4-deoxy-α-L-*threo*-hex-4-eno-pyranosyluronic acid.

Sample (ID)	OS (%)	NS (%)	6S (%)	2S (%)	NS6S (%)	NS2S (%)	2S6S (%)	TriS (%)
Control (1)	12.9±1.2	9.7±0.3	0.0±0.0	0.3±0.0	17.5±0.4	24.6±0.5	0.0±0.0	35.1±1.6
2-fold AST IV (14)	14.7±1.0	7.2±0.1	0.0±0.0	0.0±0.0	18.7±1.8	23.3±1.3	0.0±0.0	36.1±0.5
10-fold AST IV (15)	14.2±0.0	4.5±0.0	0.0±0.0	0.0±0.0	26.8±1.7	9.0±0.8	0.0±0.0	45.6±2.5

kinetics of AST IV and suggest that cofactor recycling is not the rate limiting step in sulfotransferase coupled in vitro biocatalytic systems[99].

3.2.6. Disaccharide analysis of anticoagulant bioengineered heparins containing 3-*O*-sulfo groups

There are seven different isoforms of 3-OST that act either on GlcNS or GlcNS6S. The iterative bioengineered heparin process utilizes 3-OST-1 as the last enzymatic step for completion of the pentasaccharide binding sequence responsible for heparin's anti-coagulant activity. The number of 3-*O*-sulfo groups required to impart anticoagulant activity is very low (occupying < 5% of the total C3-positions of GlcN residues). This makes the 3-OST step a relatively simpler enzymatic transformation than the 2-OST and 6-OST steps, which are required to act at 80–90% of the 2-*O*- and 6-*O*- positions within the polysaccharide chains. Combinatorial one-pot preparation of heparins, Reactions 5 and 7, were repeated at 2 mg scale with incorporation of 3-*O*-sulfo groups using 3-OST-1. After treatment with heparin lyases, the samples were analyzed using LC–MS. Disaccharide composition (on a weight basis) of Reactions 16 (10-fold level of 2-OST) and 17 (10-fold level of C_5-Epi/2-OST) are presented along with USP porcine heparins in Table 3.4. The TriS disaccharide, representative sequence of heparin, is present in a range from 66 to 84% by mass in heparin APIs suggesting that the manufacturing processes and/or

Table 3.4. Disaccharide composition of heparin products prepared using one-pot preparation with 3-*O*-sulfonation. The numbers depict mass percentage of each disaccharide in the digested product. (0S=ΔUA-GlcNAc, NS= ΔUA-GlcNS, 6S= ΔUA-GlcNAc6S, 2S= ΔUA2S-GlcNAc, NS6S= ΔUA-GlcNS6S, NS2S= ΔUA2S-GlcNS, 2S6S= ΔUA2S-GlcNAc6S, TriS= ΔUA2S-GlcNS6S). ΔUA corresponds to 4-deoxy-α-L-*threo*-hex-4-eno-pyranosyluronic acid.

Sample	OS (%)	NS (%)	6S (%)	2S (%)	NS6S (%)	NS2S (%)	2S6S (%)	TriS (%)
USP heparin	0.3-3.2	0.8-2.9	1.2-3.2	0.8-1.6	5.4-10.8	3.7-11.6	0.77-2.6	66.9-83.8
16 (10-fold 2OST)	1.4 ± 0.8	2.5 ± 0.8	0.0 ± 0.0	2.0 ± 0.7	6.5 ± 0.53	28.9 ± 0.6	0.0 ± 0.0	58.8 ± 1.6
17 (10-fold C5-epi/2OST)	2.7 ± 0.7	1.7 ± 0.4	0.0 ± 0.0	1.8 ± 0.3	7.9 ± 0.2	15.5 ± 0.6	0.0 ± 0.0	70.5 ± 0.7

source material have an impact on disaccharide composition. The one-pot bioengineered heparins, Reactions 16 and 17, were very similar to Reactions 5 and 7 with TriS disaccharide as their major component. Reaction 17 had a higher mass percentage (~71%) of TriS disaccharide, in comparison to Reaction 16, within observed range for porcine heparins[64]. Six out of eight disaccharides reported for porcine heparins were detected in Reactions 16 and 17, with significant abundance of NS2S and NS6S. The small percentage of NS disaccharide is indicative of near complete sulfation of available substrate sites on the polysaccharide chains. In Reaction 17, 5 out of 8 disaccharides (excluding only NS2S, 6S and 2S6S) were within the reported range observed for porcine heparin. The higher standard deviations (>20%) observed in analytical measurements for minor disaccharides (NS2S, 6S and 2S6S with mass percentages <5%) makes accurate determination of their abundance difficult. The impact of these individual minor disaccharides on biological activity is also not well understood. The similarity of disaccharide compositions obtained for Reactions 16 and 17 to the combinatorial study (Reactions 5 and 7) suggests a high degree of reproducibility, essential for robust process design.

3.2.7. HPLC–MS tetrasaccharide mapping of bioengineered anticoagulant heparins

Heparin binds to antithrombin III (AT) through a pentasaccharide sequence. The bound AT undergoes a conformational change that enhances its ability to inactivate thrombin, responsible for conversion of soluble fibrinogen into an insoluble fibrin clot, leading to observed anticoagulant activity of heparins. The representative pentasaccharide binding sequence of heparin is a collection of sequences and can vary depending upon the source[155]. When heparin is exhaustively treated with heparin lyase 2, in addition to the disaccharides formed, some lyase resistant tetrasaccharides are observed due to the presence of 3-*O*-sulfo containing glucosamine residues[155]. Their molecular ratio provides a fingerprint of the heparin from which they were derived as well as an insight into the structural diversity of the AT-binding pentasaccharide sequence within heparin. A positive correlation between the 3-*O*-sulfo containing glucosamine content to in vitro biological activity of USP porcine

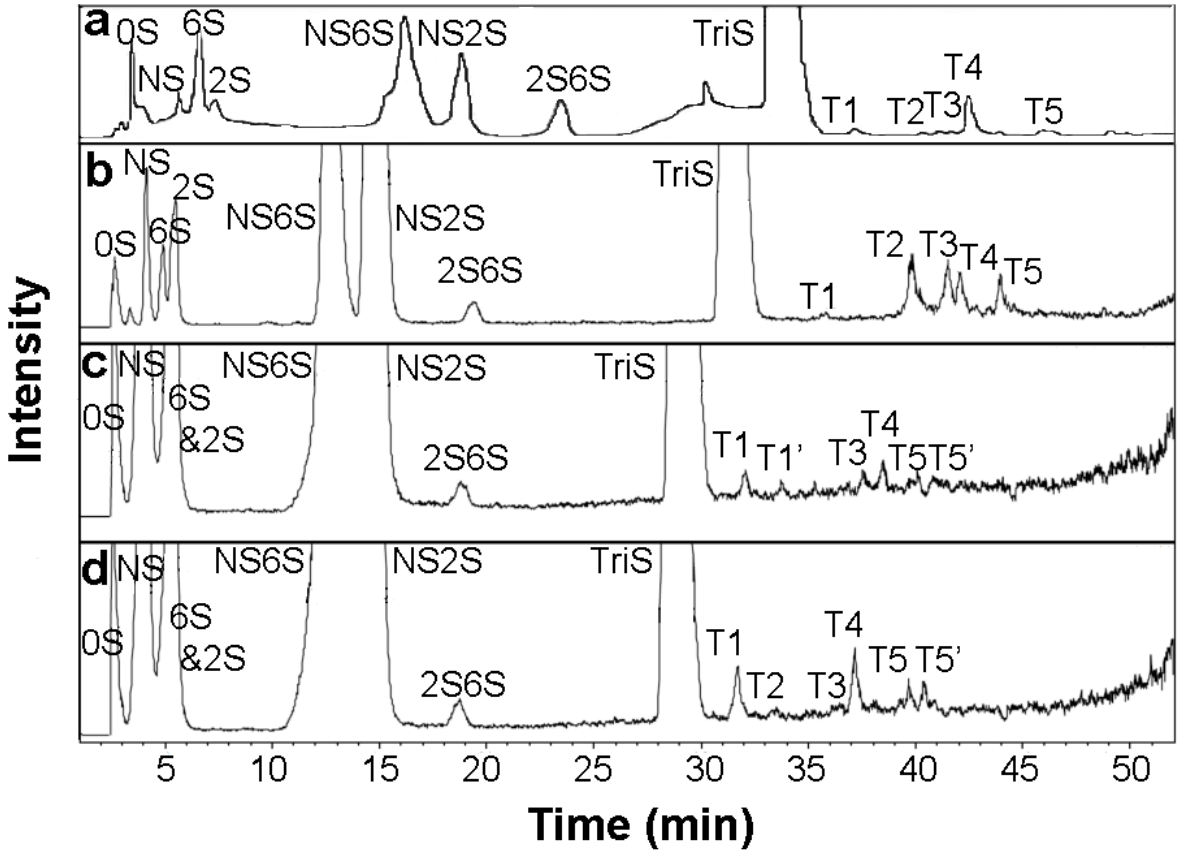

Figure 3.5. Extracted ion chromatogram (EIC) of tetrasaccharide analysis of bioengineered and natural source heparins. a. Porcine intestinal heparin T1 = 0.8 %; T2 = 0.4 %; T3 = 0.3 %; T4 = 3.0 %; T5 = 0.5 %; Total = 5.0 % (Fu et al., 2013); b. Bovine lung heparin T1 = 0.3 %; T2 = 0.3 %; T3 = 0.3 %; T4 = 3.4 %; T5 = 0.5 %; Total = 4.8 % (Fu et al., 2013); c. Bioengineered heparin 16 (T1 = 0.4 %; T1' = 0.2 %; T2 = 0.0 %; T3 = 0.4 %; T4 = 0.4 %; T5 = 0.4 %; T5' = 0.4 %; Total = 2.2 %) d. Bioengineered heparin 17 (T1 = 1.0 %; T1' = 0.2 %; T2 = 0.0 %; T3 = 0.2 %; T4 = 1.0 %; T5 = 0.4 %; T5' = 0.6 %; Total = 3.4 %). The fractions identified are T1 (m/z = $[477.4]^{2-}$, Calculated molecular mass = 956.8, Theoretical molecular mass = 956.1, Sequence = ΔUA-GlcNAc6S-GlcA-GlcNS3S), T1' having the same mass as T1, but of undetermined structure, T2 (m/z = $[496.6]^{2-}$, Calculated molecular mass = 994.4, Theoretical molecular mass = 994.0, Sequence = ΔUA-GlcNS-GlcA-GlcNS3S6S), T3 [m/z = $[496.6]^{2-}$, Calculated molecular mass = 994.4, Theoretical molecular mass = 994.0, Sequence = ΔUA-GlcNS6S-GlcA-GlcNS3S], T4 (m/z = $[517.4]^{2-}$, Calculated molecular mass= 1036.8, Theoretical molecular mass = 1036.0, Sequence = ΔUA-GlcNAc6S-GlcA-GlcNS3S6S), T5 (m/z = $[536.3]^{2-}$, Calculated molecular mass = 1074.6, Theoretical molecular mass = 1074.0, Sequence = ΔUA-GlcNS6S-GlcA-GlcNS3S6S), T5' having the same mass as T5, but of undetermined structure.

heparins has been observed[155]. We analyzed seven different USP heparins obtained from commercial sources, as described previously[156]. Five lyase resistant tetrasaccharides (**T1**, **T2**, **T3**, **T4** and **T5**) were observed in both porcine and bovine heparins. Mass spectroscopy properties and mass percentages of each individual tetrasaccharide are presented in Fig. 3.5. In porcine heparin and samples 16 and 17, **T1** (0.4–1.0%) and **T4** (0.4–3.0%) were identified as the major components with **T2** and **T5** present as minor components. Two additional lyase resistant tetrasaccharides (**T1'** and **T5'**) were identified in Reactions 16 and 17 (Fig. 3.5). The masses of **T1'** and **T5'** were identical to **T1** and **T5**, respectively, but **T1'** and **T5'** displayed different retention times from **T1** and **T5**, indicating that they have different structures. Unfortunately, their detailed sequences could not be determined owing to the small amounts of **T1'** and **T5'** formed. Presence of 3-*O*-sulfo group-containing tetrasaccharides suggests potential biological activity in Reactions 16 and 17. The total tetrasaccharide content of Reaction 17, though higher than Reaction 16, was closer to lowest tetrasaccharide content observed in porcine heparins.

3.2.8. NMR spectroscopy of bioengineered heparins

The one-pot bioengineered heparins, Reactions 16 (2.5 mg dry mass) and 17 (2.7 mg dry mass), were purified using SAX chromatography. Anticoagulant heparin consists of IdoA2S (I2S) and GlcNS3S6S (ANS3S6S). Both ^{1}H NMR and HSQC evaluation of Reactions 16 and 17 gave clear views of the 3S and I2S peaks in anomeric regions. All the anomeric peaks of I2S, A3S and ANS were visible in ^{1}H NMR and HSQC spectra of Reactions 16 and 17 (spectra not shown for Reaction 16) (Fig. 3.6). None of the product impurities coming from pharmaceutical heparins produced from animal tissues, such as xylose (Xyl), galactosamine (Gal) and the GlcA–Gal repeating units were observed in the HSQC spectra. A high level of IdoA and sulfation was detected in both Reactions 16 and 17. All the other peaks in sugar region were identified in the 1H NMR and HSQC studies. Additionally, peaks of critical features in the IdoA residues and GlcN residues, including *N*-sulfo, *N*-acetyl, 2-*O*-sulfo and 3-*O*-sulfo could be fully assigned by 1H NMR and HSQC spectra (Fig. 3.6). The percent substitution (on a molar basis), calculated using peak

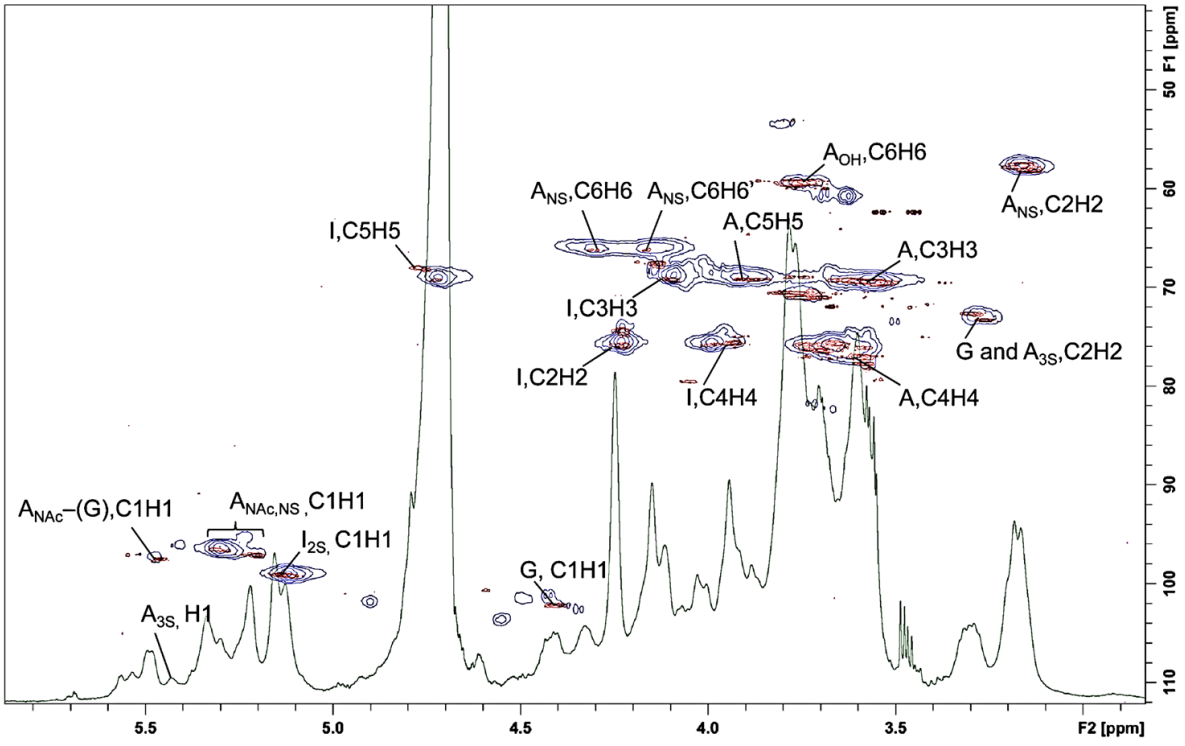

Figure 3.6. Two-dimensional heteronuclear single quantum coherence (HSQC) spectra of porcine heparin (blue), 17 (red) and one-dimensional ^{1}H spectra of 17. (A, glucosamine; I, iduronic acid; G, glucuronic acid)

integration, of glucosamine (A), iduronic acid (I) and glucuronic acid (G) in Reaction 16 (ANS = 76.2%, ANAC = 18.0%, A3S = 5.8%, I2S = 58.5%, I = 6.2% and G = 35.3%) and Reaction 17 (ANS = 73.3%, ANAC = 19.2%, A3S = 7.5%, I2S = 53.5%, I = 13.9% and G = 32.6%) were very similar to USP porcine heparins (ANS = 80 ± 0.9%, ANAC = 13 ± 0.5%, A3S = 6.7 ± 0.7%, I2S = 61 ± 2.6%, I = 10.5 ± 0.7% and G = 28.4 ± 2.0%). The total IdoA (I2S and I) content of Reaction 16 was identical to Reaction 17 despite use of excess C_5-Epi for one-pot synthesis. It has been shown that C_5-Epi complexes with 2-OST *in vivo*, and such an allosteric effect can explain identical IdoA content and marginally higher TriS levels of Reaction 17 relative to Reaction 16[157]. The presence of 3-*O*-sulfo glucosamine in Reactions 16 and 17 spectra supports tetrasaccharide analysis and suggests these products should exhibit anticoagulant activity. The requirement of excess C_5-Epi would be decided based on the measured anticoagulant activity of these

bioengineered heparins. Overall, the structural equivalence of bioengineered heparins, Reactions 16 and 17, to USP heparins was conclusively demonstrated through ^{1}H and HSQC NMR spectroscopy studies.

3.2.9. Size exclusion chromatography for molecular weight determination

Post 2008 contamination crisis, USP has actively engaged in inclusion of enhanced standards of purity and stricter quality control toward minimization of variation within commercial heparin products. For increased clinical safety, the USP has imposed several restrictions on heparin's molecular weight properties as they are known to impact its biological activity[158]. Effective May 2014, the new heparin monograph requires USP heparin APIs to comply with following molecular weight restrictions: 1. Proportion of heparin chains with molecular weight over 24,000 (M24,000) is not more than 20%. 2. Mw is between 15,000 and 19,000. 3. The ratio of heparin chains with molecular weight between 8000 and 16,000 Da (M8000–16,000) to heparin chains with molecular weight between 16,000 and 24,000 (M16,000–24,000) is not less than 1.0[159].

In the one-pot synthesis study, the molecular weight properties of USP heparin (Mw = 22,300 ± 200 Da, Mn = 15,000 ± 100 Da and PDI = 1.49 ± 0.01) were determined as an average of seven different commercial heparins previously studied[156]. SEC chromatogram of Reactions 16 and 17 showed the presence of a single major peak. Mw values of Reaction 16 (Mw = 26,200 ± 200 Da, Mn = 13,200 ± 100 Da) and Reaction 17 (Mw = 29,200 ± 500 Da, Mn = 13,900 ± 200 Da) were higher in comparison to USP heparins while their Mn values were lower than USP heparins (Fig. 3.7A). As a result, the polydispersity index (PDI) of Reaction 16 (PDI = 1.99 ± 0.02) and Reaction 17 (PDI = 2.10 ± 0.04) were significantly higher in comparison to USP porcine heparins (PDI = 1.49 ± 0.01). Higher TriS disaccharide level in Reaction 17 leads to its marginally higher molecular weight (Mw and Mn) than Reaction 16. The resulting molecular weight of bioengineered heparin products is directly related to the NSH substrate molecular weight. The high PDI of bioengineered heparin products can be attributed to the high PDI of

NSH (1.69 ± 0.01). Control over the NSH molecular weight during the chemical *N*-deacteylation/*N*-sulfonation and titanium dioxide depolymerization can effectively generate one-pot heparin products within the new regulatory requirements.

3.2.10. In vitro anticoagulant activity of bioengineered heparins

USP heparins currently are required to have an anti-factor IIa activity >180 IU/mg and anti-factor Xa/anti-factor IIa activity ratio between 0.9 and 1.1[156]. Two-stage colorimetric in vitro assays were used to evaluate anti-factor Xa and anti- factor IIa activity of bioengineered heparins Reactions 16 and 17. The activity value of USP heparin was determined as an average of reported anti-IIa and anti-Xa activity for seven different USP heparins[156]. Bioengineered heparin Reaction 17 had an anti-IIa activity of 151 ± 26 IU/mg, which was higher than 16 (73 ± 11 IU/mg) and close to 180 IU/mg required by USP (Fig. 3.7B). Reaction 17 also possessed a higher anti-Xa activity of 159 ± 15 IU/mg in comparison to Reaction 16 (96 ± 4 IU/mg). The anti-Xa to anti-IIa ratios were also determined for Reactions 17 (1.05 ± 0.20) and 16 (1.32 ± 0.21). The one-pot bioengineered heparin products possessed significant anticoagulant activity though they did not meet USP requirements. The higher in vitro anticoagulant activity of Reaction 17 can be attributed to its higher tetrasaccharide content (3.4%). The observed activity of Reactions 16 and 17 were in agreement with their measured tetrasaccharide content and supports the use of tetrasaccharide mapping for understanding heparin's anticoagulant activity at the molecular level.

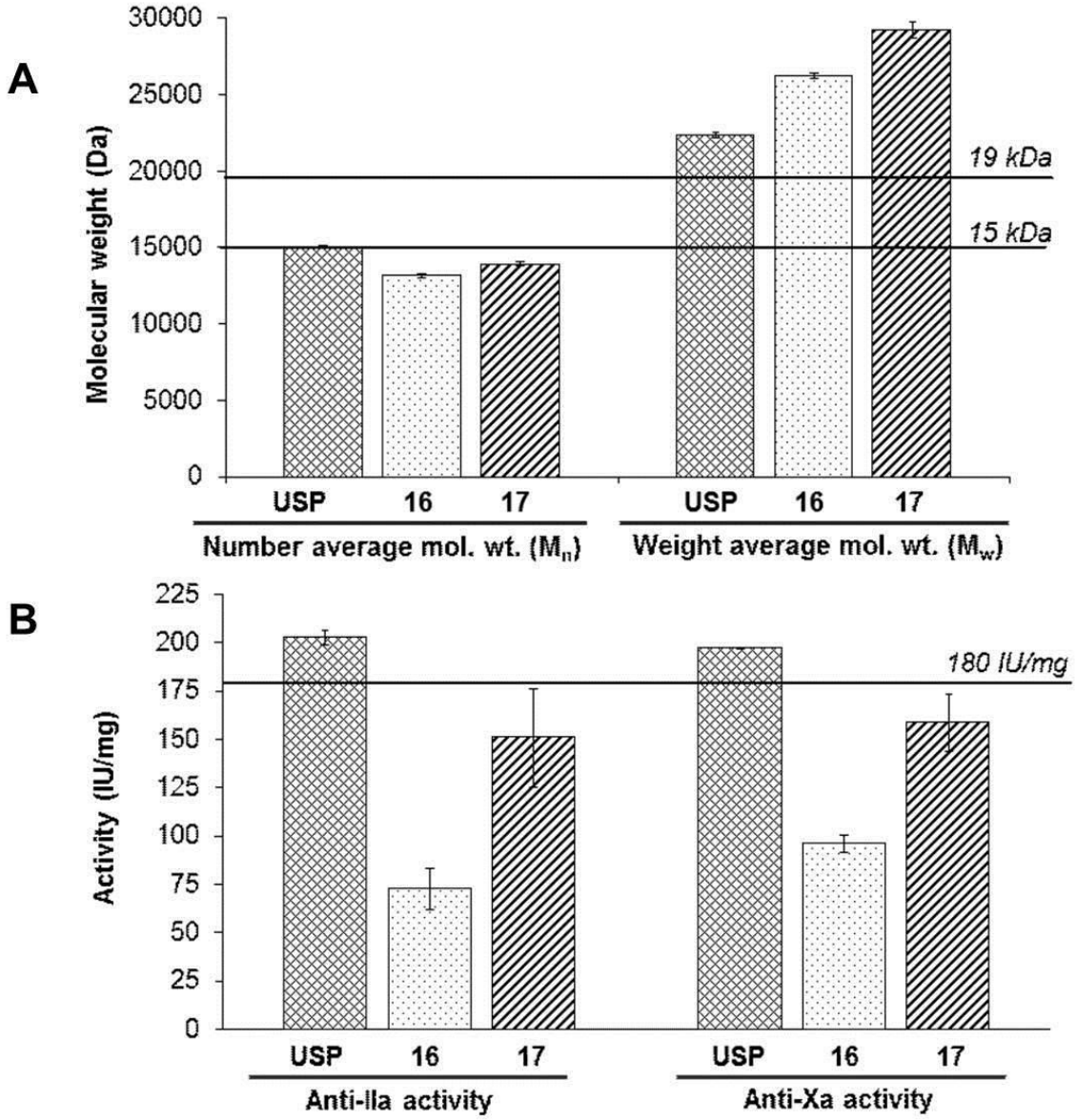

Figure 3.7. Molecular weight and anticoagulant activity of USP and bioengineered heparins. A. Molecular weight properties of 16 and 17 determined by size exclusion chromatography. New USP requirements for M_w (15000 < M_w < 19000) are depicted by horizontal lines. B. *In vitro* anti-IIa and anti-Xa activity of 16 and 17. Solid line marks the minimum anti-IIa activity of 180 IU/mg required by USP. Molecular weight and anticoagulant activity values for USP heparins were reported previously[156].

3.3. Discussion

The two studies presented in this chapter provide a road map towards the chemoenzymatic synthesis of HS and HP oligosaccharide targets. The application of fluorous tagging polysaccharides has the potential to streamline a bioengineered heparin process by greatly reducing the purification time after successive enzyme treatments. The enzymatic process of backbone elongation provides an alternative to an E. coli K5 capsular polysaccharide starting material, as used in the one-pot heparin study. This iterative approach using KfiA and PmHS2 glycosyltransferases allows for specific, controlled sequences to be built. By feeding either GlcNAc or GlcNTFA into the elongation reaction, a set of oligosaccharides with defined GlcNAc and GlcNS content could be synthesized to exact specifications and used to sort out the complex structure activity relationship of HS oligosaccharides on binding partners such as growth factors and extracellular matrix components.

The bioengineered heparins produced in the one-pot reaction show that despite heparin's enormous structural complexity, a bioengineered alternative to animal sourced heparin is feasible. Compared to USP heparin, the bioengineered heparins were similar in disaccharide content, slightly higher in molecular weight, and reasonably close to the USP anti IIa and Xa activity. Tighter control of the K5 capsular polysaccharide MW could easily bring the bioengineered heparin with USP limits, and fine tuning the 3-OST enzyme concentration could bring anticoagulant activity up to par with USP heparin. Using more than one 3-OST isoform in the reaction could also generate a wider variety of AT binding sites, thereby increasing the anticoagulant activity.

The concentration of enzyme and the ratio of enzyme to substrate needs careful fine tuning in a chemoenzymatic synthesis. The approach of modulating enzymatic activity through use of an optimized E:S ratio is well suited for high throughput screening studies aimed at better understanding of heparin's structural heterogeneity and its impact on structure activity relationship. Diversity in 3-OST family (7 different isoforms) is primarily responsible for a wide array of biological functions attributed to

heparin/HS glycosaminoglycans. One-pot chemoenzymatic synthesis of heparin/HS chains provides a way to decipher the substrate specificity of various 3-OST isoforms with easy availability of polysaccharide/oligosaccharide substrates. The one-pot approach would also be useful for evaluating combinations of different OST isoforms not used in this study.

3.4. Conclusions and future directions

In conclusion, we have successfully applied the FBoc linker and FSPE technique in our chemoenzymatic synthesis of heparan sulfate oligosaccharides. The fluorous-linked disaccharide was extended with glycosyltransferases KifA and PmHS2 respectively, and recognized by 6-OSTs, revealing that the FBoc linker does not interfere with the action of these enzymes. The FSPE technique was suitable for the purification of heparan sulfate oligosaccharides as well.

In addition, a successful one-pot chemoenzymatic synthesis of complex full-length heparin/HS polysaccharides has been achieved beginning from NSH. Rapid oligosaccharide synthesis can be realized through this one step scheme, and in the future could be modified with the inclusion of glycosyltransferases and UDP sugar-based chain elongation, as in the fluorous tagged oligosaccharide study. Scale up of this process to metric ton scale is relatively infeasible but it is a robust process for laboratory scale preparation of full-length polysaccharides and oligosaccharides, especially in combination with the fed-batch enzyme fermentations detailed in Chapter 2.

3.5. Materials and methods

3.5.1. Expression of HS biosynthetic enzymes

A total of four enzymes were used for the chemoenzymatic synthesis, including 6-OST-1, 6-OST-3, KfiA, and pmHS2. All enzymes were expressed in *E. coli* and purified by appropriate affinity chromatography as described in section 3.5.6.

3.5.2. Preparation of enzyme cofactors

Preparation of UDP-GlcNTFA was completed using GlcNH2-1-phosphate (Sigma) and glucosamine-1 phosphate acetyltransferase/Nacetylglucosamine-1-phosphate uridyltransferase (GlmU) as described previously. Briefly, $GlcNH_2$-1-phosphate was converted to GlcNTFA using S-ethyl trifluorothioacetate. The resultant GlcNTFA-1-phosphate was then converted to UDP-GlcNTFA using glucosamine-1-phosphate acetyltransferase/*N*-acetylglucosamine-1-phosphate uridyltransferase (GlmU) in a buffer containing 50 mM Tris-HCl (pH 7.0), 5 mM $MgCl_2$, 200 M dithiothreitol, 2.5 mM UTP and 0.012 U/L inorganic pyrophosphatase. A sulfo donor, 3'-phosphoadenosine 5'-phophosulfate (PAPS), was prepared using adenosine phosphokinase and ATPsulfurylase.

3.5.3. Backbone elongation procedures

To introduce a GlcNTFA into the backbone: Acceptor substrate (1.2 mmol) was incubated with KfiA (20 µg mL-1) in buffer containing Tris (25 mmol, pH 7.2), $MnCl_2$ (15 mmol) and UDP-GlcNTFA (1.5 mmol), at room temperature overnight. The product after elongation step was purified using FSPE. The identity of the product was confirmed by electrospray ionization (ESI)-MS and NMR.

To introduce GlcA into the backbone: Acceptor substrate (1.2 mmol) was incubated with PmHS2 (20 µg mL-1) in a buffer containing Tris (25 mmol, pH 7.2), $MnCl_2$ (15 mmol) and UDP-GlcA (1.5 mmol), at room temperature overnight. The product after elongation step was purified using FSPE. The identity of the product was confirmed by ESI-MS and NMR.

3.5.4. Enzymatic sulfation methods

Backbone substrate (0.3 mmol) was incubated with 2-(*N*-morpholino)ethanesulfonic acid (MES) buffer solution (50 mmol, pH 7.0), PAPS (1.5 mmol), 6-OST-1 (200 µg mL-1) and 6-OST-3 (200 µg mL-1) overnight at 37 ˚C. The product after 6-*O*-sulfation step was purified using FSPE (Fluorous Solid Phase Extraction). The identity of the product was confirmed by ESI-MS and NMR.

3.5.5. Fluorous solid phase extraction method

FSPE cartridge (FluoroFlash® SPE Cartridges, 2 grams, 8 cc tube) was purchased from Fluorous Technologies. Inc. LC-MS analysis was performed to monitor each cycle of enzymatic reaction, and mixed solution (1~2 mL) was directly loaded into the FSPE cartridge after the completion of enzymatic reaction after detection by LC-MS. Double-distilled water (6 mL) was employed to wash all non-fluorous substrates including salts, peptides etc. Subsequently, 80% methanol aqueous solution (6 mL) was added to elute fluorous compounds from the cartridge. Finally, 100% methanol (6 mL) was used to wash and regenerate the FSPE cartridge.

3.5.6. Enzymes and *N*-sulfo heparosan production

Recombinant *E. coli* strains expressing fusion proteins of C_5-Epi, 2-OST, 6-OST-1, 6-OST-3, 3-OST-1 and AST IV were grown in LB medium (MP Biomedicals) at 37◦C using rotary air shaker (New Brunswick Scientific Innova 44R)[97,107,119,160]. Recovered cell pellets were stored at −80◦C until purified. Recombinant enzymes were purified from clarified cell lysates using either MBP- or His- affinity chromatography. Briefly, cell pellets were re-suspended in respective extraction buffers, lysed and centrifuged to obtain a clear cell lysate. The clarified cell lysate was then loaded onto respective affinity column connected to a GE Äkta purifier system. Elution was carried out using either high maltose (for MBP tagged proteins) or high imidazole (for His tagged proteins) containing buffers. The eluted protein was stored at −80◦C with 10–15% glycerol, until further use. *E. coli* K5 capsular polysaccharide, heparosan, was purified from the supernatant of fed batch fermentation using ammo- nium sulfate precipitation[108]. *N*-sulfo heparosan (NSH) was prepared by partial chemical *N*-deacetylation and *N*-sulfonation of heparosan as described earlier[108]. Titanium dioxide based depolymerization was employed to reduce the molecular weight, if required[161]. Analysis of the NSH product obtained indicated following characteristics: Number average molecular weight (Mn) = 11,100 ± 200 Da; weight average molecular weight (Mw) = 18,800 ± 200 Da; polydispersity index (PDI) = 1.69 ± 0.01; % N-sulfo groups = 81.4 ± 0.9%.

3.5.7. Combinatorial one pot synthesis of heparin

Initial combinatorial chemoenzymatic heparin synthesis experiments were carried out using 1 mg of NSH as substrate in 50 mM MES, pH 7 buffer. The reaction mixture consisted of 0.1 mg/mL of NSH substrate and 300 µM of sulfo group donor 3'- phosphoadenosine-5'-phosphosulfate (PAPS), an essential cofactor for sulfotransferases. A 5 mM concentration of p-nitrophenyl sulfate (PNPS, Sigma) was used in the reaction mixture as the sulfo group donor to establish an AST IV based co-factor recycling system for PAPS regeneration (Burkart et al., 2000). The control reaction contained 0.1 mg/mL each of C_5-Epi, 2OST, 6-OST-1, 6-OST-3 and AST IV. The 3-OST-1 was not included in the initial combinatorial synthesis of heparin to reduce product complexity in order to simplify analysis (3-*O*-sulfo group containing sequences are resistant to heparin lyases and thus do not afford disaccharide products). The concentration of three groups of enzymes was varied combinatorially by either 2-fold (0.2 mg/mL) or 10-fold (1 mg/mL): 1. C_5-Epi & 2-OST individually as well as together; 2. 6-OST-1 & 3 individually as well as together; and 3. AST IV alone. All enzymes not varied were maintained constant at 0.1 mg/mL, as was the reaction control. The reaction mixtures were incubated overnight at 37◦C. The resulting products were analyzed using disaccharide analysis and optimal conditions were identified. In the second set of experiments, 2 mg of the product formed using the two best conditions, identified through the combinatorial experiments, were treated with 3-OST-1 at a final concentration of 0.1 mg/mL, after the end of overnight incubation and the reaction mixture was incubated for an additional day. The product was purified using anion exchange chromatography and further evaluated using chemical and biological assays.

3.5.8. Strong anion exchange (SAX) purification of bioengineered heparin

Reaction product, obtained after the second enzymatic one-pot preparation, was boiled and centrifuged, and the supernatant was filtered using a 0.22 µm filter. The clarified permeate was then dialyzed using centrifugal ultrafiltration units (Amicon centrifugal filter units, Millipore) and DI water.

Dialyzed polysaccharide solution was then loaded onto a 20 mL Q-Sepharose fast flow (GE life sciences) strong anion exchange (SAX) glass column connected to a GE Äkta purifier FPLC system. Prior to loading the sample, Q- Sepharose column was washed with 4 column volumes of DI water, 4 column volumes of 20% v/v ethanol and 4 column volumes of DI water. After loading the sample, column was washed using 4 column volumes of buffer A (DI water) and 4 column volumes of 0.4 M NaCl by mixing buffer A and buffer B (2 M NaCl in DI water). This was followed by step elution at 2 M NaCl by buffer B. Fractions eluted with 2 M salt were collected, dialyzed and lyophilized. These samples were used for further analysis.

3.5.9. Enzymatic digestion for disaccharide analysis and tetrasaccharide mapping

For disaccharides analysis, heparin lyases 1, 2, and 3 (10 mU each) in 5 µl of 25 mM Tris, 500 mM NaCl, 300 mM imidazole buffer (pH 7.4) were added to 10 µg heparin sample in 100 µl of distilled water and incubated at 35◦C for 10 h to degrade heparin sample completely[162]. The products were recovered by centrifugal filtration using a YM- 10 micro-concentrator (Millipore), and the heparin disaccharides were recovered in the flow-through and freeze-dried. The digested heparin disaccharides were dissolved in water to concentration of 50–100 ng/2 µl for liquid chromatography (LC)–mass spectrometric (MS) analysis. For tetrasaccharide analysis, 40 mU of heparin lyase 2 in 20 µL of 25 mM Tris, 500 mM NaCl, 300 mM imidazole buffer (pH 7.4) was added to 50–100 µg heparin sample in 100 µL of distilled water and incubated at 35◦C for 10 h. The resulting product was freeze-dried for further LC–MS analysis[155].

3.5.10. Disaccharide analysis and tetrasaccharide mapping using liquid chromatography–mass spectrometry

LC–MS analyses were performed on an Agilent 1200 LC/MSD instrument (Agilent Technologies, Inc. Wilmington, DE) equipped with a 6300 ion trap and a binary pump followed by a UV detector equipped with a high-pressure cell. The column used was a Poroshell 120 C18 column (2.1 × 100 mm,

2.7 µm, Agilent, USA). Eluent A was water/acetonitrile (85:15) v/v, and eluent B was water/acetonitrile (35:65) v/v. Both eluents contained 12 mM tributylamine (TrBA) and 38 mM ammonium acetate with pH adjusted to 6.5 with acetic acid. For disaccharide analysis, a gradient of solution A for 5 min followed by a linear gradient from 5 to 15 min (0–40% solution B) was used at flow rate of 150 µl/min. For tetrasaccharide analysis, a gradient of solution A for 2 min followed by a linear gradient from 2 to 40 min (0–30% solution B) was used at flow rate of 150 µl/min. The column effluent entered the source of the electrospray ionization (ESI)–MS for continuous detection by MS. The electrospray interface was set in negative ionization mode with a skimmer potential of −40.0 V, a capillary exit of −40.0 V, and a source temperature of 350◦C, to obtain the maximum abundance of the ions in a full-scan spectrum (200–1500 Da). Nitrogen (8 l/min, 40 psi) was used as a drying and nebulizing gas. Quantification analysis of di- or tetra-saccharides was performed using calibration curves established by separation of increasing amounts of unsaturated di- or tetrasaccharide standards (0.1, 0.5, 1, 5, 10, 20, 50, 100 ng/each). Linearity was assessed based on the amount of di- or tetra-saccharide and peak intensity in extracted ion chromatogram (EIC). Disaccharide and tetrasaccharide analyses were performed in duplicates and singlet, respectively.

3.5.11. NMR spectroscopy

Heparin products were analyzed by 1H nuclear magnetic resonance (NMR) and two-dimensional NMR spectroscopy heteronuclear single quantum coherence (HSQC) to fully characterize its structure[64]. All NMR experiments were performed on a Bruker Advance II 600 MHz spectrometer (Bruker BioSpin, Billerica, MA) with Topsin 2.1.6 software (Bruker). Briefly, samples were each dissolved in 0.5 ml $^{1}H_2O$ (99.996%, Sigma) and freeze- dried repeatedly to remove the exchangeable protons. The samples were re-dissolved in 0.4 ml $^{2}H_2O$ and transferred to NMR micro tubes (OD 5 mm, Norell, tubes). The conditions for one-dimensional 1H NMR spectra were as follows: wobble sweep width of 12.3 kHz, acquisition time of 2.66 s, and relaxation delay of 8 s at 298 K. The conditions for two-dimensional HSQC

spectrum were as follows: 32 scans, sweep width of 6.15 kHz, acquisition time of 0.33 s, and relaxation delay of 0.90 s.

3.5.12. Molecular weight determination

Molecular weight and polydispersity of prepared heparin products was determined using size exclusion chromatography as described earlier[156]. TSK-GEL G3000PWxl size exclusion column (Tosoh Bioscience), maintained at 40◦C with an Eppendorf column heater, was connected to a HPLC system consisting of a Shimadzu LC-10Ai pump, a Shimadzu CBM-20A controller and a Shimadzu RID-10A refractive index detector. The mobile phase consisted of 0.1 M $NaNO^3$. A sample injection volume of 20 µL and a flow rate of 0.6 ml/min were used. The SEC chromatograms were recorded with the LC solution Version 1.25 software and molecular weight properties determined using the "GPC Postrun" function. Heparin sodium oligosaccharides (Iduron, UK) of different molecular weights (2687 Da, 4300 Da, 5375 Da, 6449 Da and 8060 Da) were used as calibrants for the standard curve. The molecular weight measurements were carried out in duplicates.

3.5.13. In vitro anticoagulant activity measurement

The anti-factor Xa and anti-factor IIa activities of heparin products was determined by two stage Biophen heparin anti-Xa and anti-IIa colorimetric kits (Aniara, US) using manufacturer's supplied instructions[106]. USP heparin (Celsus Laboratories) with anti-IIa activity of 200 IU/mg and anti-Xa/anti-IIa activity ratio of 1 was used as a standard for the colorimetric assays. The *in vitro* activity measurements were carried out in duplicate.

4. HEPARAN SULFATE AND HEPARIN IN FIBROBLAST GROWTH FACTOR SIGNALING

4.1. Introduction

The glycosaminoglycan (GAG) heparan sulfate (HS) is abundant on the cell surface and within the extracellular matrix (ECM), and plays a role in cell signaling due to its ability to interact with growth factors, chemokines, and other ECM proteins. The wide array of potential binding partners for HS is due to its structural heterogeneity, which can vary based on the cell or tissue type where it is produced. As such the function of HS in cell signaling is highly complex and not well understood. Mammalian heparan sulfate contains a domain structure comprised of undersulfated sequences rich in GlcNAc residues (called 'NA domains') and highly sulfated sequences rich in GlcNS residues (called 'NS domains') (Figure 4.1)[161,162,164]. These domains structurally vary based on the species and tissues from which a HS is obtained[12,165] and the NS domain is of particular importance in cellular behavior and disease processes[166]. HS is biosynthesized in the endoplasmic reticulum and Golgi as a constituent of proteoglycans (PGs) attached to one of a number of core proteins[167,168]. The biosynthesis of the GAG chain within the Golgi controls the placement of domains within HS[3,168]. These PGs are primarily localized to the cell membrane or in the extracellular matrix[167,168] where they play a critical biological role as a co-receptor in growth factor signaling[21,169]. HS domains structure and position on the GAG chain can also be catabolically modified through the action of extracellular sulfatases[167,170] and heparanase[167,171]. A plethora of HS structures are possible and many are observed in animals.

In the past, heparan sulfate used in biochemical studies was generally extracted from animal tissues following proteolysis. The resulting HS GAG is a large (Mr >10 kDa), polydisperse (for Mr 10-30 kDa, Mw/Mn values of 1.2-1.6), and microheterogeneous (e.g., possessing multiple structural domains

Portions of this chapter previously appeared as: Schultz, V. *et al.* Heparan sulfate domains required for fibroblast growth factor 1 and 2 signaling through fibroblast growth factor receptor 1c. *J. Biol. Chem.* **292,** 2495–2509 (2017).

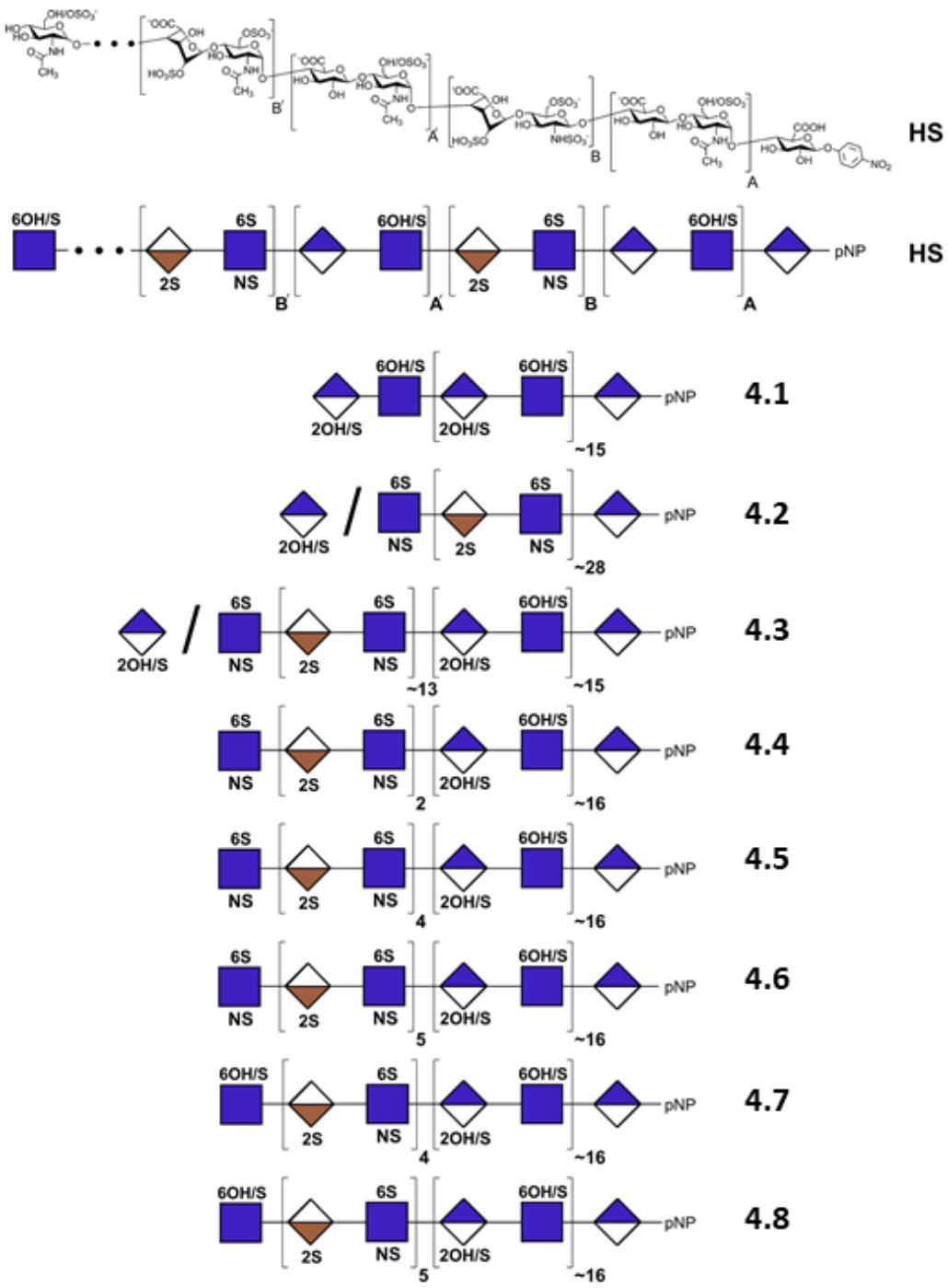

Figure 4.1. Structures of synthetic heparan sulfates. A generalized chemical structure of heparan sulfate (HS) is shown and below it, the same structure is drawn using conventional symbols. Synthetic heparan sulfates 4.1-8 are shown in their symbolic representations. The presence of substituents is indicated above and below the symbols with the carbon position number (or 'N' for nitrogen substituent) and 'OH' for unsubstituted or 'S' for sulfo group substituted. An 'OH/S' indicates that the position can be either unsubstituted or sulfated. The '/' at the non-reducing terminus indicates an ambiguous monosaccharide that was not controlled during the final step of synthesis.

and variable saccharide sequences)[165,172-174]. The structural complexity of heparan sulfate GAG complicates the study of its structure-activity relationship (SAR), with regard to its protein-mediated signaling activities. Related, less heterogeneous and more highly sulfated heparin, chemically modified heparins or heparin-derived oligosaccharides have been applied to simplify these SAR studies[78,103,175,176]. Unfortunately, natural heparan sulfate has highly variable compositions and sequences and only a very limited number of chemically modified heparin structures can be reliably prepared from natural polysaccharides and in quite small quantities (e.g., micrograms to milligrams). Structurally defined heparan sulfate-derived or heparin-derived oligosaccharides from natural GAGs or organic synthesis are often too small to exhibit many important biological activities in comparison to the 'full length' native polysaccharides[103,175,176].

Recently, it has become possible to chemoenzymatically synthesize larger heparan sulfate chains having domain structures[177]. Recombinant heparan sulfate polymerizing and modifying enzymes have been utilized for reactions *in vitro*[73,119]. The GAG chain backbones can be efficiently and controllably synthesized in vitro using GAG synthases to add the monosaccharide units from UDP-sugar donors onto an acceptor (Figure 4.2). When building GAGs from natural UDP-sugars (UDP-GlcNAc and UDP-GlcA) or non-natural UDP-sugars (UDP-GlcNTFA, where TFA is trifluoroacetyl)[79], *in vitro* GAG chain synthesis can be performed in one of two preferred formats: step-wise elongation (i.e. one sugar unit at a time) or in a synchronized polymerization reaction (i.e. block addition via multiple sugar units). Both of these formats yield well-defined products with narrow size distributions (monodisperse or nearly so) and potentially much more controllable compositions than the GAG produced *in vivo*[82,103,178,179]. In our approach, the polysaccharide backbone is assembled with blocks of either [→4)-β-D-GlcA (1→4)-β-D-GlcNAc(1→] or [→4)-β-D-GlcA (1→4)-β-D-GlcNTFA(1→]. Mild chemical

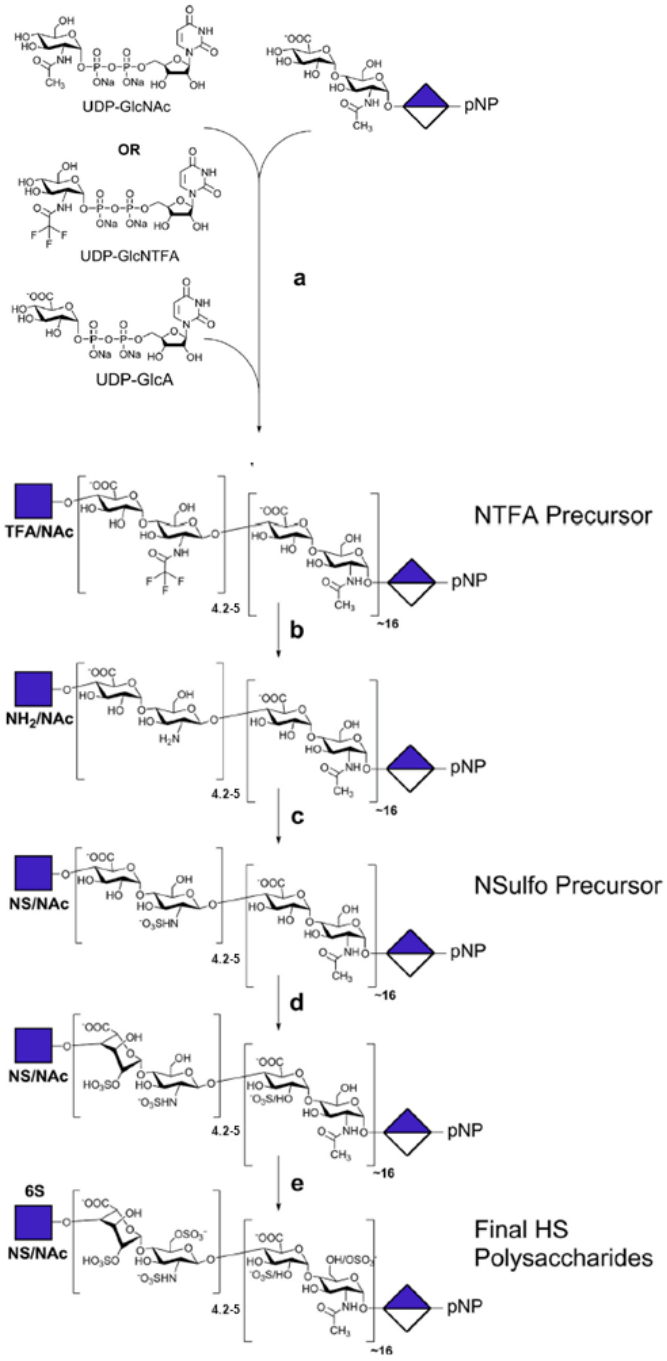

Figure 4.2. Chemoenzymatic synthesis of heparan sulfates. The first step involving the iterative synthesis of the trisaccharide acceptor, from GlcA-pNP and UDP-donor sugars, is not shown. a. The second step is polysaccharide backbone synthesis from the trisaccharide acceptor and UDP-donor sugars are shown at the *top* and are under stoichiometric control. b. The chemical conversion of GlcNTFA to GlcN (for a GlcNAc-containing domain, this part of the chain remains basically untransformed at this step). c. The chemical conversion of GlcN to GlcNS. d. Enzymatic treatment with C_5-epimerase and 2-*O*-sufotransferase. e. Enzymatic treatment with 6-*O*-sufotransferase-1 and 6-*O*-sufotransferase-3.

treatments remove the TFA moieties from the glucosamine and replace it with *N*-sulfo groups to generate a precursor structure with blocks of [→4)-β-D-GlcA (1→4)-β-D-GlcNAc(1→] or [→4)-β-D-GlcA (1→4)-β-D-GlcNS(1→] that is enzymatically modified with C_5-epimerase (C_5-Epi), which converts GlcA into iduronic acid (IdoA), *O*-sulfotransferases (STases) that transfer sulfo groups from the donor 3'-phosphoadenosine-5'-phosphosulfate (PAPS) to the various hydroxyl groups of the GAG. The resulting synthetic heparan sulfate chains have a controlled domain structure useful for SAR studies[99].

Heparan sulfate regulates the activity of the 22-member family of extracellular fibroblast growth factors (FGFs) involved in critically important cellular activities including angiogenesis, cellular proliferation, cellular motility, differentiation[180-182] and adhesion[183,184]. The FGFs signal through their cognate membrane-bound fibroblast growth factor receptors (FGFRs), a group of 7 distinct protein receptors and a HS co-receptor[185-187]. Kinetic experiments using surface plasmon resonance suggest that two extracellular FGFs first bind to the HS chain(s) of membrane-anchored HSPGs and then recruit two FGFRs to assemble into a signaling complex[188]. Assembly of a FGF:HS:FGFR ternary complex[189] then activates signaling across the transmembrane helix, which then activates the intracellular tyrosine-kinase domain[190]. The individual binding affinities of the HS chains for FGFs and FGFRs have been determined, but the actual structure of the ternary complex remains unclear[188]. The dimeric protein complex, FGF_2FGFR_2, forms a positively charged cleft or 'canyon' lined with basic amino acid residues that interact with one or two complementary negatively charged HS chains with high (nM range) affinity[186,191]. The FGF:HS:FGFR ternary complex is believed to be a symmetric structure of 2:2:2 stoichiometry[25]. Previous studies show that highly sulfated NS domains at the non-reducing terminus of heparan sulfate, bind with higher affinity and promote FGF2-FGFR1 signaling[99,192].

The following study examines the impact of the domain structure and the structure at the non-reducing terminus of chemoenzymatically synthesized heparan sulfate GAG chains on FGF-1 and FGF-2 signaling through FGFR-1c. Heparan sulfate mediated FGF-FGFR signaling was determined using a

murine immortalized bone marrow (BaF3) cell line developed by Ornitz and coworkers[186,191] that expresses FGFR type 1c without expressing either HSPGs or FGF. The ternary complex signaling process is determined by measuring heparan sulfate-mediated cellular proliferation.

4.2. Results

4.2.1. Design of synthetic heparan sulfate targets

The domains present within natural heparan sulfate consist of sequences of high sulfation (NS domains) and low sulfation (NA domains)[161,162,164]. While these domains vary in size and number of sulfo-groups between species and tissues[165], the regions do share some common features. First, their placement and sizes are believed to be controlled through the placement of *N*-sulfo groups by the action of the different *N*-deacetylase *N*-sulfotransferase isoforms[3,162,164,169]. Second, the domain closest to the core protein at the heparan sulfate chain's reducing end is generally an NA domain, while the domain at the non-reducing end of non-signaling and signaling heparan sulfate chains are typically NA and NS domains, respectively[161,164]. Moreover, the conversion of a non-signaling heparan sulfate chain to a signaling heparan sulfate chain in disease processes associated with rapid cell proliferation, such as cancer, can also take place through the action of heparanase, that cleaves between a high and low sulfate domain, thus, exposing a GlcN residue associated with an NS domain at the chain's non-reducing end[167,168].

Eight heparan sulfate chains were designed to begin to study the contribution of domain structures in HS for FGF-FGFR signaling (Figure 4.1, **4.1**-**8**). These chains consist of one or two long domains assembled at the non-reducing end of a GlcA-pNP acceptor. One chain, **4.2**, contained a long (~28 disaccharide repeats) NS domain assembled at the non-reducing end of a GlcA-pNP acceptor, resembling heparin, serving as a positive control in signaling assays. A second chain, **4.1**, contained a

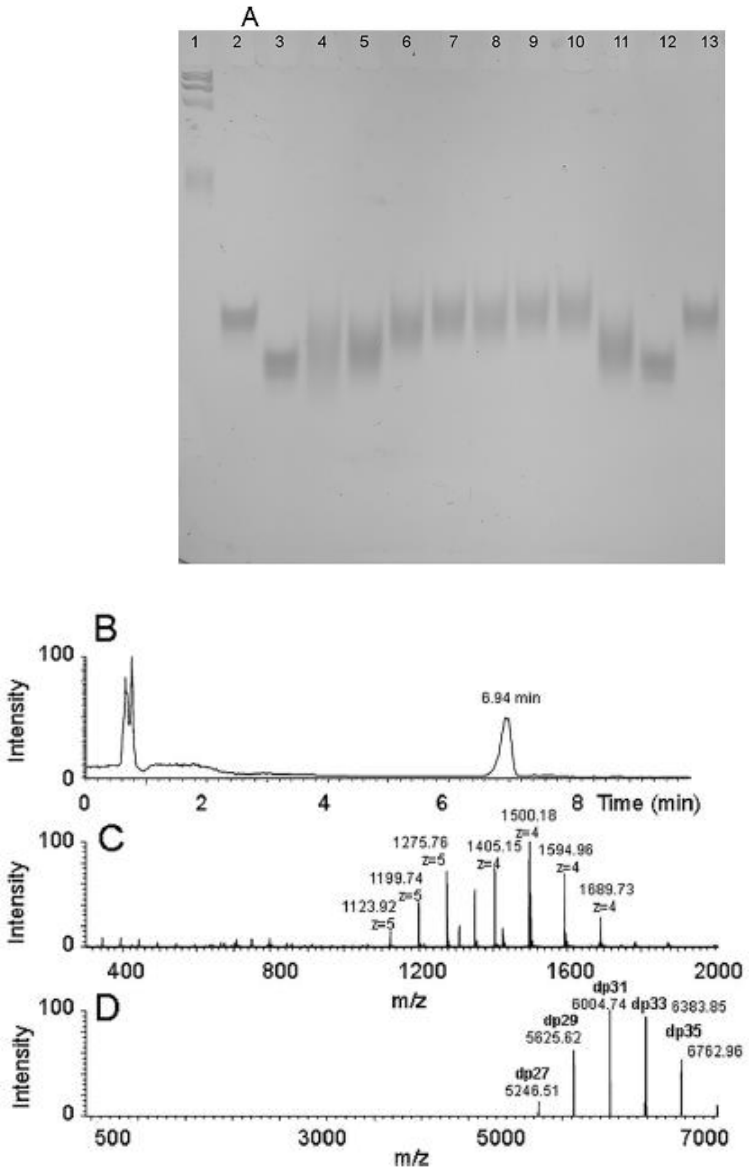

Figure 4.3. PAGE analysis of various synthetic heparosan and TFA-protected heparosan precursors and HPLC-MS analysis of the precursor to synthetic heparan sulfate 4.1. The heparosan polysaccharide and TFA-protected heparosan precursors were assembled on the GlcA-GlcNAc-GlcA-pNP *or* GlcA-GlcNTFAGlcA-pNP acceptors analyzed by HPLC-MS. *A*, 8% PAGE was used to analyze these samples together with individual hyaluronan and a mixture of hyaluronan (*HA*) standards (Hyalose, LLC; note that hyaluronan and heparosan migrate similarly but not identically on PAGE). Samples (~1 µg) were loaded onto the gel and run at 250 V applied for 20 min. The gel was stained overnight with 0.05% Alcian Blue stain. *Lane 1*, hyaluronan LoLadder (fastest migrating band is 27 kDa); *lanes 2* and *13*, 10-kDa hyaluronan; *lanes 3* and *12*, 6.5-kDa hyaluronan; *lane 4*, NAc precursor of 4.1; *lanes 5* and *11*, NAc precursor of 4.1 (SAX-polished); *lane 6*, NTFA precursor of 4.4 (five sugars added); *lane 7*, NAc precursor of 4.7 (nine sugars added); *lane 8*, NTFA precursor of 4.5 (nine sugars added); *lane 9*, NAc precursor of 4.8 (11 sugars added); *lane 10*, NTFA precursor of 4.6 (11 sugars added). HPLC-MS analysis of the precursor to synthetic heparan sulfate 4.1 (purified; same as shown in *A*, *lanes 5* and *11*) was performed. *B*, the HPLC chromatogram with the broad peak at 6.94 min corresponding to the polysaccharide chain. *C*, the mass

spectrum of polysaccharide chains in the HPLC peak eluting at 6.94 min. *D*, the deconvoluted mass spectrum of polysaccharide chains in the 6.94-min HPLC peak with a degree of polymerization (*dp*; the number of monosaccharides in the chain) and molecular mass distribution of precursor to synthetic heparan sulfate 4.1 showing a molecular mass consistent with the 6.4-kDa target.

long (~15 repeats) NA domain assembled at the non-reducing end of the acceptor (Figure 4.3), resembling a single domain heparan sulfate chain, serving as a negative control in signaling assays. A third chain, **4.3**, contained two domains comprised of a long (~13 repeats) NS domain assembled at the non-reducing end of a long (~15 repeats) NA domain assembled at the reducing end of the GlcA-pNP acceptor. On the remaining five synthetic heparan sulfate chains (**4.4**-**8**) this long (~16 repeats) reducing end NA domain was terminated at the non-reducing end with NS domains of variable lengths capped with a single GlcN residue substituted with either an *N*-sulfo or *N*-acetyl group.

4.2.2. Block Copolymer elongation and formation

Chain synthesis began on a commercially available GlcA-pNP acceptor. This acceptor was iteratively extended through the alternative addition of UDP-GlcNAc and UDP-GlcA donors, to prepare the precursor for targets **4.1** and **4.3**-**8,** or UDP-GlcNTFA and UDP-GlcA donors, to prepare precursor for target **4.2,** resulting in trisaccharides GlcA-GlcNAc-GlcA-pNP and GlcA-GlcNTFA-GlcA-pNP. These trisaccharides were characterized by electrospray ionization MS (ESI-MS) and anion exchange HPLC.

The synthesized trisaccharides are excellent acceptors for stoichiometrically controlled extension. The length of the long domain was controlled by the ratio of the trisaccharide acceptor and the UDP-sugar donors. The molecules are quasi-monodisperse due to the synchronization of the synthase-catalyzed polymerization reaction with acceptor as described[82]. The size of the resulting chains $[GlcA\text{-}GlcNAc]_{15}$-GlcA-pNP (as well as all the other synthetic HS chains) was determined by HPLC-MS. The $[GlcA\text{-}GlcNTFA]_{28}$-GlcA-pNP chain corresponds to the first precursor to synthetic heparan sulfate **4.2** (Figure 4.1).

The [GlcA-GlcNAc]$_{16}$-GlcA-pNP chains were further modified by iterative transfer of UDP-GlcNTFA and UDP-GlcA adding 5, 9 or 11 additional monosaccharide units. In each case, these chains were capped with either a final GlcNTFA or a GlcNAc residue (Figure 4.1) to afford the first precursor of the designed synthetic heparan sulfates **4.4**-**8**. It is important to note that these non-reducing terminal extensions were completely defined structures. While there are multiple species (~8 major) observed for the block portion of the synthetic chain, the step-wise synthesis results in precise additions. This control is needed to assess the SAR of the end of HS chains.

4.2.3. Glucosamine de-*N*-trifluoroacetylation and *N*-sulfonation

Once the precursors to synthetic heparan sulfates **4.2**-**8** were synthesized with the desired GlcNAc- and GlcNTFA-containing domains, the NTFA groups were deprotected and subsequently *N*-sulfonated. Each

Table 4.1. Disaccharide composition of the precursors and the oligosaccharides after *O*-sulfation
Disaccharide composition was calculated from HPLC-MS peak integration (Fig. 4.4) using appropriate response factors. The theoretical percentage of dp2 (NS) (where dp is the degree of polymerization) was calculated as NS/(NS + NAc - 1), and the percentage of dp2(NAc) was calculated as (NAc - 1)/(NS + NAc - 1) (see structure in Fig. 1). TriS, NS6S, NS2S, and NS disaccharides arise from the NS domains, and 2S6S, 6S, 2S, and 0S disaccharides arise from the NS domains. —, not detected.

	Disaccharide composition								Experimental		Theoretical	
	TriS	NS6S	NS2S	NS	2S6S	6S	2S	0S	Total -NS	Total - NAc	Total -NS	Total -NAc
***N*-sulfo precursor 4.4**	—	—	—	17%	—	—	—	83%	17%	83%	12%	88%
***N*-sulfo precursor 4.5**	—	—	—	26%	—	—	—	74%	26%	74%	21%	79%
***N*-sulfo precursor 4.6**	—	—	—	30%	—	—	—	70%	30%	70%	25%	75%
***N*-sulfo precursor 4.7**	—	—	—	28%	—	—	—	72%	28%	72%	21%	79%
Heparan sulfate **4.1**	—	16%	—	—	—	7%	—	77%	16%	85%	0%	100%
Heparan sulfate **4.2**	65%	23%	—	—	—	1%	7%	3%	88%	11%	100%	0%
Heparan sulfate **4.3**	37%	15%	—	—	—	10%	3%	36%	52%	49%	48%	52%
Heparan sulfate **4.4**	2%	6%	—	—	—	15%	32%	44%	8%	91%	12%	88%
Heparan sulfate **4.5**	6%	14%	—	—	—	21%	17%	41%	20%	79%	21%	79%
Heparan sulfate **4.6**	5%	14%	—	—	—	19%	29%	31%	19%	79%	25%	75%
Heparan sulfate **4.7**	5%	12%	—	—	—	21%	23%	39%	17%	83%	21%	79%
Heparan sulfate **4.8**	—	20%	—	—	—	17%	—	63%	20%	80%	25%	75%

TFA-containing block co-polymer was dissolved in a mildly basic solution of Et_3N, MeOH, and H_2O and stirred overnight. Under these conditions, the GlcNTFA residues were completely deprotected exposing free amino groups, which were chemically *N*-sulfonated using $NMe_3{\cdot}SO_3$ to afford GlcNAc- and GlcNS-domains containing block co-polymers, the *N*-sulfo precursors to synthetic heparan sulfates **4.2**-**8**. On the other hand, the acetyl groups of NA domains remain virtually intact throughout this process.

The sizes of the resulting di-copolymer intermediates, as examined using PAGE and LC-MS, were consistent with those expected based on their synthesis. The disaccharide composition of the N-sulfo precursors to synthetic heparan sulfates **4.4**, **4.5**, **4.6** and **4.7** were examined by disaccharide compositional analysis using HPLC-MS analysis to confirm that the expected extensions had taken place (Table 4.1).

The structure of the NTFA and N-sulfo precursors for each synthetic heparan sulfate was evaluated by 1D ^{1}H NMR. The ^{1}H spectra for the NTFA and N-sulfo precursors of synthetic heparan

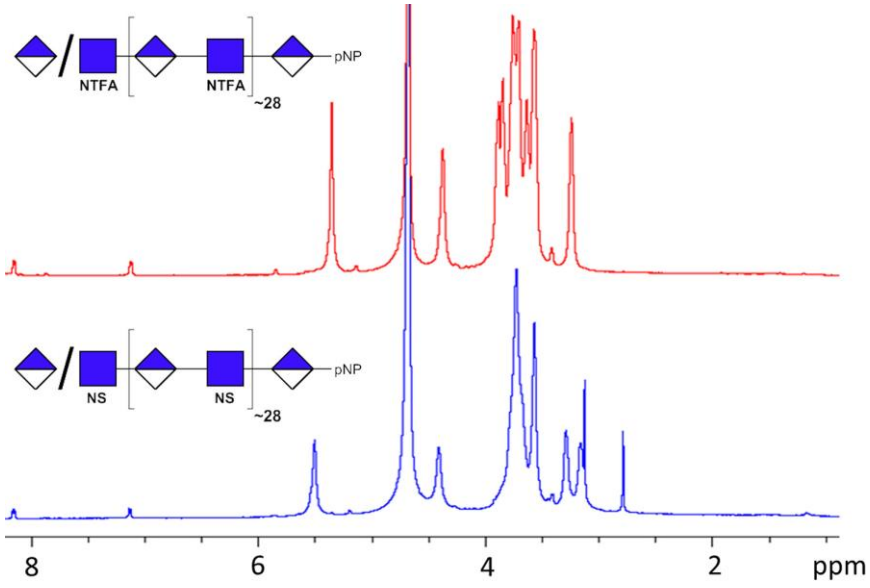

Figure 4.4. NMR analyses of HS intermediates. Proton NMR (600 MHz) of the first and second intermediate products of synthetic heparan sulfate 2. Panel A. The NTFA precursor, corresponding to compound 2. Panel B. The *N*-sulfo precursor is formed through de-*N*-trifluoracetylation and *N*-sulfonation of the NTFA precursor.

sulfate **4.2** is shown in Figure 4.4. The conversion of the GlcNTFA residue to GlcNS residue was confirmed by the change in chemical shift of the anomeric proton (H1) signal. NMR spectra of all block co-polymers show two signals in the anomeric region of ~4-6 ppm. The signal at ~5.5 ppm and ~4.4 ppm corresponds to the anomeric proton of GlcNTFA and GlcA, respectively. Incomplete *N*-sulfonation would be indicated by a peak at ~5.6 ppm, but such a signal cannot be seen in the spectra. Taken together, the NMR data indicate that the block co-polymers were successfully *N*-sulfonated.

4.2.4. Disaccharide composition of heparan sulfate precursors

The disaccharide composition of the heparan sulfate N-sulfo was next determined by

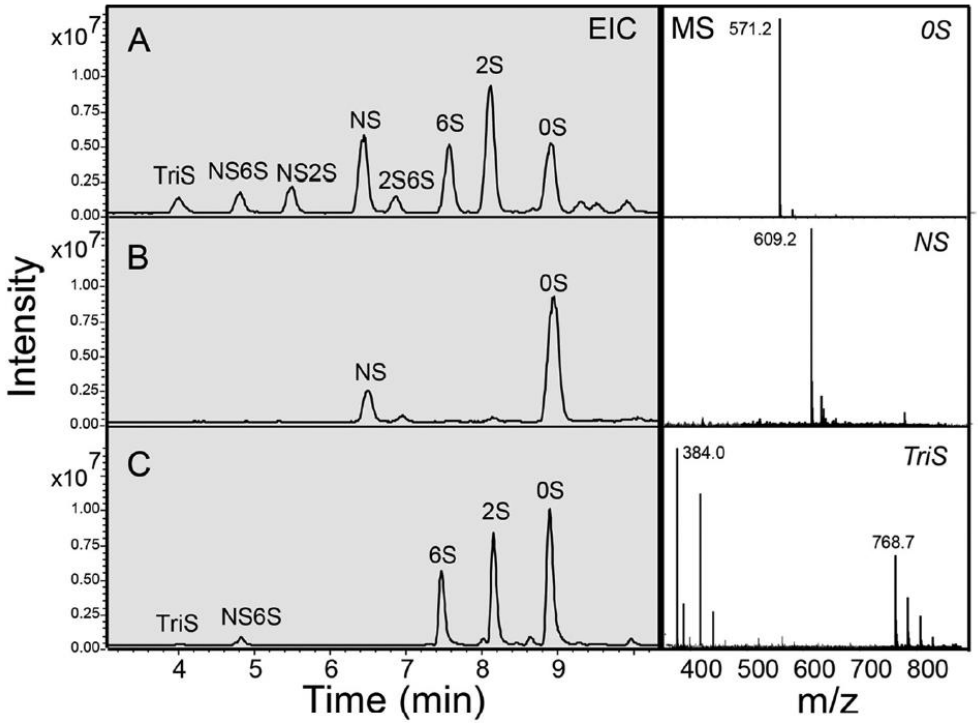

Figure 4.5. Disaccharide compositional analysis of synthetic HS. Disaccharides afforded through the treatment with heparin lyases 1, 2 and 3 were analyzed using HPLC-MS. Extracted ion chromatograms (EICs) were shown in the left, mass spectra are shown in the right (0S before any modification, NS after *N*-sulfonation, and TriS after *O*-sulfation.) Panel A. HPLC analysis of heparan sulfate disaccharide standards with detection by ion-trap mass spectrometer. Panel B. Disaccharide analysis of the *N*-sulfo precursor intermediate for synthetic heparan sulfate 4.4. Panel C. Disaccharide analysis of synthetic heparan sulfate 4.4 (complete with *O*-sulfotransferase modifications).

exhaustively treating each with heparin lyases, labeling with 2-aminoacridone (AMAC) and performing HPLC-MS. The resulting total ion chromatogram obtained by HPLC-MS analysis showed only 0S and NS disaccharides associated with each of the HS block co-polymers. The HPLC-MS analysis of the *N*-sulfo precursor of heparan sulfate **4.4** shown in Figure 4.5, for example, is consistent with its structure after compensating for the different response factors for the 0S and NS disaccharides. The experimentally observed disaccharide compositions of the N-sulfo precursor of heparan sulfates **4.4-7**, having a complex block structure correspond quite well to their theoretical compositions (Table 4.1). The data suggest that these polysaccharide compounds have the anticipated structures.

4.2.5. C_5 epimerization and *O*-sulfonation

The HS block copolymers were treated exhaustively with C_5-epimerase in the presence of 2-*O*-sulfotransferase, followed by 6-*O*-sulfotransferase-1 and 6-*O*-sulfotransferase-3. These enzymes all act in the *N*-sulfo domains to form fully modified high sulfo S-domains comprised of →GlcNS6S→IdoA2S→ repeating units. The 6-*O*-sulfotransferases could also modify the *N*-acetyl *N*-domains to a limited extent.

4.2.6. Characterization of heparan sulfate products

The disaccharide composition of the synthetic heparan sulfates obtained through C_5-epimerization and *O*-sulfonation were next analyzed by LC-MS (Figure 4.2 and Table 4.1). The disaccharide analysis of synthetic heparan sulfate **4.4** is shown in Figure 4.5. On treatment with heparin lyases, all the synthetic heparan sulfates afforded complex mixtures containing different amounts of the eight possible disaccharides (Table 4.1). The NS domains were comprised of TriS and NS6S, consistent with expectation. The NA domains were primarily of comprised 0S, 2S and 6S. High levels of 0S and 6S were anticipated. The exhaustive treatment of NA domains with C_5-Epi in the presence of 2-OST affording surprising amounts of 2S containing sequences most likely the result of the presence of unexpectedly large amounts of GlcA2S.

4.2.7. Bioactivity/cellular proliferation of synthetic heparan sulfates

The synthetic heparan sulfates were tested for cellular proliferation with the FGFR1c expressing cells in the presence of FGF1 or FGF2 in a 96-well plate[99]. The assay was performed in in a single 96-well plate in triplicate giving a small standard deviation confirming the precision of this measurement. First, a standard curve of the optical density (at 590 nm) as a function of *y* was constructed to demonstrate the linearity of the cellular proliferation assay (Figure 4.6A). The negative control, no added heparan sulfate, gave a baseline cell count of 4,000 ± 750 and 33,000 ± 1,100 for FGF1 and FGF2 signaling through FGFR1c, respectively (Figure 4.6B). The difference in baseline may be an indication that FGF2 may promote some signaling in the absence of GAG, though signaling is greatly augmented by addition of these polysaccharides. Porcine intestinal mucosal heparin served as a positive control showing a cell

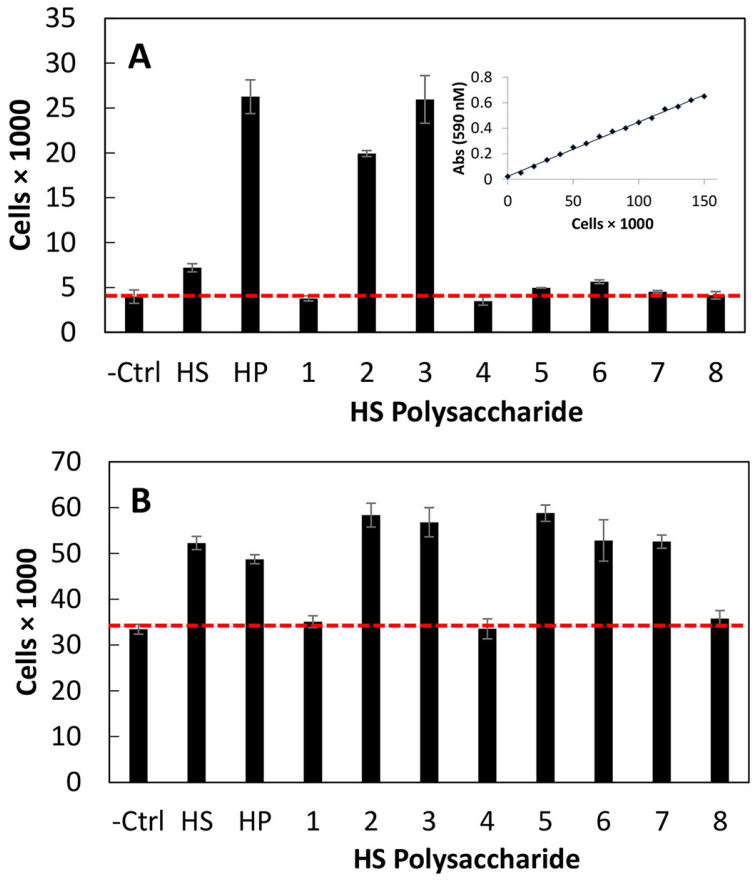

Figure 4.6. Fibroblast growth factor receptor bioactivity of natural and synthetic HS. Heparan sulfate-mediated FGF-FGFR signaling using a BAF3 cellular proliferation assay in a 96-well plate. Panel A. FGF1 signaling through FGFR1c. The inset shows a standard curve of cell proliferation assay. Panel B. FGF2 signaling through FGFR1c.

count of 26,000 ±1,900 through FGF1, but a significantly higher cell count of 49,000 ± 990 through FGF2. Next, porcine intestinal heparan sulfate was tested and while it showed a very low cell count of 7,000 ± 460 through FGF1, it unexpectedly showed a slightly higher signaling cell count of 52,000 ± 1,400 than observed for heparin through FGF2. This observation implies potential for the variability for natural-sourced GAGs.

As expected, synthetic heparan sulfate **4.2**, containing only a single NS domain with ~28 repeating disaccharides and terminated with a GlcNS residue at the non-reducing end, showed high FGF1 and FGF2 signaling activities (26,000 ± 330 and 49,000 ± 2,600, respectively) similar to that observed for heparin. Similarly, the two-domain synthetic heparan sulfate **4.3**, with an NA domain of ~15 repeating disaccharides at the reducing end and an NS domain of ~15 repeating disaccharides at the non-reducing end also showed potent FGF1 and FGF2 signaling activities (26,000 ± 2,600 and 57,000 ± 3,200, respectively) comparable with the positive control heparin.

Synthetic heparan sulfate **4.1** having a single NA domain of ~15 repeating disaccharides and terminated with a GlcA residue showed no FGF1 and FGF2 signaling activities (*i.e.* buffer alone baseline values), suggesting that a non-reducing terminal NS domain is critical for robust signaling.

Of particular interest were the signaling activities of synthetic heparan sulfates **4.4**-**8**, having NA domain of ~16 repeating disaccharides (derived from **4.1**, the inactive HS) at the reducing end with defined short variable length NS domains at their non-reducing ends. Synthetic heparan sulfates **4.7** and **4.8**, with reducing end NA domain of ~16 repeating disaccharides and non-reducing end NS domains of 4 and 5 repeating disaccharides were terminated with a GlcNAc residue. Synthetic heparan sulfates **4.7** and **4.8** behave similarly to synthetic heparan sulfate **4.1**, showing no FGF1 signaling activities. Interestingly, synthetic heparan sulfates **4.7** and **4.8** showed some FGF2 signaling activity. Synthetic heparan sulfates **4.4**, **4.5**, and **4.6** with non-reducing end NS domains of 2, 4 and 5 disaccharides and terminated with a GlcNS residue showed differential FGF1 and FGF2 signaling activities. Synthetic

heparan sulfates **4.5** and **4.6**, with longer 4 and 5 disaccharide non-reducing end NS domains showed low FGF1 and high FGF2 signaling activities. In contrast, synthetic heparan sulfate **4.4**, with the shortest non-reducing end NS domain showed no FGF1 and FGF2 signaling activities, suggesting that a non-reducing end terminal NS domain of at least 4-5 disaccharides is necessary for signaling. The BaF3 cell-based assay was performed a second time and confirmed the relative similar levels of signaling for the various synthetic heparan sulfates.

4.3. Discussion

Using our chemoenzymatic approach for the synthesis of heparan sulfate polysaccharides on simple aglycone acceptors, we had previously synthesized block polysaccharides having different

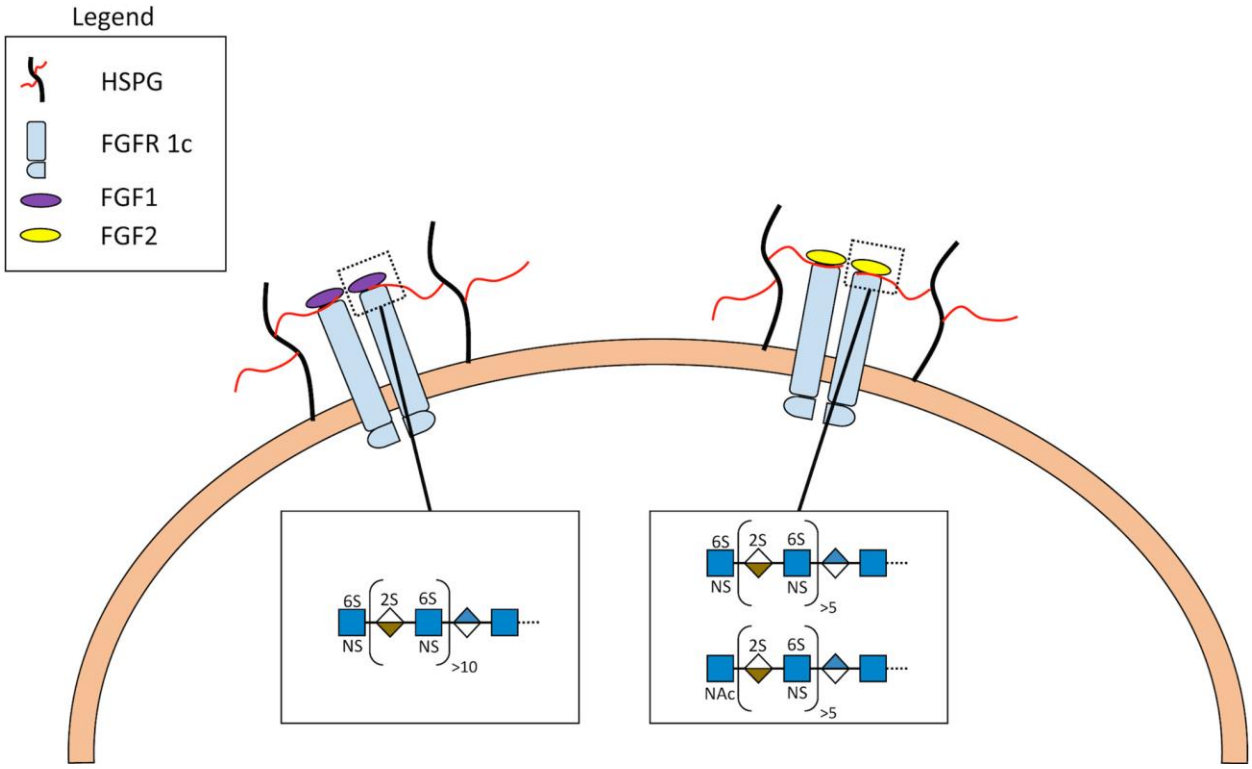

Figure 4.7. Proposed model and Structure/Activity Relationship of heparan sulfate mediated FGF-FGFR signaling through a FGF_2:$HSPG_2$:$FGFR1c_2$ complex. Heparan sulfate structural characteristics required to facilitate signaling complex formation differ between FGF1 and FGF2. FGF1 (*left*) requires a terminal NS domain of 10-11 disaccharides, and a terminal GlcNS for signaling. In contrast, FGF2 (*right*) utilizes a shorter non-reducing NS domain (~5 disaccharides) and is tolerant of a non-reducing end GlcNAc.

arrangements of uniform size NS and NA domains[99]. The symmetric FGF_2:HS_2:$FGFR_2$ ternary complex model[25] was best supported by the results of our prior study suggested that NS domains at the non-reducing end were required for FGF signaling[99]. Due to the topological constraints of the two heparan sulfate chains being attached to the core protein through their reducing ends, in the native FGF_2:$HSPG_2$:$FGFR_2$ complex the two heparan sulfate chains are attached core protein through their reducing ends, the interacting NS domains must be located on the non-reducing end of each heparan sulfate chain (Fig. 4.7). These two heparan sulfate chains are docked through their non-reducing ends into the basic canyon located on the top face of the FGF_2-$FGFR_2$ protein complex, called the heparin-binding site. Furthermore, the electrostatic and topological characteristics of the basic canyon are different for each protein signaling complex, *i.e.* the canyon of $FGF1_2$-$FGFR1c_2$ should be distinct from $FGF2_2$-$FGFR1c_2$[193].

Most SAR studies in the past focused on the structural characteristics of heparin or HS required for binding to various FGFs in the absence of receptor[194]. These studies provide only limited information since they do not consider the FGFR component of the interaction[193]. Furthermore, without a cellular component, such as employed in the BAF3 assay, it is always unclear whether binding is sufficient for signaling. Biochemical studies directly assessing FGF-FGFR signaling clearly support the symmetric FGF_2:HS_2:$FGFR_2$ ternary complex model in which the non-reducing ends of two HS chains are involved in the interaction[177,195]. Studies on chemically modified heparins and various chondroitin sulfates generally show heparin giving the greatest signaling among the heparin derivatives and dermatan sulfate (chondroitin sulfate B) giving the greatest signaling for the various chondroitin sulfates[196]. While these previous studies provide a better understanding of the SAR they provide no information about the precise structural features directly at the non-reducing ends of the chains involved in FGF signaling.

FGF2 signaling through FGFR1c has been shown to interact via the NS domains of HS chains[197] and FGF2 binding to FGFR1c[193]. The current study is focused on developing a more precise SAR for heparan sulfate-mediated signaling through one pair of homologous growth factor-receptor complexes, $FGF1_2$-$FGFR1c_2$ and $FGF2_2$-$FGFR1c_2$. A new paradigm for the chemoenzymatic synthesis of a variety of larger heparan sulfate chains, having between 16 and 28 repeating units, was required to carry out this study.

Our synthetic approach utilized three enzymatic steps employing UDP-sugar donors to build the polysaccharide backbone. The first step with a commercially available glycoside acceptor GlcA-pNP that was iteratively extended to the heparosan trisaccharide acceptors GlcA-GlcNAc-GlcA-pNP or GlcA-GlcNTFA-GlcA-pNP. In the second step, the trisaccharide acceptors were efficiently elongated through stoichiometrically controlled extension to afford either an NA block or the NTFA precursor of an NS block. In the third step, either a second block was added under stoichiometric control or a short oligosaccharide domain was added through iterative synthesis. For the end-capped polymers, the last residue added at the non-reducing end of the chain was controlled to be either GlcNAc or GlcNTFA.

Once the suitable polysaccharide precursors were assembled, the GlcNTFA residues were quantitatively converted to GlcNS, as could be demonstrated by NMR and through the use of HPLC-MS based disaccharide analysis. It is important to note that in comparison to the natural *N*-deacetylase *N*-sulfotransferase-based processes, our strategy for chemical installation of the N-sulfo groups is both (*i*) virtually complete, and (*ii*) allows strict placement and segregation of the NA and NS domains.

Final enzymatic treatment with C_5-Epi and 2-OST followed by 6-OST-1 and 6-OST-3 afforded synthetic heparan sulfates **4.1**-**8**. After confirming their structures, a 96-well plate BaF3 cell proliferation assay was conducted to afford a more detailed SAR of heparan sulfate signaling through $FGF1_2$-$FGFR1c_2$ or $FGF2_2$-$FGFR1c_2$.

The heparan sulfate binding site canyon in $FGF1_2$-$FGFR1c_2$ appears to prefer a longer non-reducing terminal NS than that of $FGF2_2$-$FGFR1c_2$ (Fig. 4.7). Porcine intestinal heparin strongly signals through $FGF1_2$-$FGFR1c_2$ as do synthetic heparan sulfates **4.2** and **4.3**, but porcine intestinal heparan sulfate and synthetic heparan sulfate **4.6** only weakly signal. This suggests the minimum NS binding domain of 4-5 disaccharide repeats terminated with a GlcNS residue for weak signaling and a NS binding domain of ~15 disaccharide sequences terminated with a GlcNS for robust signaling. In contrast, the heparan sulfate binding site canyon in $FGF2_2$-$FGFR1c_2$ appears to utilize a shorter non-reducing terminal NS domain. Robust signaling was observed for synthetic heparan sulfates **4.5** and **4.6,** but no signaling is observed for **4.4,** suggesting that the optimal length of the non-reducing terminal NS domain is >4-5 disaccharides with a terminal GlcNS residue. Furthermore, in contrast to $FGF1_2$-$FGFR1c_2$, signaling is observed for synthetic heparan sulfates **4.7** and **4.8**, with a non-reducing terminal NS domain of 4 or 5 disaccharides, respectively, with a terminal GlcNAc residue, demonstrating flexibility in the requirement for terminal NS domains.

4.4. Conclusions and future directions

The results of this study demonstrate that, at least for the $FGF1_2$-$FGFR1c_2$ and $FGF2_2$-$FGFR1c_2$ signal transduction complexes, it is possible to design and chemoenzymatically synthesize heparan sulfates that can selectively mediate signaling. Basically, in this case, our HS species with shorter NS terminal domains allow differential targeting of one FGF signaling complex over another homologous complex. The application of this approach to the other 20 members of the FGF family and the other 6 FGFRs needs to be explored. Ultimately, the use of synthetic heparan sulfates to selectively control FGF-FGFR signaling might play an important role in the control of stem cell differentiation, or developmental biology and might suggest new therapeutic approaches for the treatment of cancer and enhancement of wound healing.

4.5. Materials and methods

4.5.1. Defined polysaccharide synthesis

Polysaccharides containing either (i) alternating NA blocks of GlcA-GlcNAc- or NS-precursor blocks of GlcA-GlcNTFA repeating disaccharide units, or (ii) a NA block with various specific sugar extensions at the non-reducing termini were synthesized.

Initially, in all syntheses, a heparosan trisaccharide was prepared from the successive transfer of UDP-GlcNAc (or GlcNTFA) and UDP-GlcA, donors to GlcA-*p*-nitrophenyl glycoside by a series of addition reactions catalyzed by PmHS2. Here, the recombinant pmHS2 was constructed as an *N*-terminal fusion to $(His)_6$ using a PET-15b vector (Novagen) expressed in BL21 star (DE3) cells (Invitrogen).

In subsequent block reactions, 0.5-2 mM heparosan trisaccharide (GlcA-GlcNAc (or TFA)-GlcA-pNP) was used as an acceptor to maintain a continuous block as desired. All block reactions received 12-28 mM UDP-GlcA and, depending on the desired block, either 25 mM UDP-GlcNAc or 12-20 mM UDP-GlcNTFA (for preparing the N- or S-domain, respectively)[78,105]. Reaction buffer contained 50-130 mM HEPES, pH 7.2, and 1 mM $MnCl_2$. Each reaction received 1 μg/μL purified MBP-Chimera G enzyme. This enzyme, PmHS2(1–167) PmHS1(134–318) PmHS2(353–651), was selected as the catalyst for NS block polysaccharide synthesis because it exhibits at least a 10- and 2-fold higher specific activity using UDP-GlcNAc and UDP-GlcNTFA when compared with PmHS2, respectively. Also, Chimera G is roughly twice as acceptor-dependent as PmHS2 due to a lower level of *de novo* synthesis (*i.e.*, the initiation with UDP-sugars only, not an exogenously supplied oligosaccharide). Each step was incubated at 30°C for 16 h. After polymerization was complete, the bulk of the enzyme was removed by extraction with an equal volume of *n*-butanol and vortexing, followed by phase separation via centrifugation at 14,000 × *g* for 5 min. The various HS precursors in the lower aqueous phase were then purified as described later.

The molecular mass of each block section and the total polymer was determined by a combination of polyacrylamide gel/Alcian blue staining analyses with size-defined standards[177,198], size exclusion chromatography coupled to multi-angle light scattering[179], and/or by LC/MS[198].

The precursor for HS **4.2** was isolated from the extracted reaction mixture using strong anion exchange (SAX) chromatography on Sepharose Q resin (GE) with an ammonium formate step gradient (0.2 M wash for 10 column volumes, then an elution with 0.7 M, 0.8 M and 0.9 M for 1.5 column volumes each). The pooled 0.7 M-0.9 M eluates were then frozen and the volatile salt removed by repeated lyophilization from water. It is important to note that the SAX step was employed here instead of paper chromatography (described later) for this long TFA-containing block because polymers composed solely of this more hydrophobic heparosan derivative migrated away from the origin thus complicating facile and efficient recovery.

The reaction mixture containing the precursor for HS polysaccharide **4.1** was used as the starting material for targets **4.3**-**8**. To create a more homogenous polymer with equivalent and defined non-reducing terminus, the repeating GlcNAc-GlcA-pNP polysaccharide **4.1** product was further treated with a synthase and one UDP-sugar, and then purified to reduce its size heterogeneity. First, the HS precursor was end-capped to ensure all chains terminated with a GlcA residue via reaction with ~5 molar equivalents of UDP-GlcA and 0.5 µg/µL wild-type MBP-PmHS1 enzyme[82] to create a uniform population of NA polysaccharide acceptor. Second, a SAX chromatography step on Sepharose Q resin with a linear gradient (0.15 M wash for 5 column volumes, then a gradient to 1M over 10 column volumes in 25 min) followed by repeated lyophilization of the target fractions from water was employed. The end-capping and SAX steps were then repeated in tandem for another cycle. The final central SAX peak was harvested to reduce the sample complexity from the original ~12 major species to ~8 major species (where 'major' is defined as any species that is present at an intensity level of at least 30% or more of

the most abundant peak ion) as observed by LC-MS[199]. The MW of the central peak polymer of resulting precursor **4.1** was 6.4 kDa by LC-MS.

The precursor for HS **4.3** (made in a reaction of the pre-SAX-purified precursor for HS **4.1** as the acceptor for reactions with UDP-GlcNTFA and UDP-GlcA donors) was isolated by preparative descending paper chromatography (65:35 ethanol:1 M ammonium acetate, pH 5.5, development solvent with Whatman 3MM); the polysaccharide remains at the origin of the paper strip while any excess UDP-sugars and the UDP byproduct migrate substantially down the paper. The origin with the target was cut out, air-dried, washed with ethanol, dried again, then eluted with water. The samples were then frozen and the volatile salt removed by three cycles of lyophilization from water (typical overall yield >95%).

To create precursors for HS **4.4**-**8**, extensions ranging from 5 to 11 monosaccharide units were sequentially added to the non-reducing terminus of the SAX-polished, GlcA end-capped precursor to HS **4.1** acceptor. These step-wise addition reactions (*e.g.,* first add UDP-hexosamine, purification, then add UDP-GlcA, etc.) used 1.2 molar equivalents of donor and 1 μg/μl of the appropriate monofunctional Chimera G catalyst (*e.g.,* first the hexosamine-transferase, then the GlcA-transferase, etc.) under the same general reaction conditions as described for the block polymers. The choice of hexosamine in any position of the chain was controlled by the UDP-sugar, either UDP-GlcNAc or UDP-GlcNTFA, employed in a given step. At some steps, an intermediate polymer was split into two parallel reactions that received either one or the other hexosamine precursor thus affording control of the *N*-sulfation status of the terminal non-reducing sugar.

After each step-wise sugar addition, the target molecule was isolated by batch mode paper chromatography; in this high capacity method, the polysaccharide was spotted onto squares of Whatman 3MM paper at ~ 0.3 mg/cm^2, air-dried, and washed with 8 changes of 65:35 ethanol:1M ammonium acetate, pH 5.5 (15-45 min each) to remove excess UDP-sugars and UDP. The squares were

then washed with ethanol twice (10 min each), air-dried, then eluted with water. The volatile salt was removed by repeated lyophilization from water as described before.

4.5.2. De-*N*-trifluoroacetylation and *N*-sulfonation

Briefly, the *N*-trifluoroacetylated containing block copolymer was dissolved in a solution of 1:1:0.5 MeOH:H_2O:Et_3N at a concentration of 1 mg/ml and stirred overnight at room temperature to expose the amine functionality protected by the TFA group. The de-*N*-trifluoroacetylated block co-polymer was then loaded onto a 3,000 MWCO Amicon Ultra spin unit and washed with distilled H_2O three times at 14,000 × *g* for 10 min. The retentate containing the de-*N*-trifluoroacetylated block copolymer was recovered and lyophilized.

N-sulfonation of block copolymers was then performed according to a modified procedure from Maruyama *et al.*[200] using $NMe_3{\cdot}SO_3$ as the sulfonating agent. The lyophilized de-*N*-trifluoroacetylated polysaccharide was then dissolved in distilled H_2O (1 mg/ml) at pH 7. Na_2CO_3 and $NMe_3{\cdot}SO_3$ were then added in a 3:1 w/w ratio to polysaccharide (*e.g.*, 3 mg each of Na_2CO_3 and $NMe_3{\cdot}SO_3$ for 1 mg of starting polymer) were added and stirred for 12 h at 45 °C. A second equivalent portion of Na_2CO_3 and $NMe_3{\cdot}SO_3$ was then added to the reaction and stirred for an additional 12 h at 45 °C. The reaction mixture was loaded into a 3000 MWCO Amicon Ultra spin unit and washed with distilled H_2O three times at 14,000 × *g* for 10 min. The retentate containing the *N*-sulfonated polysaccharide was recovered and lyophilized to afford a white fluffy powder.

4.5.3. NMR characterization of HS block copolymer intermediates

Analysis of the resulting block copolymers using *PAGE* confirmed that the polymer backbone remained intact following the de-*N*-trifluoroacetylation and *N*-sulfonation reactions. The four block co-polymers were also characterized by one-dimensional (1D) ^1H nuclear magnetic resonance (NMR) spectroscopy after the chemical *N*-sulfonation step. All samples were dissolved in 400 µl D_2O (99.9 %,

Sigma-Aldrich, St. Louis, MO) and lyophilized three times to remove the exchangeable protons. The samples were re-dissolved in 400 µL 99.9 % D_2O and transferred to NMR microtubes. All NMR experiments were performed at 298 K on Bruker Advance II 600 MHz instrument with Topspin 2.1.6 software. One-dimensional ^1H spectra were recorded for 32 scans.

4.5.4. Enzymatic *O*-sulfonation

The *N*-sulfonated polysaccharide backbones were subjected to the modifications by C_5-Epi, 2-OST and 6-OST-1 and -3 to introduce IdoA residues, 2-*O*-sulfo groups, and 6-*O*-sulfo groups, respectively. For the C_5-Epi and 2-OST modifications, the reaction was carried out in one-pot format to drive the reversible epimerization reaction forward. Briefly, the backbone polysaccharides (0.1 mg/ml) were incubated with C_5-Epi (0.2 mg/ml) in a buffer containing 1 mM $CaCl_2$ and 50 mM MES pH 7.0 at 37°C. After 30 min incubation, 2-OST (0.1 mg/ml) and PAPS (100 µM) was added to the reaction mixture. The reaction mixture was then incubated at 37°C overnight. The product was purified using DEAE Sepharose column chromatography as described previously[173]. After 2-*O*-sulfonation, the product (0.1 mg/ml) was further modified with 6-*O*-sulfotransferase 1 (0.1 mg/ml) and 6-*O*-sulfotransferase 3 (0.1 mg/ml) in 50 mM MES, pH 7.0, and PAPS (100 µM) at 37°C overnight. The 6-*O*-sulfonated products were then also purified through a DEAE Sepharose column.

4.5.5. Polysaccharide purification

Each chemoenzymatically synthesized HS sample was freeze-dried and then dissolved in endotoxin-free water at a concentration of 2-8 mg/ml. Each HS sample (0.8-3.1 mg) was bound on the Vivapure® Q Maxi H mini-SAX columns that had been pre-equilibrated with water by centrifugation at 2,000 × *g* for 10 min. Columns were washed thrice with 400 µl water and thrice with 400 µl 0.2 M aqueous NaCl. The HS was then eluted by washing thrice with 400 µl of 1.0 M and thrice with 2.0 M aqueous NaCl. The combined eluted samples were desalted by 1000 MWCO dialysis membranes and

filtered through 0.2 µm syringe filters. The recovered samples were subjected to carbazole assay[201] to measure each HS used to prepare stock solutions for chemical and biological analyses.

4.5.6. Disaccharide compositional analysis of precursor and block copolymer products by HPLC

The disaccharide compositions of block co-polymers were analyzed by high-performance liquid chromatography-mass spectrometry[161]. Heparosan oligosaccharides (1-10 µg) were digested by adding 100 µl digestion buffer (50 mM ammonium acetate containing 2 mM calcium chloride adjusted to pH 7.0) and recombinant heparin lyase I, II, III (10 mU each in Tris-HCl buffer, pH 7.0). The samples were digested at 37 °C overnight. The reaction was terminated by eliminating the enzyme via trapping in the retentate of 3 kDa MWCO spin columns. The filter units were washed twice with 300 µl distilled water and the filtrates with disaccharides were collected, combined, and lyophilized. The dried digested HS samples were AMAC-labeled by adding 20 µl of 0.1 M AMAC in DMSO/acetic acid (17:3, v/v) incubating at room temperature for 10 min, followed by adding 20 µl of 1 M aqueous sodium cyanoborohydride and incubating for 1 h at 45 ℃. A mixture containing all 8 disaccharide standards prepared at 12.5 ng/µl was similarly AMAC-labeled and used for each run as an external standard. After the AMAC-labeling reaction, the samples were centrifuged and each supernatant was recovered.

For the disaccharide analysis of intermediate samples before extensive purification, LC-MS analyses were performed on an Agilent 1200 LC/MSD Instrument (Agilent Technologies, Inc., Wilmington, DE) equipped with a 6300 ion-trap and a binary pump. LC was performed at 45 °C using an Agilent Poroshell 120 ECC18 (2.7 µm, 3.0 × 50 mm) column. Mobile phase A was 50 mM ammonium acetate aqueous solution, and the mobile phase B was methanol. The flow rate was 300 µl/min. The concentration of A increased from 5% to 45% during 10 min, then rose to 100% B in the following 0.2 min, and a 4 min hold at 100% B was applied to elute all compounds. The mass spectrometer was operated in negative ionization mode with a skimmer potential of -40.0 V, a capillary exit of -40.0 V, and

a source temperature of 350 ℃. Mass range of the spectrum is 300-900 m/z. Nitrogen (8 l/min 40 psi) was used as drying and nebulizing gas.

For disaccharide analysis of samples after purification, a triple quadrupole mass spectrometry system equipped with an ESI source (Thermo Fisher Scientific, San Jose, CA) was used as a detector. The online MS analysis was in the Multiple Reaction Monitoring (MRM) mode. The conditions and collision energies for the all of the disaccharides MRM transitions are as described before[202].

4.5.7. BaF3 cell culture

BaF3 cell cultures were grown in RPMI-1640 media supplemented with 10% newborn calf serum, 5 ml PenStrep, and 50 μM β-mercaptoethanol, and 400 μg/ml G418, as previously described[186,191]. In the absence of the FGF and GAG combination, BaF3 cells can be grown with the addition of 5 ng/ml murine IL3 (Life Technologies) to the media. Cells were grown at 37°C with 5% CO_2 in T75 culture flasks. Cells were passaged every three days, with initial seeding densities of 2×10^5 cells/ml.

Prior to use in the signaling assay, cells were centrifuged at $200 \times g$ for 5 min, spent media removed through vacuum aspiration and the cell pellet washed with 5 ml of IL3-free RPMI media. The centrifugation and washing step were repeated four times to remove any residual IL3. The resulting cell pellet was then used in the signaling assay below.

4.5.8. BaF3 signaling assay

RPMI media with FGF1 or FGF2 (5 μM final) or no growth factor was added to the washed BaF3 cell pellet to form a suspension (5×10^6 cells/ml) that was dispensed into a 96-well plate at 50,000 cells/well. Solutions of the individual HS block copolymers or heparin (positive control) in PBS were added to obtain a final concentration of 2 μg/l. The negative control was PBS vehicle only. The plate was incubated at 37˚C/5% CO_2 for 24 h. Each sample was tested in triplicate wells.

Cell proliferation was measured with a 3-(4,5- dimethylthiazol-2-yl) -2,5-diphenyl tetrazolium bromide (MTT) assay. Briefly, 40 µl of a 2.5 mg/mL MTT solution was added to each well, and incubated for 3 hours. Then 100 µl of 10% sodium dodecyl sulfate (SDS) in 0.01 N HCl was added to each well and gently shaken overnight to dissolve the formazan crystals. Optical density was measured at 590 nm and 690 nm as a control, which was subtracted from the absorbance at 590 nm to give a background corrected optical density. Optical density was correlated to cell count using a standard curve.

5. HEPARAN SULFATE IN HUMAN HEALTH AND DISEASE

5.1. Introduction

The endothelial glycocalyx is a heparan sulfate (HS)-rich layer of glycosaminoglycans and associated proteoglycans that line the micro- and macro-vascular intima. *In vivo*, glycocalyx glycosaminoglycans become highly hydrated, forming a substantial gel-like endothelial surface layer (ESL) that projects 0.5 μm to >10 μm into the vascular lumen[200]. An intact ESL contributes to the endothelial barrier to fluid and protein, regulates leukocyte-endothelial adhesion, and transduces fluid shear stress into endothelial nitric oxide synthesis[201]. Accordingly, a number of acute and chronic vascular diseases are characterized by degradation of the glycocalyx/ESL (here forth collectively referred to as the "ESL"). For example, rapid induction of endothelial heparanase (a TNFα-activated, HS-specific mammalian endoglucuronosyl hydrolase) degrades ESL HS during sepsis, leading to lung[202] and kidney[205] injury.

Given the importance of ESL integrity to vascular homeostasis, endothelial cells would be expected to rapidly repair a damaged ESL. However, little is known about the endogenous mechanisms driving ESL reconstitution. Mouse cremasteric ESL recovery occurred within 5 days of intravenous heparinase-III (a bacterial HS-specific endoglucuronosyl lyase) or intrascrotal TNFα[206]. It is unclear if a similarly slow pace of ESL recovery occurs within the lung, an organ characterized by a thicker ESL[202] and greater functional susceptibility to edema. Indeed, in vitro studies of endothelial cells under shear stress demonstrate that glycocalyx recovery is capable of occurring as rapidly as 12 h after enzymatic HS degradation[207].

Portions of this chapter previously appeared as: Yang, Y. *et al.* Fibroblast Growth Factor Signaling Mediates Pulmonary Endothelial Glycocalyx Reconstitution. *Am. J. Respir. Cell Mol. Biol.* **56,** 727–737 (2017)., and Schmidt, E. P. *et al.* Urinary Glycosaminoglycans Predict Outcomes in Septic Shock and Acute Respiratory Distress Syndrome. *Am. J. Respir. Crit. Care Med.* **194,** 439–449 (2016).

As HS is a critical contributor to ESL structure and function[202], ESL reconstitution likely requires induction of HS biosynthesis. We hypothesized that pulmonary ESL reconstitution would occur rapidly after (non-septic) HS degradation with heparinase-III, reflecting the critical homeostatic functions of an intact pulmonary ESL. We hypothesized that ESL repair would be promoted by activation of endothelial growth factor signaling by highly-sulfated HS fragments released into the circulation during ESL degradation. Finally, we hypothesized that these homeostatic processes of ESL reconstitution would be impaired during sepsis, suggesting that septic vascular dysfunction may arise not only from ESL degradation but also delayed reconstitution.

Today, sepsis and its associated infections remain the major cause of in-hospital death in the United States[208] and intensive care units (ICUs) worldwide[209,210]. As sepsis mortality increases with the incremental onset of organ failure[211], early identification of at-risk organ systems may enable personalization of therapies that could benefit patients with evolving sepsis.

There is increasing appreciation for the importance of the endothelial glycocalyx to lung[202] and kidney[205,212] homeostasis. Accordingly, dysfunction of the endothelial glycocalyx may contribute to the tissue edema, aberrant vascular tone, and inappropriate inflammation characteristic of septic organ injury.

Using a mouse model of polymicrobial sepsis, we recently observed septic induction of renal heparanase, a heparan sulfate-specific endoglucuronidase[205]. Renal heparanase activation was associated with fragmentation of glomerular HS, leading to loss of glomerular filtration. This early, pathogenic induction of glomerular heparanase could be detected in mice via urinary assays, including HS degradation activity[205].

We recently developed a high-sensitivity, mass spectrometry-based approach to detect and characterize fragmented GAGs within biologic samples from critically-ill patients[202]. This high-sensitivity approach allows for not only quantification/characterization of HS fragments, but detection of other

glycocalyx GAGs including chondroitin sulfate (CS, a sulfated linear polysaccharide comprised of repeating hexuronic acid-*N*-acetylgalactosamine disaccharides) and hyaluronic acid (HA, an unsulfated linear polysaccharide of repeating glucuronic acid-*N*-acetylglucosamine disaccharides).

Building on these mechanistic animal data (and leveraging our newly-developed GAG analytical techniques), we conceived the second of two studies presented below. We hypothesized that septic shock in humans would be associated with early induction of glomerular heparanase, leading to pathologic degradation of the glomerular endothelial glycocalyx and excretion of HS fragments into the urine. Urinary HS and heparanase activity would therefore be associated with the development of kidney injury and, ultimately, mortality in septic shock. We performed a prospective pilot study of patients with septic shock to test this hypothesis. We compared our findings to samples obtained from cohorts of critically ill trauma[202] and acute respiratory distress syndrome (ARDS) patients[213].

The first of these studies identifies a fibroblast growth factor-mediated mechanism governing the reconstitution of pulmonary ESL in response to septic injury[203]. A second complementary study takes a clinical approach, drawing on data from actual sepsis patients. This study found urinary GAGs were robust predictors of sepsis-related mortality, which led to the development of a cost effective prognostic method for identifying high-risk patients[204].

5.2. Results

5.2.1. Homeostatic pulmonary ESL reconstitution occurs rapidly after heparinase-III-mediated degradation but is delayed after sepsis-associated degradation

The pulmonary ESL is a substantial endovascular structure with HS-dependent size and function[202]. To determine the mechanisms underlying ESL recovery after non-septic HS degradation, we treated mice with intravenous heparinase-III, a HS-specific endoglucuronosyl lyase that rapidly degrades the pulmonary ESL[202,214]. Using a previously-established, intravital microscopy-based dextran exclusion technique[215], we observed that the pulmonary ESL is completely reconstituted within 24 h of

heparinase-III-mediated degradation (Fig 5.1a). This rapid ESL reconstitution coincided with induction of pulmonary EXT1, an enzyme necessary for HS polymerization[216]. The increase in lung homogenate EXT1 protein (Fig 5.1b) occurred before a statistically-significant increase in lung homogenate EXT1 mRNA (Fig 5.1c), potentially reflecting both transcriptional and post-transcriptional control of EXT1 expression. HS synthesis was necessary to pulmonary ESL recovery, as timely reconstitution did not occur in mice treated with the artificial glycan 4-fluoro-*N*-acetyl-glucosamine (4-F-GlcNAc, Fig 5.1d), which interrupts EXT1-mediated HS polymerization[217,218]. While heparinase-III alone was insufficient to induce lung edema 6 h (wet/dry ratio 4.42 ± 0.25 in heparinase-III treated wild-type mice; 4.40 ± 0.52 in heat-inactivated heparinase-III-treated wild-type mice, n =4., p = 0.96) or 24 h (Fig 5.1e)

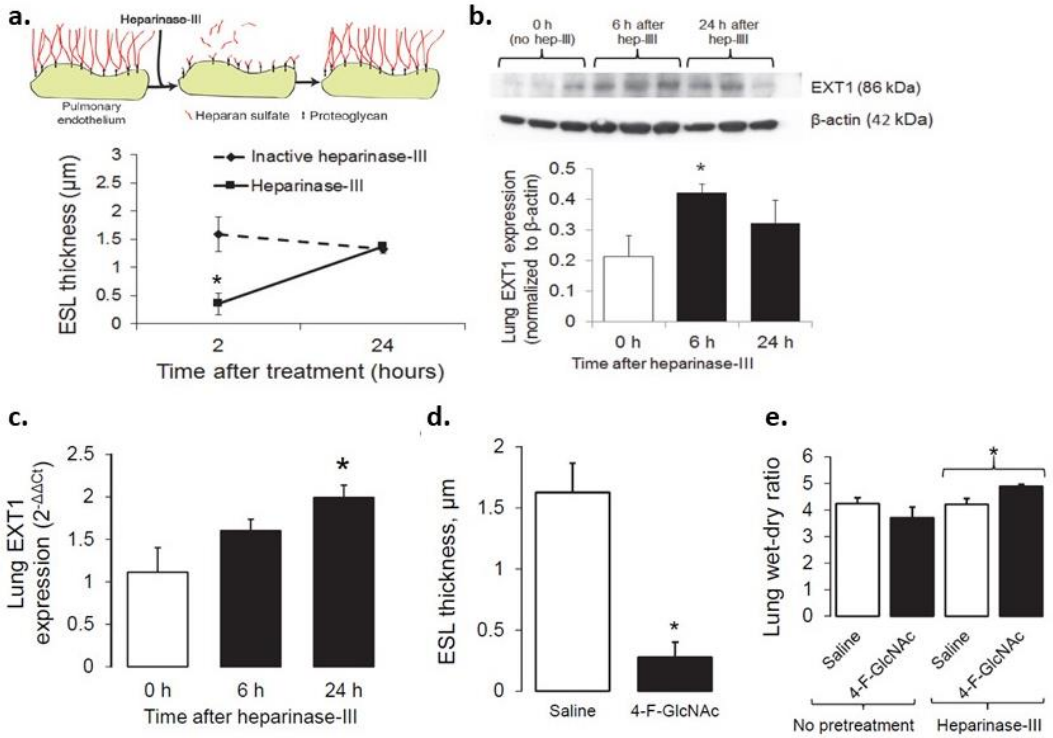

Figure 5.1. Homeostatic pulmonary ESL reconstitution occurs rapidly after heparinase-III-mediated degradation. (a) Thickness of the heparan sulfate-rich pulmonary ESL (measured via intravital microscopy) rapidly declines after non-septic degradation (heparinase-III, 1 unit *intravenously* administered (IV)) but recovers within 24 h. Lungs from heparinase-III-treated mice demonstrated increased protein (b) and mRNA (c) expression of EXT1, a glucosyltransferase required for heparan sulfate synthesis. EXT1 is necessary for homeostatic ESL reconstitution, as inhibition of EXT1 activity after heparinase-IIII-mediated ESL degradation (4-F-GlcNAc, 2.5 mg IP 6, 12, and 18 h after heparinase-III) delayed ESL recovery (d) and induced lung edema (e) 24 h after ESL degradation. n > 3 per group, * $p < 0.05$

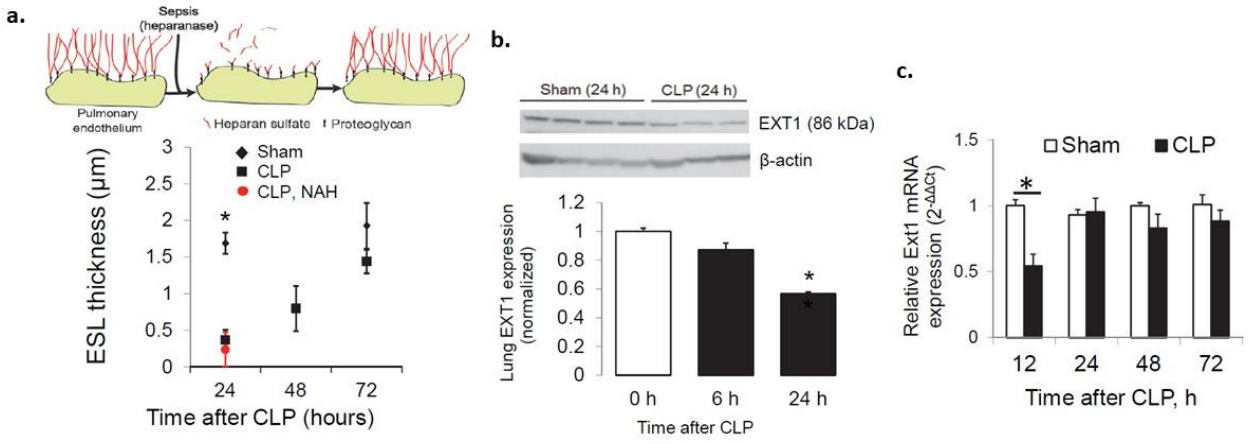

Figure 5.2. Homeostatic pulmonary ESL reconstitution occurs slowly after sepsis-mediated degradation. In contrast to heparinase-III, cecal ligation and puncture (CLP)-induced ESL degradation (a process mediated by heparanase, a mammalian heparinase-III analog) is delayed (f). ESL recovery 24 h after CLP is not accelerated by heparanase inhibition (150 μg *N*-desulfated re-*N*-acetylated heparin (NAH) administered subcutaneously 6, 12, and 18 h after CLP), indicating that delayed reconstitution is not a function of ongoing septic heparan sulfate degradation. Consistent with impaired ESL recovery, lungs from CLP-treated mice demonstrated decreased EXT1 protein (g) and mRNA (h) expression. n > 3 per group, * $p < 0.05$

after injection, heparinase-III treatment followed 6 h later by 4-F-GlcNAc-mediated inhibition of HS polymerization induced pulmonary edema at 24 h (Fig 5.1e), demonstrating that processes of pulmonary ESL recovery are homeostatic.

After determining the rapidity of homeostatic pulmonary ESL reconstitution after non-septic degradation, we sought to determine if similar recovery occurs during sepsis. We have previously demonstrated that sepsis (as modeled in mice using cecal ligation and puncture, CLP) induces expression of mammalian heparanase, an enzyme that degrades pulmonary ESL thickness with similar rapidity (i.e. < 30 min) as heparinase-III[202]. Despite similar rapidity of degradation, pulmonary ESL reconstitution after CLP was significantly delayed (72 h, Fig 5.2a) in comparison to heparinase-III (24 h, Fig 5.1a). Administration of the heparanase inhibitor *N*-desulfated, re-N-acetylated heparin (NAH) after septic ESL degradation did not accelerate ESL reconstitution (Fig 5.2a), suggesting that delayed ESL reconstitution during sepsis was not simply due to ongoing degradation but instead reflected aberrant ESL repair. Indeed, CLP-treated mice demonstrated an early loss of pulmonary EXT1 expression (Fig 5.2b-c),

contrasting EXT1 induction observed after heparinase-III (Fig 5.1b-c). CLP-treated mice eventually demonstrated return of baseline pulmonary EXT1 expression (Fig 5.2c), coincident with ESL recovery. CLP-treated mice had no evidence of compensatory induction of pulmonary Exostosin 2 (EXT2) or Exostosin-like 2 (EXTL2), salvage HS polymerases previously noted[219] to produce (albeit-truncated) HS in EXT1-deficient cells (data not shown).

5.2.2. FGFR1 mediates pulmonary ESL reconstitution after heparinase-III but is suppressed after CLP

We first sought to define the mechanisms responsible for rapid pulmonary ESL reconstitution after heparinase-III to determine the mechanisms underlying delayed pulmonary ESL reconstitution during sepsis. Recent reports have implicated fibroblast growth factor receptors in endothelial recovery after vascular injury[220]. Fibroblast growth factor receptor 1 (FGFR1) is the predominant FGFR expressed in pulmonary endothelial cells[221]. Accordingly, heparinase-III-mediated ESL degradation was followed by increased pulmonary FGFR1 expression (Fig 5.3a). Pulmonary endothelial FGFR1 induction after heparinase-III was ESL-reparative, as Tie2-Cre FGFR-1/2f/f mice (which lack endothelial FGFR1[220]) demonstrated absence of pulmonary EXT1 induction (Fig 5.3b) and delayed ESL reconstitution (Fig 5.3c) after heparinase-III. These transgenic investigations were complemented by experiments using AZD4547, a high-affinity FGFR1 inhibitor[222] (Fig 5.3d-e). Similar to 4-F-GlcNAc (Fig 5.1e), AZD4547-induced impairment of ESL reconstitution induced lung edema, again suggesting that FGFR1/EXT1-mediated ESL reconstitution was homeostatic (data not shown). However, this partial impairment in reconstitution was not sufficient to cause lung edema in Tie2-Cre FGFR-1/2f/f mice, suggesting the presence of compensatory lung-protective pathways in these mice constitutively lacking endothelial FGFR1 signaling.

In contrast to the reparative induction of FGFR1 in wild-type mice after heparinase-III-mediated ESL degradation, FGFR1 expression was suppressed after CLP-mediated ESL degradation (Fig 5.4a). We

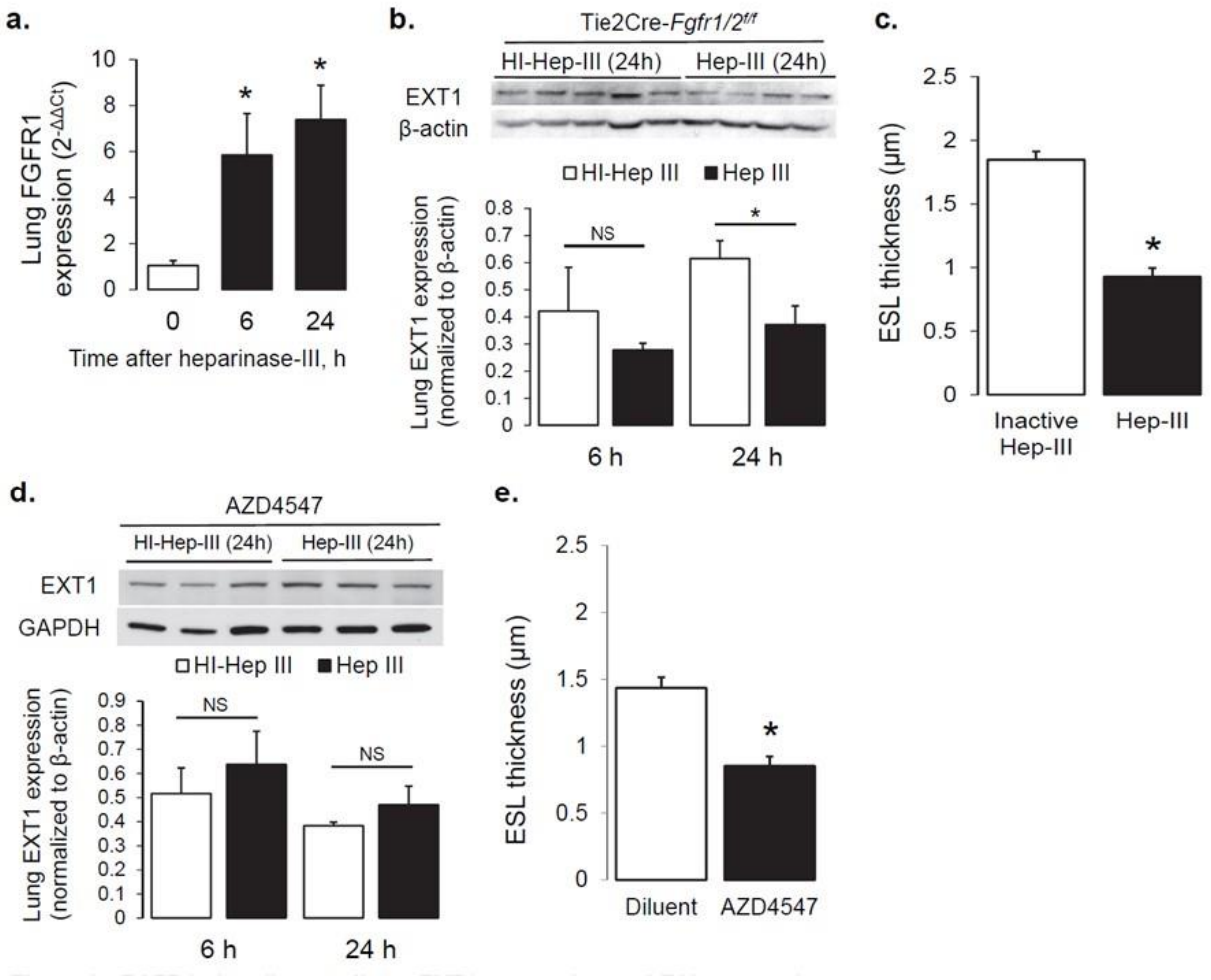

Figure 5.3. FGFR1 signaling mediates EXT1 expression and ESL reconstitution after heparinase-III. (a) Heparinase-III treatment (1 unit IV at time = 0) induces pulmonary expression of FGFR1 within wild-type C57BL/6 mice. (b) Tie2Cre-*Fgfr1/2*f/f mice, which feature loss of pulmonary endothelial FGFR1, demonstrated loss of EXT1 expression after heparinase-III (1 unit IV, (b)) and, accordingly, delayed 24 h ESL recovery (c) in comparison to heat-inactivated heparinase-III (HI-Hep-III). Western blot images (b, d) demonstrate one mouse per lane. Pretreatment of wild-type C57BL/6 mice with the FGFR1 inhibitor AZD45457 (12.5 μg/g body weight by gavage 3h prior to heparinase-III) similarly prevented EXT1 induction (d) and delayed 24 h ESL reconstitution (e). n > 3 per group, * $p < 0.05$.

treated primary mouse lung microvascular endothelial cells (MLMVECs) with lipopolysaccharide (LPS) and observed decreased endothelial FGFR1 expression to determine if this septic loss of FGFR1 expression occurred within the pulmonary endothelium (Fig 5.4b).

Previous studies have demonstrated that endothelial FGFR1 expression can be decreased by miR-16[223], an endothelial-expressed microRNA previously observed in the plasma of humans[224] and animals[225] with sepsis. We similarly noted a trend (p = 0.09) towards increased plasma miR-16 12

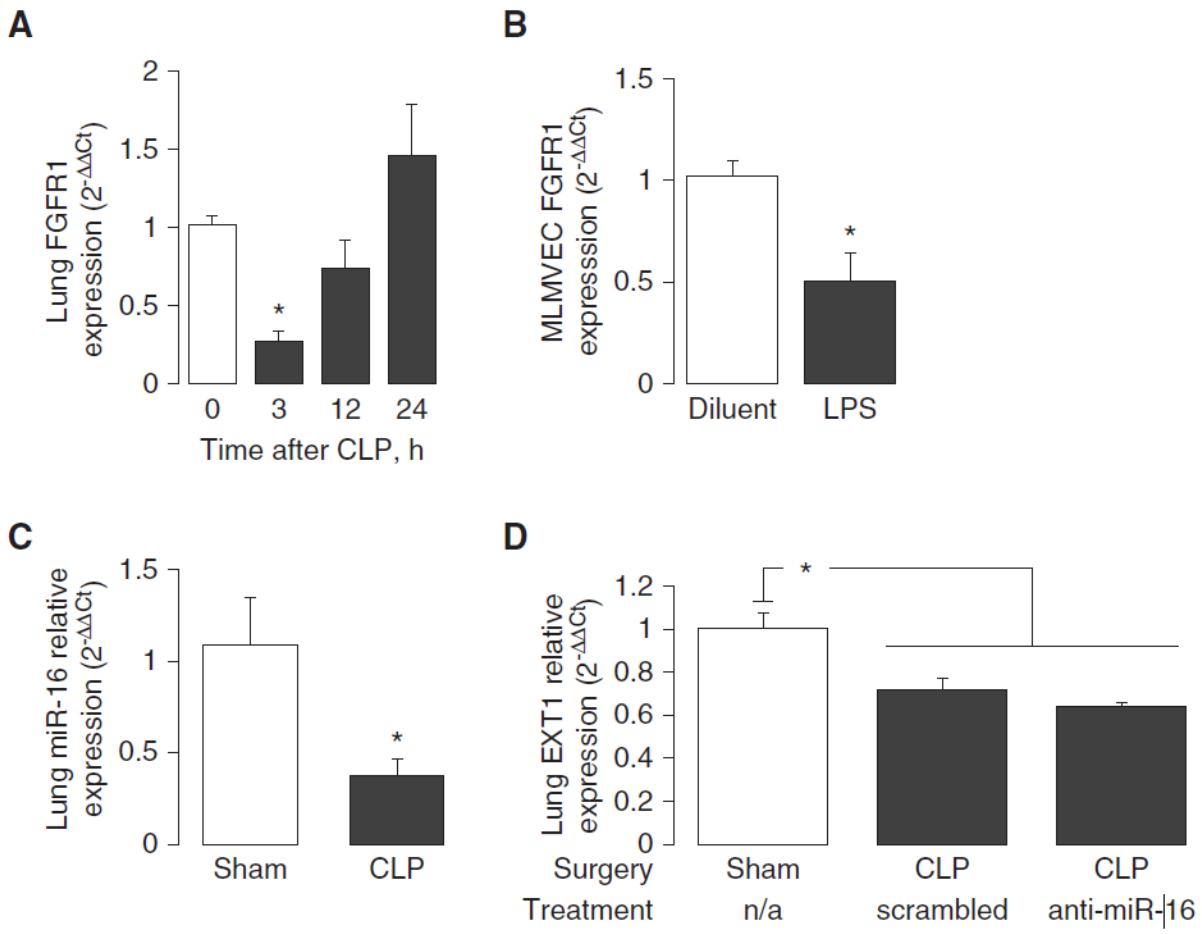

Figure 5.4. Sepsis is associated with suppression of pulmonary FGFR1. (A) In contrast to heparinase-III treatment, CLP was associated with loss of pulmonary FGFR1 expression. (B) Mouse lung microvascular endothelial cells (MLMVECs) similarly demonstrated diminished FGFR1 mRNA 6 h after LPS treatment (10 mg/ml 3 45 min, followed by media change). (C) Expression of microRNA (miR)-16 (a sepsis-associated miR that suppresses FGFR1) was decreased within the lung 3 h after CLP, a time point characterized by maximal FGFR1 suppression; expression normalized to sham and housekeeping miR103 (22ΔΔCt). (D) Accordingly, antagonism of miR-16 with an antimiR (5 μg/g body weight intraperitoneally, given 12 h before CLP) had no effect on EXT1 expression 12 h after CLP. Similar findings were noted with 25 μg/g anti-miR dosing (data not shown). N>3 per group; *P<0.05 compared with sham/diluent/untreated control. All graphs demonstrate mean values (±SE). n/a, not applicable.

h after CLP (data not shown). However, pulmonary miR-16 expression was decreased 3 h after CLP (Fig 5.4c), suggesting that miR-16 was unlikely to be active in the lung concurrent with CLP-induced loss of pulmonary FGFR1 (Fig 5.4a). Furthermore, treatment of mice with a miR-16 blocking oligonucleotide had no impact on pulmonary expression of EXT1 (Fig 5.4d) 12 h after CLP, indicating that septic loss of pulmonary EXT1 occurred in a miR-16-independent fashion.

5.2.3. HS fragments released after heparinase-III-mediated ESL degradation activate FGFR1 signaling

In human diseases characterized by ESL degradation, HS fragments are released into the circulation[226]. We previously observed[31] that these plasma HS fragments include hexasaccharides to octasaccharides (degree of polymerization 6 to 8, dp6 to dp8) as well as larger-weight fractions, with high degrees of glucosamine amino-sulfation (*N*-sulfated, Fig 5.5a). These structural characteristics suggest that circulating HS fragments are capable of influencing growth factor signaling, as they meet typical size and sulfation requirements necessary for interaction with positively-charged residues of growth factor ligands and their cognate receptors[201,227].

We therefore sought to determine if heparinase-III-mediated ESL degradation in mice similarly released highly-sulfated HS fragments capable of regulating endothelial-reparative FGFR1 signaling. Treatment of mice with heparinase-III was associated with increased plasma N-sulfated HS fragments (as measured by mass spectrometry, Fig 5.5b) in a time course consistent with loss of ESL thickness (Fig 5.1a). As measurement of HS fragment size in mouse plasma is technically infeasible (given low plasma concentrations and small sample volumes), we instead isolated HS from whole mouse lungs, then treated extracted HS ex-vivo with heparinase-III and performed gel electrophoresis. The vast majority of lung HS fragments yielded after heparinase-III treatment were dp6 or larger in size (Fig 5.5c).

We next determined if highly-sulfated, > degree of polymerization (dp6) HS fragments can influence endothelial FGFR1 signaling. Using surface plasmon resonance, we examined the ability of HS to interact with FGF2, a FGFR1 ligand constitutively expressed within the lung[228] and implicated in endothelial repair[220,223]. FGF2 avidly bound to full-length glycosaminoglycans with high concentrations of N-sulfated glucosamines (Fig 5.6a), suggesting that N-sulfation was important for FGF2 binding. The necessity of N-sulfation to FGF2 binding was confirmed by selectively *N*-desulfating heparin, which dramatically attenuated FGF2 binding (Fig 5.6b). FGF2-HS interactions were additionally size-dependent, with only fragments > dp6 in size having substantial binding (Fig 5.6c). Together, these

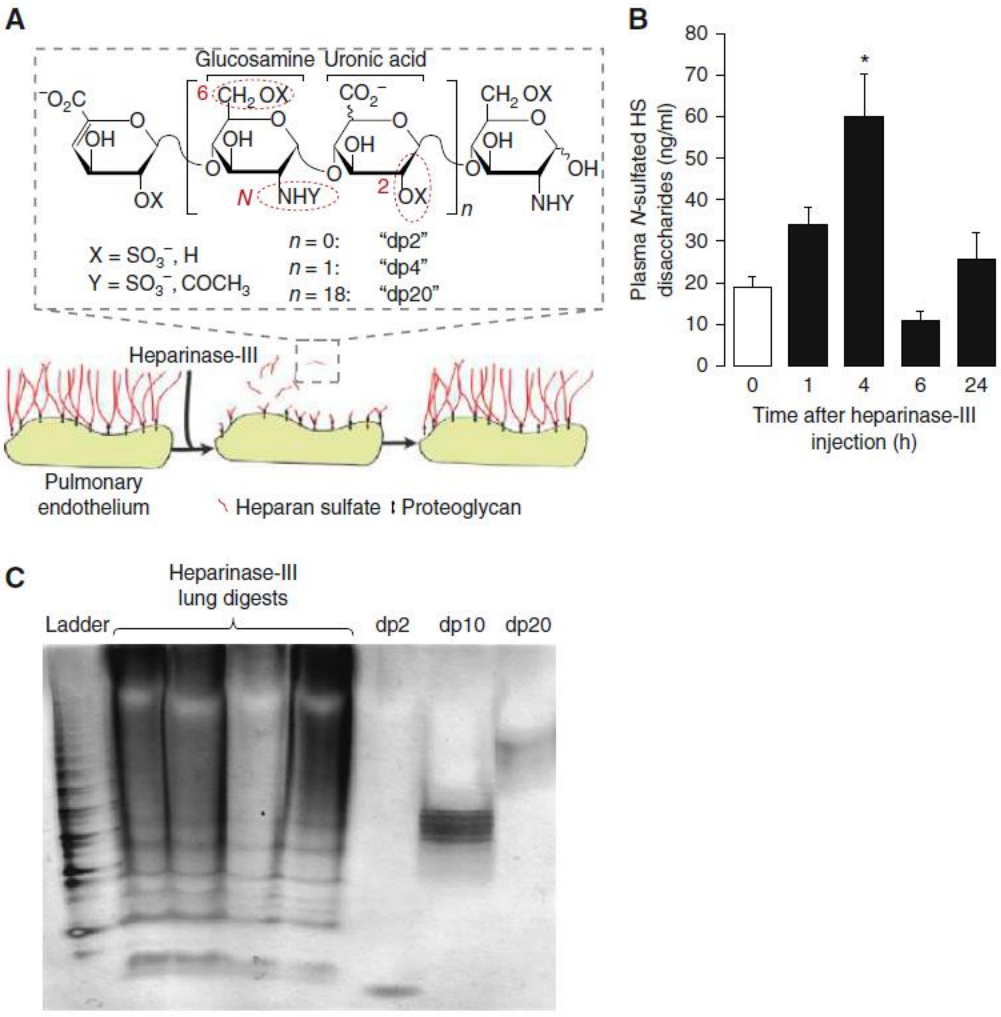

Figure 5.5. Structural characteristics of HS fragments released during heparinase-III-mediated ESL degradation. (a) Heparan sulfate (HS) is a polymer of repeating disaccharide units (with size quantified as degree of polymerization, dp) that can be sulfated at 2-*O*, 6-*O*, and/or *N*-positions. *n* = number of repeats. (b) Heparinase-III treatment (1 unit IV) is associated with increased plasma *N*-sulfated HS, as measured by mass spectrometry. * $p < 0.05$ compared to time = 0; n > 3 per group. (c) Heparinase-III treatment cuts lung HS in low sulfation domains (X & Y are primarily H and OCCH3, as per panel a) yielding a range of fragment sizes, predominantly 6 saccharides (dp6) or larger, where X & Y (panel a) are primarily SO^{3-}. Heparinase-digested heparin ladder (left) shows disaccharides of all dp values found in heparin, and purified heparin dp2, dp10, and dp20 fragments (right) serve as size standards of gel electrophoresis.

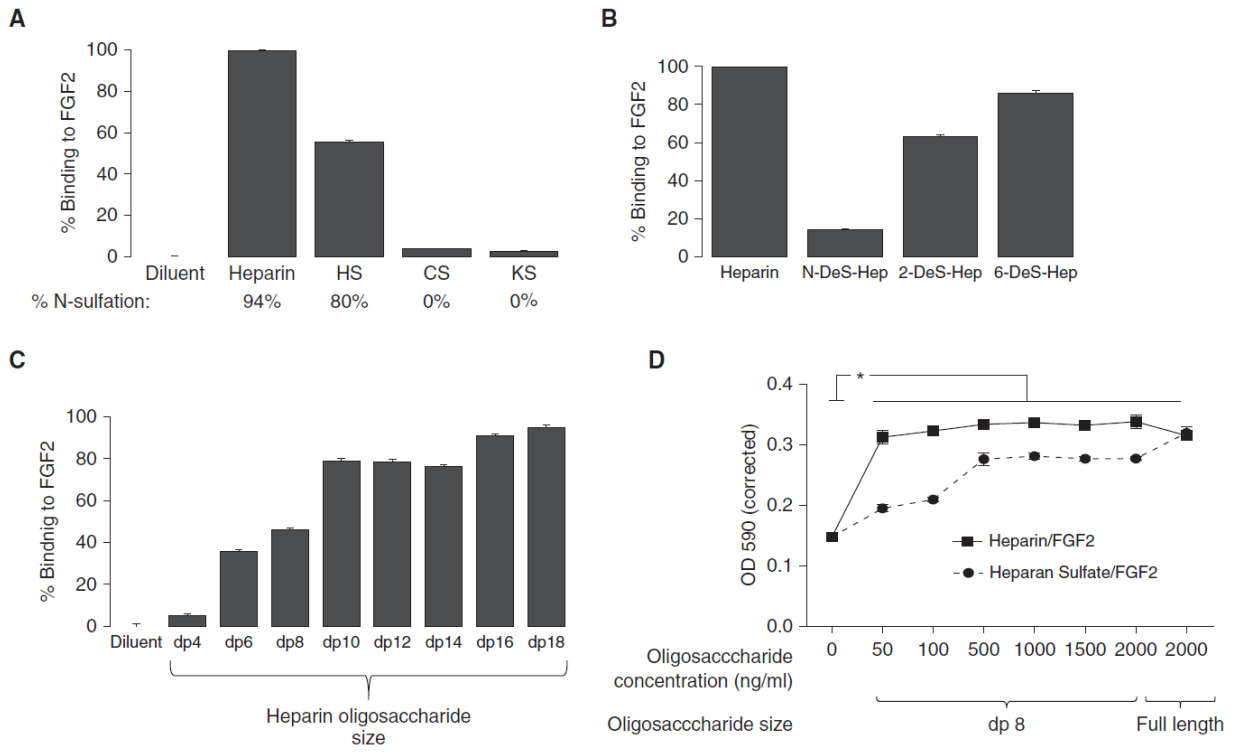

Figure 5.6. *N*-sulfated HS fragments can bind FGF2 and promote FGFR1c activation. Surface plasmon resonance studies revealed that highly *N*-sulfated glycosaminoglycans (such as HS or heparin, (a)) readily bind FGF2 in an *N*-sulfation- (b) and size-(c) dependent fashion. KS: Keratin Sulfate. CS: Chondroitin Sulfate. All group differences in (a - c) are statistically significant ($p < 0.05$). (d) HS or heparin octasaccharides augment FGF2 (5 nmol/l) activation of FGFR1c (the endothelial-expressed FGFR1 isoform), as demonstrated by increased growth/survival of FGFR1c-expressing BaF3 cells (* $p < 0.05$ for each concentration of heparin or heparan sulfate, compared to oligosaccharide-unexposed control). Full-length (> dp18) heparin or HS serve as a positive control. n > 3 for all groups.

findings indicate that circulating HS fragments released during heparinase-III-mediated ESL degradation are of sufficient size and sulfation to bind to FGF2.

The primary FGF2 receptor splice variant expressed in pulmonary endothelial cells to determine the impact of HS fragment-FGF2 binding on FGFR1 signaling, we used BaF3 cells stably transfected with FGFR1c[221,227]. These cells require FGFR1 activation to grow/survive, as quantified by optical density. FGF2-induced BaF3 cell survival/growth was significantly augmented (Fig 5.6d) by the addition of highly-sulfated heparin or HS octasaccharides (representative of > dp6 fragments released after heparinase-III). FGFR1c activation occurred at similar octasaccharide concentrations as those observed in the plasma of heparinase-III-treated mice (~50 ng/ml *N*-sulfated HS as per Fig 5.5b, approximated in BaF3 experiments

by similar concentrations of highly-sulfated heparin oligosaccharides). Heparin or HS octasaccharides were incapable of activating FGFR1c in the absence of FGF2 (data not shown). We confirmed activation of endothelial FGFR signaling by measuring FGFR induction of ERK signaling[223] in HPMVEC-1.6R cells (a human pulmonary microvascular endothelial cells line[229], Fig 5.7a, c) treated with dp8 HS and FGF2. FGFR dependence of ERK activation was confirmed by pretreatment with AZD4547 (Fig 5.7b, c). HS/FGF2 treatment of HPMEC-ST1.6R cells (Fig 5.7d) or primary mouse lung microvascular endothelial

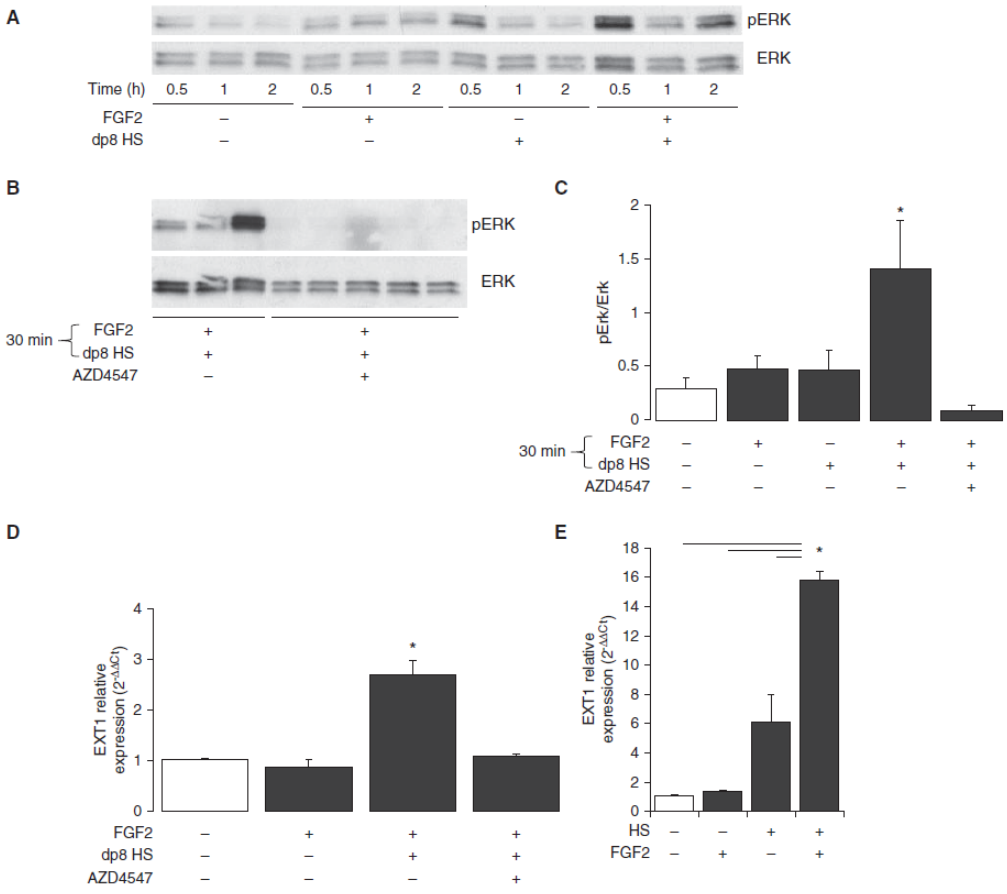

Figure 5.7: HS-FGF2 activates endothelial growth factor signaling and EXT1 expression. (a) dp8 HS (0.5 µg/ml) and FGF2 (5 ng/ml) activated growth factor signaling in HPMEC-ST1.6R cells, as measured by ERK phosphorylation. (b) Pretreatment (12 h, 20 nmol/l) with the FGFR1 inhibitor AZD4547 confirmed that ERK phosphorylation (induced by 30 min dp8 HS/FGF2) was FGFR-dependent. (c) Densitometry quantification of 30 min FGF2/dp8 HS treatments in panels a, b. (d) dp8 HS and FGF2 (3 h treatment) of HPMEC-ST1.6R cells similarly induced EXT1 mRNA expression in a FGFR-dependent fashion. (e) Similar induction of EXT1 expression was noted in primary mouse lung microvascular endothelial cells treated with HS (5 µg/ml) and FGF2 (20 ng/ml) for 5 h. * $p < 0.05$. $n > 3$ for all groups.

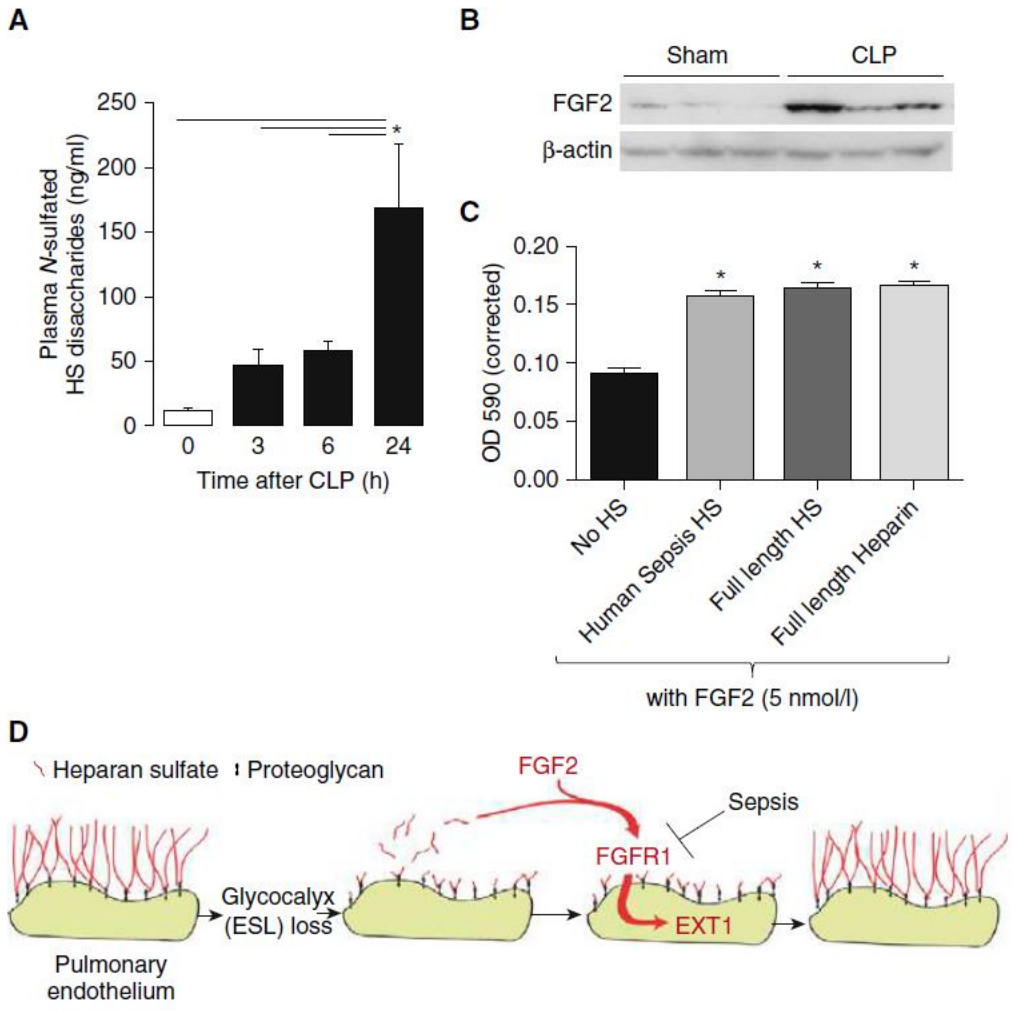

Figure 5.8. Septic loss of HS-FGF2-FGFR1 signaling occurs downstream of HS-FGF2. CLP was associated with increased plasma *N*-sulfated HS (a) and pulmonary FGF2 (b, 24 h after CLP). (c) HS fragments (1 μg/ml) pooled from the plasma of septic patients were capable of activating FGFR1c in BaF3 cells. (d) Proposed pathway of ESL reconstitution. As septic plasma HS fragments remain capable of activating FGF2/FGFR1, impairment of FGFR1-mediated ESL reconstitution during sepsis likely occurs due to loss of endothelial FGFR1 expression. n > 3 per group, * $p < 0.05$.

cells (MLMVECs, Fig 5.7e) significantly induced EXT1 expression in a FGFR-dependent fashion (Fig 5.7d). Taken together with the absence of EXT1 induction in FGFR-inhibited mice (Fig 5.3b, d), these findings suggest that HS fragments, released during heparinase-III-mediated ESL degradation, activate endothelial FGF2/FGFR1 signaling and promote EXT1-mediated ESL reconstitution.

5.2.4. HS fragments released after CLP-mediated ESL degradation activate FGFR1 signaling

Given the observed loss of pulmonary EXT1 induction and delay in ESL reconstitution after CLP, we sought to determine if sepsis was associated not only with loss of reparative endothelial FGFR1 expression (Fig 5.4a) but also impaired FGFR1 activation by circulating HS fragments. Similar to heparinase-III treatment, CLP-treated mice demonstrated increased circulating *N*-sulfated HS fragments (Fig 5.8a) in concentrations sufficient to induce FGFR1c signaling in BaF3 cells (Fig 5.6d). Furthermore, there was an abundance of pulmonary FGF2 during sepsis (Fig 5.8b). We treated BaF3 cells with HS fragments (dp6-dp8 oligosaccharides or larger[31]) pooled from plasma of human patients with sepsis to confirm that sepsis-produced HS fragments were capable of augmenting FGFR1 activation. These human-derived fragments augmented FGFR1 signaling in a manner consistent with full-length HS (Fig 5.8c). In contrast, HS fragments collected from the plasma of non-septic patients with pneumonia had minimal impact on FGFR1 signaling (data not shown), likely reflecting their undersulfated state[31]. Taken together, these findings indicate that the delayed ESL reconstitution observed after CLP is not due to an inability of circulating HS fragments (released during septic ESL degradation) to activate FGFR1, but rather reflects the downstream absence of endothelial FGFR1 expression during sepsis (Fig 5.8d).

5.2.5. Urinary GAGs in medical and surgical ICU patients

Between July 2013 and October 2014, we enrolled 30 medical ICU patients with vasopressor-dependent septic shock. Twenty-five concurrently-enrolled surgical ICU patients with severe trauma served as a contemporaneous ICU control group. As expected, septic shock patients were much more likely than trauma patients to develop new/worsening renal dysfunction in the 72 h after study enrollment or to die during their hospitalization.

Urine GAGs were significantly elevated in septic shock patients as compared to their surgical ICU comparators (Fig 5.9a). While HS concentrations were independent of severity of illness (Fig 5.9b), urinary concentrations of HA and CS correlated with Acute Physiology And Chronic Health Evaluation II

(APACHE II) scores (Fig 5.9c, d). Accordingly, total GAGs correlated with APACHE II ($p < 0.01$, r2 = 0.2059). To investigate the association of GAG sulfation (e.g. HS, CS) with the cause of critical illness, we enzymatically digested isolated GAGs into constituent disaccharides and determined sulfation patterns by mass spectrometry. As detailed in Fig 5.9e, urine NS2S, NS, 6S, 2S, and unsulfated heparan disaccharides were significantly elevated in septic shock patients as compared to trauma patients. Furthermore, urine 2S6S, 4S, and unsulfated chondroitin disaccharides were elevated in patients with septic shock (Fig 5.9f).

The observed elevation in N-sulfated (NS, NS6S, NS2S, Tri-sulfated) HS fragments suggested the action of heparanase, which preferentially releases *N*-sulfated heparan fragments. Consistent with our previous findings using a mouse model of polymicrobial sepsis[205], patients with septic shock demonstrated elevated urinary HS degradation activity (a marker of heparanase activity). Urinary HS degradation activity correlated closely with urinary HS, suggesting that the fragmentation was a consequence of heparanase activity. Furthermore, in a manner consistent with urinary HS (Fig 5.9b), urinary HS degradation activity did not correlate with severity of illness.

Given the significant septic shock-associated elevation in urine chondroitin 4S disaccharides, we sought to determine if urinary bikunin (a urine proteoglycan enriched in 4S-CS) was elevated in septic shock patients. While urinary bikunin and 4S-CS concentrations were correlated ($p = 0.03$), this association was weak ($r^2 = 0.08$), and there were no differences between septic shock and trauma patients (0.331 ng bikunin/mg creatinine vs. 0.359 ng bikunin/mg creatinine; $p = 0.72$).

5.2.6. Urinary GAGs predict the development/progression of renal dysfunction in septic shock

Based upon our previous animal investigations[205], we hypothesized that urinary GAG fragmentation would be an early event in the development of septic kidney injury in humans. Indeed, increasing urinary concentrations of HS (Fig 5.10a, b, f) and urine HS degradation activity within 24 h of septic shock onset correlated with later (i.e. within 72 h of enrollment) renal dysfunction, as defined by

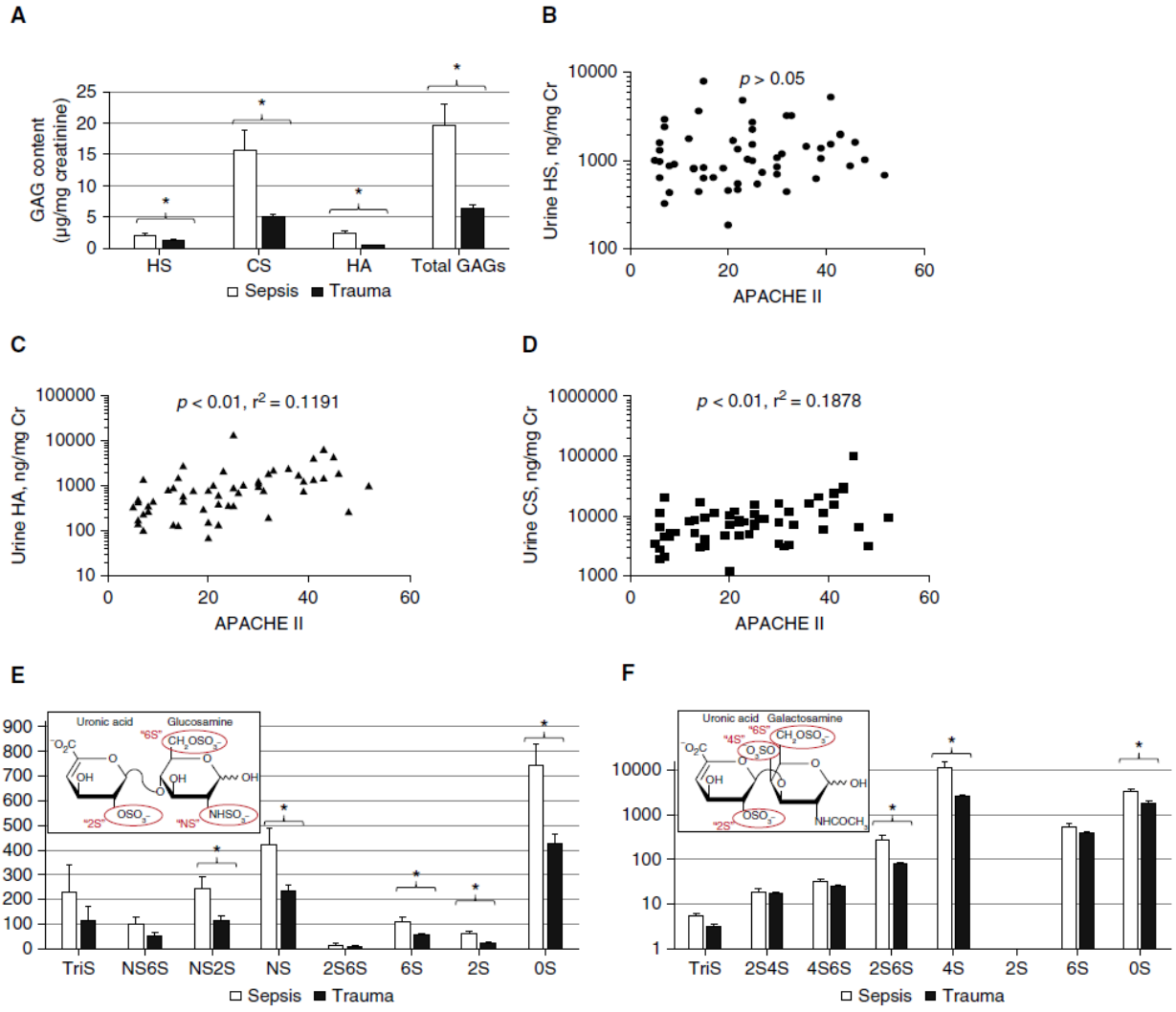

Figure 5.9. Urinary glycosaminoglycans (GAGs) in septic shock and trauma. (A) Urine GAGs (including heparan sulfate [HS], chondroitin sulfate [CS], and hyaluronic acid [HA]) were significantly elevated in patients with septic shock (collected within 24 h of shock diagnosis) in comparison to surgical intensive care unit–admitted trauma patients. (B) Urine HS was not associated with severity of illness (Acute Physiology and Chronic Health Evaluation [APACHE] II) in the combined surgical/medical population. In contrast, urine HA (C) and CS (D) were associated with severity of illness. Mass spectrometry measurements revealed that patients with septic shock had distinct patterns of urine HS (E) and CS (F) disaccharide sulfation (inset). *P,0.05. NS = *N*-sulfated.

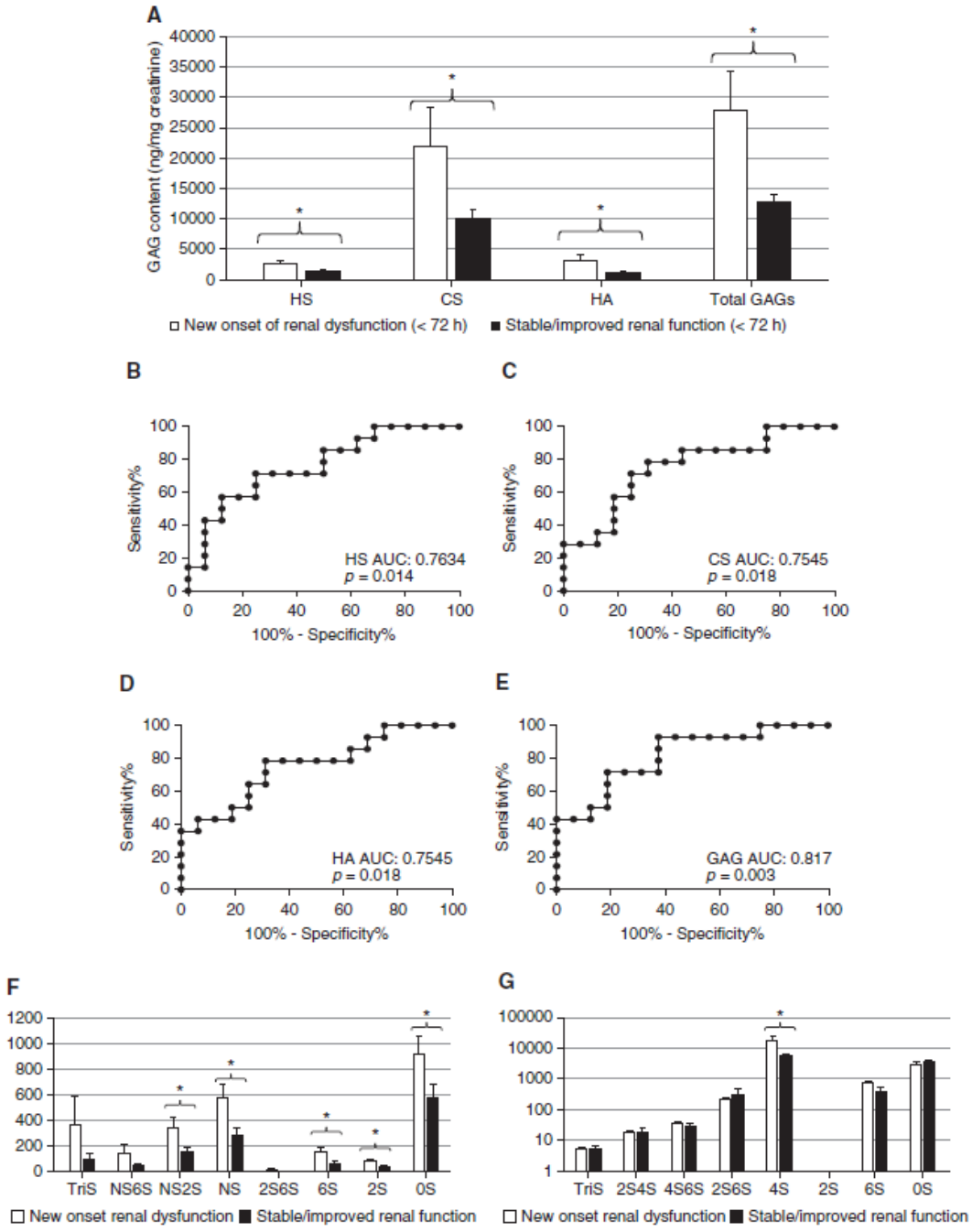

Figure 5.10. Urine glycosaminoglycans (GAGs) predict the development/progression of renal dysfunction in septic shock. (A) In urine collected within 24 h of the diagnosis of septic shock, GAG concentrations (heparan sulfate [HS], chondroitin sulfate [CS], and hyaluronic acid [HA]) were significantly elevated in patients who developed new Acute Kidney Injury Network 2 criteria (twofold increase in serum creatinine or ,0.5 ml/kg/h urine output) between 24 and 72 h after urine collection. (B–E) Urine HS (B), CS (C), HA (D), and total GAGs (E) have significant predictive value for the development of renal dysfunction, as demonstrated by receiver operating characteristic curves. Mass spectrometry measurements revealed that patients with septic shock who developed new/progressive renal dysfunction had distinct patterns of urine HS (F) and CS (G) disaccharide sulfation. *P,0.05. AUC = area under the receiver operating characteristic curve; NS = N-sulfated.

new onset of AKIN 2 criteria. Changes in urinary CS and HA similarly predicted new renal dysfunction (Fig 5.10a, c, d, g), with total GAGs demonstrating a high (0.817) area-under-the receiver-operating characteristic (ROC) curve as a kidney injury predictor (Fig 5.10e). Similarly robust ROC curves were seen with HS disaccharides including NS2S, NS, 2S, and 0S (data not shown). Of CS disaccharides, only 4S sulfation patterns predicted the onset/progression of renal dysfunction (data not shown). The predictive ability of urine GAGs (HS, CS, HA, total GAGs) remained even after controlling for severity of illness.

For these analyses, patients with abnormal serum creatinine at enrollment were retained because of the relatively low enrollment. As such, our findings are not direct predictors of *de novo* AKI, but rather the onset or progression of renal dysfunction from baseline function at study enrollment. However, in sensitivity analyses limited to septic shock patients with creatinine < 2.0 mg/dl at enrollment, HS ($p = 0.05$) and total GAGs ($p = 0.0287$) remained associated with renal dysfunction onset/progression. Additional analyses inclusive of all critically-ill patients (both septic shock and trauma) showed strong associations between HS, CS, HA, or total GAGs and renal dysfunction ($p < 0.001$ for each); these associations remained statistically significant when limited to patients with baseline serum creatinine < 2.0 mg/dl (data not shown).

In accordance with previous studies of urinary GAGs, we elected to normalize GAG concentrations to urine creatinine, thereby controlling for urine dilution[230,231]. However, raw concentrations of urine HS, CS, HA, and total GAGs remained statistically associated with worsening renal dysfunction ($p < 0.05$), with robust ROC AUCs (0.8884, 0.8348, 0.8705, and 0.8482, respectively). As with normalized GAGs, raw concentrations of heparan NS2S, NS, 6S, 2S, and 0S disaccharides remained statistically associated with renal dysfunction. In contrast to normalized CS, raw concentrations of chondroitin 2S4S, 4S6S, 4S, and 6S disaccharides were associated with later renal dysfunction ($p < 0.05$).

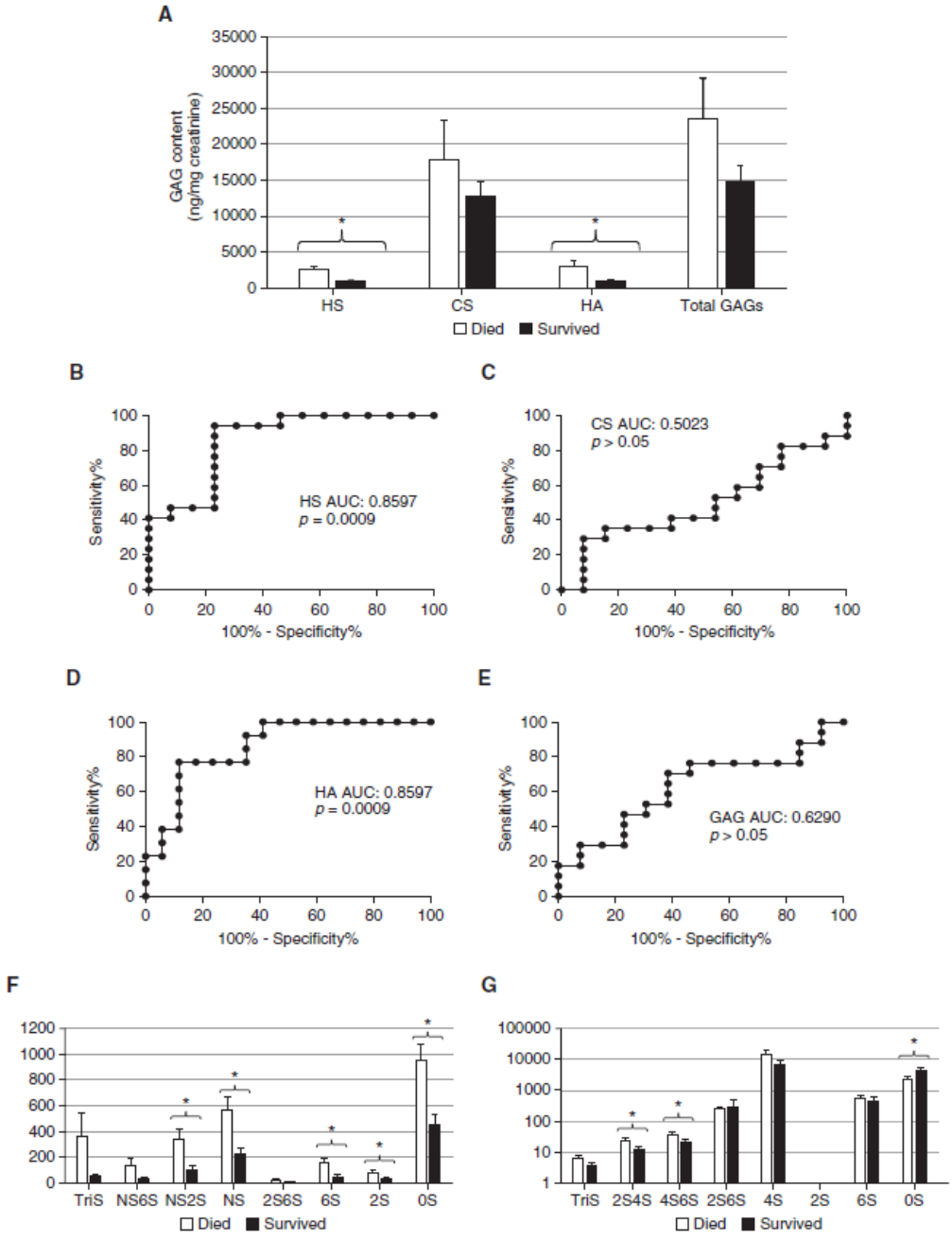

Figure 5.11. Urine glycosaminoglycans (GAGs) predict hospital mortality in septic shock. (A) In urine collected within 24 h of the diagnosis of septic shock, urine heparan sulfate (HS) and hyaluronic acid (HA) were significantly elevated in patients who died during their hospitalization. Urine HS (B) and HA (D) have significant predictive value for mortality, as demonstrated by receiver operating characteristic curves. Conversely, urine chondroitin sulfate (CS) (C) and total GAGs (E) did not predict mortality. Mass spectrometry measurements revealed that patients with septic shock who died had distinct patterns of urine HS (F) and CS (G) disaccharide sulfation. *P,0.05. AUC = area under the receiver operating characteristic curve.

5.2.7. Urinary HS and HA predict hospital mortality in patients with septic shock

As demonstrated in Fig 5.11a, urinary HS and HA (collected within 24 h of diagnosis and normalized to urine creatinine) were significantly elevated in septic shock patients who later died during their hospitalization. This predictive ability of HS and HA (Fig 5.11b, c) persisted when controlling for severity of illness (data not shown).

Similar to renal dysfunction (Fig 5.10f), NS2S, NS, 6S, 2S, and 0S heparan disaccharides were strongly predictive of hospital mortality (Fig 5.11d). In contrast to kidney dysfunction (Fig 5.10g), 4S chondroitin disaccharides did not predict mortality, although 2S4S, 4S6S, and 0S did (Fig 5.11d). Identical associations with hospital mortality were observed when we repeated analyses using raw urine concentrations (ng/ml) of HS, CS, HA, total GAGs, and CS/HS disaccharides (data not shown).

5.2.8. Alternative measures of urinary GAGs

As mass spectrometry is expensive and cannot be easily performed at the bedside, we sought to determine the predictive value of simplified measurements of urinary GAGs. DMMB is a colorimetric assay that detects sulfated GAGs in urine at a fraction of the cost of mass spectrometry (cost per sample in our study: $2 vs. $200). To best approximate a simple, point-of-care assay, DMMB measures were not normalized to urine creatinine. These DMMB measures of sulfated GAGs correlated well with mass spectrometry measures of total GAGs (Fig 5.12a). Accordingly, urine DMMB (collected within 24 h of septic shock onset) predicted progressive renal dysfunction (Fig 5.12b) and hospital mortality (Fig 5.12c).

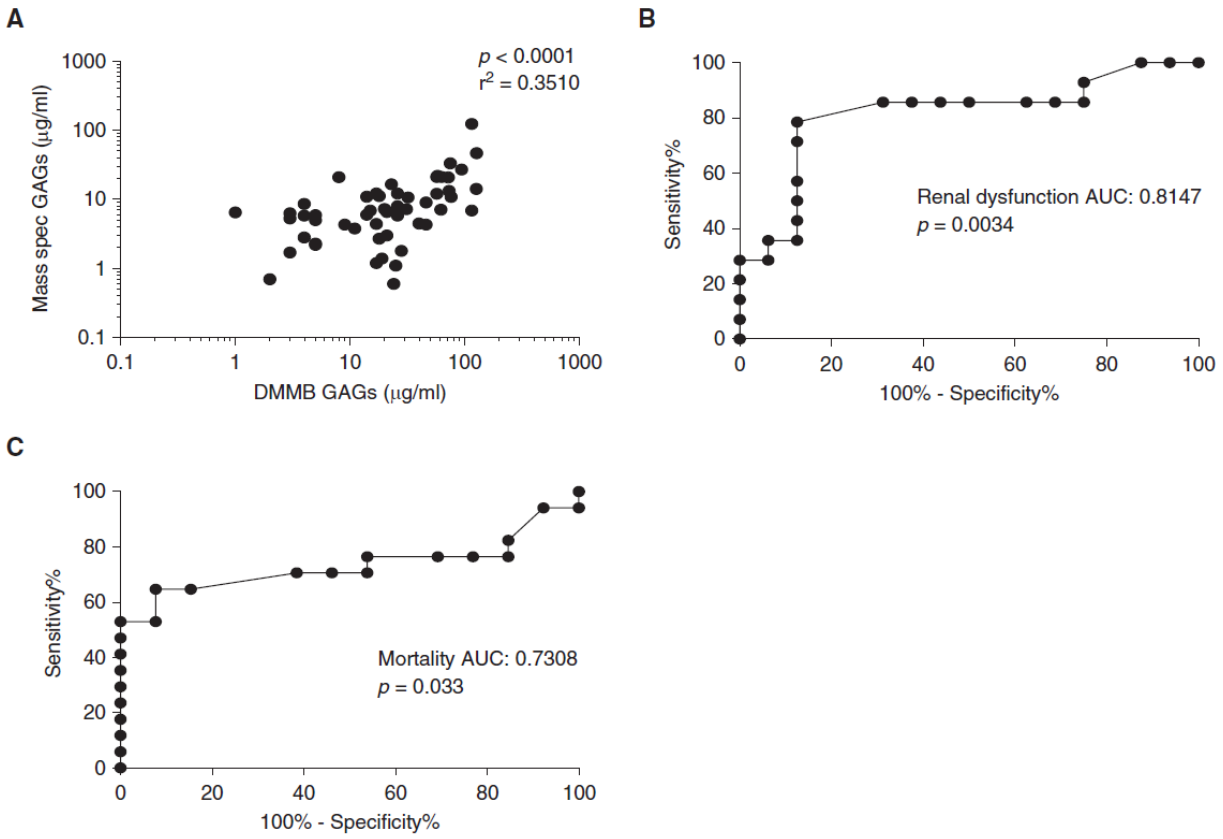

Figure 5.12. Dimethylmethylene blue (DMMB) colorimetric assay of urinary glycosaminoglycans (GAGs). (A) DMMB, a colorimetric assay that identifies sulfated glycosaminoglycans (GAGs), correlates with urine GAGs as measured by mass spectrometry. Accordingly, DMMB predicted the onset/progression of renal dysfunction (B) and in-hospital mortality (C) in patients with septic shock. AUC = area under the receiver operating characteristic curve.

5.2.9. Urinary GAG fragmentation in ARDS patients with normal baseline renal function

We obtained urine samples collected from patients with ARDS 0, 1, and 3 days after enrollment in the ARDS Network ARMA study[243]. As previously described[213], all 70 patients in this cohort had normal renal function at baseline; 22 patients later developed AKI. These patients had significantly elevated urinary total glycosaminoglycans at days 0 and 3, largely derived from a consistently elevated urinary CS (Fig 5.13). Disaccharide analyses revealed that urine CS was largely 4-*O* sulfated (data not shown). While total HS demonstrated a nonsignificant association with AKI (p = 0.08) at day 0, *N*-sulfated and 6-*O*-sulfated HS fragments were statistically different between AKI and non-AKI groups (Fig 5.13).

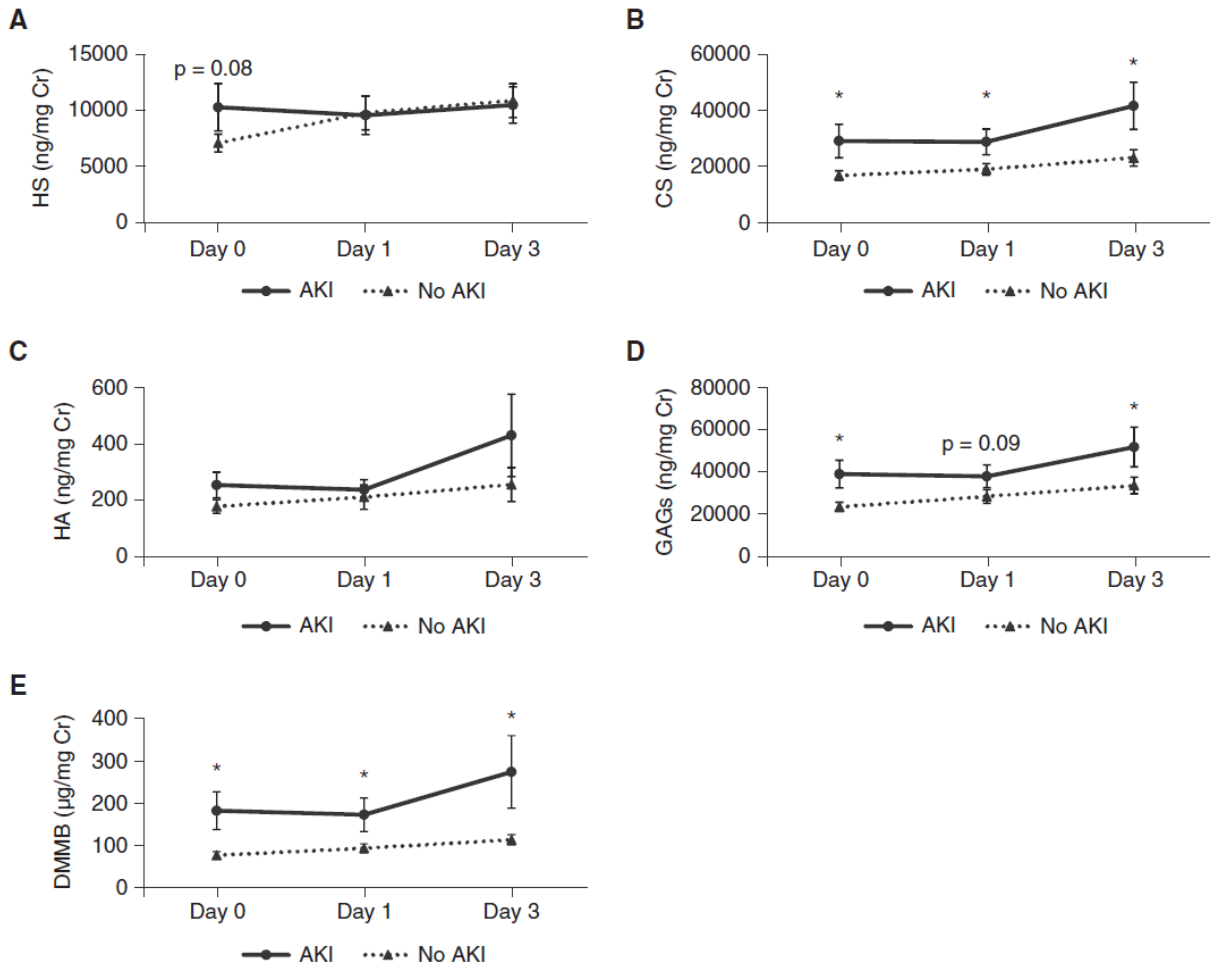

Figure 5.13. Urinary indices of glycosaminoglycan (GAG) degradation and acute kidney injury (AKI) in acute respiratory distress syndrome. Urine was collected from patients with acute respiratory distress syndrome 0, 1, and 3 days after study enrollment and analyzed by mass spectrometry for (A) heparan sulfate (HS), (B) chondroitin sulfate (CS), (C) hyaluronic acid (HA), or (D) total GAGs (reflecting the sum of HS, CS, and HA). In addition, sulfated glycosaminoglycans were measured using the colorimetric dimethylmethylene blue (DMMB) assay (E). At baseline, all patients had normal renal function. A subset of patients later developed AKI; the remainder of patients remained with normal renal function. *P,0.05 between AKI and no AKI groups.

Raw day 0 glycosaminoglycan data revealed similar associations as normalized data, with the exception that raw HS was significantly elevated in patients who later developed AKI (5877.42 ± 1501.63 ng/ml vs. 3306.44 ± 430.80 ng/ml, p = 0.03). There were no differences in raw urine glycosaminoglycan levels at day 1. At day 3, only raw CS was significantly different between AKI and non-AKI groups (12012.98 ± 2162.19 ng/ml vs. 8300.30 ± 821.58 ng/ml, p = 0.05).

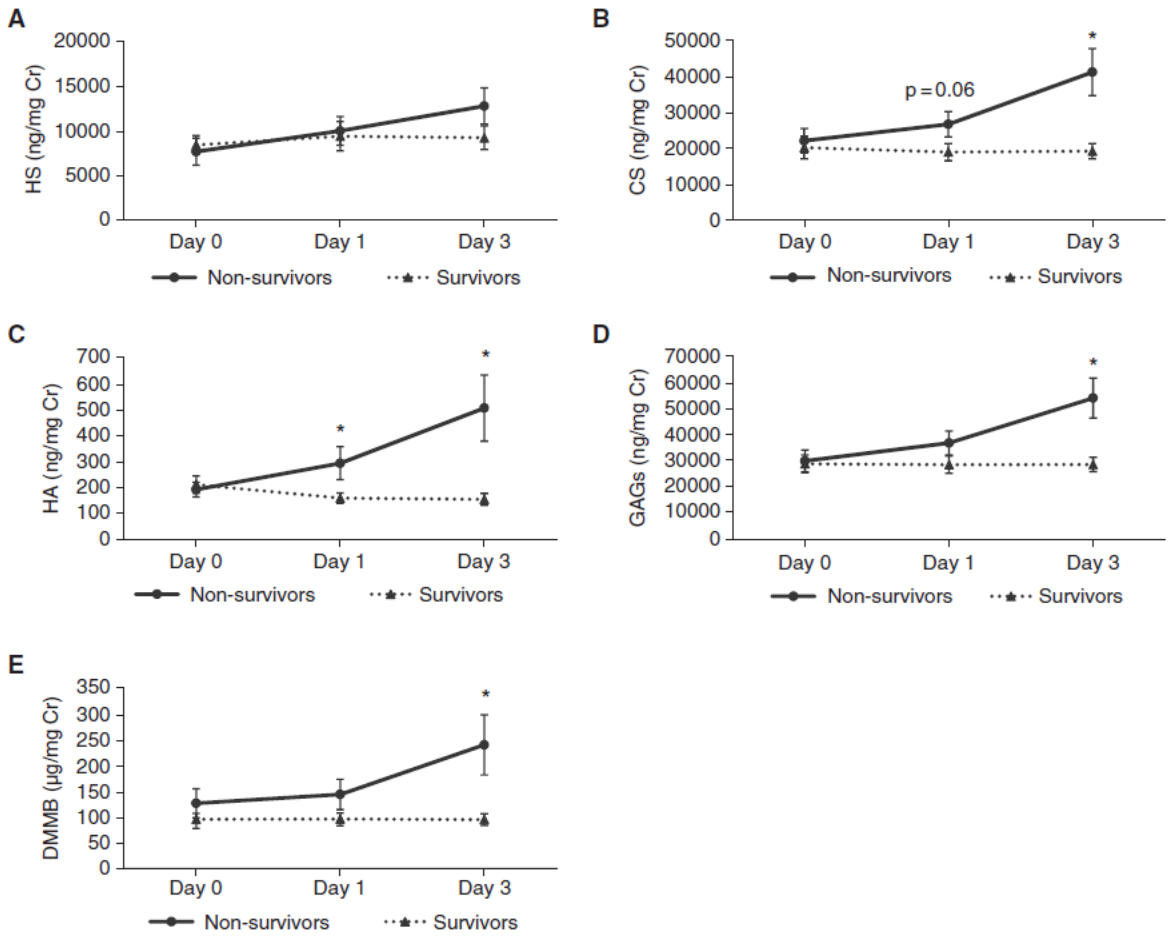

Figure 5.14. Urinary indices of glycosaminoglycan (GAG) degradation and hospital mortality in acute respiratory distress syndrome. Urine was collected from patients with acute respiratory distress syndrome 0, 1, and 3 days after study enrollment and analyzed by mass spectrometry for (A) heparan sulfate (HS), (B) chondroitin sulfate (CS), (C) hyaluronic acid (HA), or (D) total GAGs (reflecting the sum of HS, CS, and HA). In addition, sulfated glycosaminoglycans were measured using the colorimetric dimethylmethylene blue (DMMB) assay (E). *P,0.05 between nonsurvivors and survivors.

As with septic shock, urinary glycosaminoglycan indices were directly (and temporally) associated with in-hospital mortality in patients with ARDS (Fig 5.14). At day 3, *N*-sulfated and unsulfated HS disaccharides were associated with mortality; nearly every CS sulfation pattern (with the exception of TriS and 2S) was associated with mortality (data not shown). In contrast to patients with septic shock, the predictive ability of urinary indices in ARDS was lost when values were not normalized for urine creatinine.

5.2.10. Urinary GAGs and pulmonary vs. nonpulmonary etiologies of illness

As we have previously observed distinct plasma GAG fragmentation patterns in pulmonary and non-pulmonary sepsis[31], we measured the correlation of urinary GAG fragments with the infectious site causative of septic shock. Urinary GAG fragments in septic shock patients did not correlate with source of infection (pulmonary vs. nonpulmonary, $p > 0.3$ for all GAGs studied). In patients with ARDS, there was a nonsignificant trend of elevated HS (day 0) in patients with non-pulmonary sepsis-induced ARDS as opposed to direct (pneumonia) injury (10123.62 ± 1980.71 ng/mg Cr vs. 6979.37 ± 784.75 ng/mg Cr, $p = 0.08$).

5.3. Discussion

The first study identifies the endogenous mechanisms driving reconstitution of a degraded ESL. We found that non-septic (i.e. heparinase-III mediated) ESL degradation was followed by a rapid induction of endothelial FGFR1 expression, triggering homeostatic, EXT1-mediated pulmonary ESL reconstitution. ESL repair after heparinase-III was additionally promoted by the release of *N*-sulfated HS oligosaccharides capable of activating FGF2-FGFR1 signaling. Rapid induction of ESL repair by the very products of ESL degradation is biologically efficient, reflecting the critical importance of an intact ESL to endothelial homeostasis. In contrast to heparinase-III, CLP-mediated ESL degradation was associated with loss of reparative endothelial FGFR1 expression and, accordingly, delayed ESL reconstitution. However, HS fragments released during septic ESL degradation maintained FGFR1-promoting activity, indicating that septic suppression of ESL recovery occurs downstream of HS/FGF2 (Fig 5.8d). Taken together, these findings suggest that sepsis may cause vascular injury via not only ESL degradation but also suppressed FGFR1/EXT1-mediated ESL recovery.

Our investigations (Figs 5.2, 3, 5) of the mechanisms governing pulmonary ESL reconstitution are largely derived from a non-septic model of heparinase-III (a bacterial HS-specific glucuronosyl lyase)-mediated pulmonary ESL degradation. We have previously demonstrated that sepsis is characterized by

similarly-rapid pulmonary ESL degradation by endothelial heparanase, a mammalian HS-specific glucuronosyl hydrolase[202]. Heparinase-III (also known as heparitinase) and heparanase have been shown to act similarly upon matrix HS, releasing biologically-active HS fragments[232]. However, heparinase-III-mediated ESL degradation was insufficient to induce pulmonary vascular leak *in vivo* (Fig 5.1e[233]), while heparanase-mediated ESL degradation during sepsis directly contributed to lung edema and inflammation[202]. These differences in the physiologic consequence of ESL degradation can be potentially explained by a concomitant loss of reparative HS biosynthetic enzymes (e.g. EXT1) during sepsis (Fig 5.2b, c), leading to a prolonged suppression of ESL integrity (Fig 5.2a). Indeed, heparinase-III treatment was able to induce lung edema at 24 h only if subsequent HS biosynthesis was pharmacologically inhibited (Fig 5.1e).

Our work (Fig 5.3) specifically identifies endothelial FGFR1 as a critical regulator of EXT1 induction and homeostatic pulmonary ESL reconstitution. Endothelial FGFR signaling is an important mediator of vascular repair, with previous studies of Tie2Cre-*Fgfr1/2* knockout mice demonstrating impaired retinal microvascular responses to injury[220]. While these mice are characterized by endothelial loss of both FGFR1 and FGFR2, the relative absence of FGFR2 expression in the pulmonary microvascular endothelium[221] provides reassurance that our pulmonary EXT1 findings are largely FGFR1-driven.

While we observed that sepsis is associated with loss of (ESL-reparative) FGFR1 expression, the mechanisms responsible for this suppression remain uncertain. One potential mediator of septic FGFR1 downregulation is miR-16, an endothelial microRNA (miR) that decreases FGFR1 expression and suppresses angiogenesis[223]. Previous reports have observed increased plasma miR-16 in human and murine sepsis[224,225]. Surprisingly, we found little evidence of pulmonary miR16 induction at time points coincident with loss of pulmonary FGFR1 (Fig 5.4c). Furthermore, inhibition of miR-16 failed to prevent the septic loss of pulmonary EXT1 expression (Fig 5.4d). The apparent miR-16-independence of septic suppression of ESL recovery is compatible with the observation that elevated plasma miR-16, despite

being a marker of sepsis, is correlated with improved septic outcomes in humans[234]. The mechanisms governing loss of endothelial FGFR1 during sepsis will require further study.

In addition to identifying FGFR1 expression as a mediator of ESL repair, our work highlights the importance of ESL-derived HS fragments in promoting FGFR1 activation. While others have reported circulating HS as a biomarker of ESL degradation, the biological function of these oligosaccharides has been largely relegated to serving as a damage-associated molecular pattern, with less attention to impact on other signaling pathways. When anchored to cell-surface proteoglycans, HS may function as a *cis*-activating co-receptor for growth factor ligand-receptor interaction[227]. Our findings suggest that endothelial growth factor signaling can be paradoxically augmented by HS degradation, provided that the products of this degradation (HS oligosaccharides) are of sufficient size (> dp 6) and sulfation (*N*-sulfated) to bind soluble FGF2 and activate FGF2-FGFR1 signaling. This sulfation requirement for growth factor activation suggests that HS degradation might release cryptic, highly-sulfated HS domains not participatory in *cis*-activation of growth factor signaling. Alternatively, released HS oligosaccharides might access basolateral growth factor receptors otherwise unengaged by apical heparan sulfate proteoglycans. Determination of the geographic localization of these interactions will require future development of highly-sensitive glycosaminoglycan labeling and sequencing techniques.

The critical necessity of ESL integrity to the maintenance of vascular physiology suggests that there likely exist additional systems of glycosaminoglycan biosynthesis and ESL recovery complementary to FGF2/$FGFR_1$ signaling. Indeed, inhibition of FGFR1 signaling did not completely suppress EXT1 expression or ESL recovery 24 h after heparinase-III (Fig 5.3), and this partial suppression of ESL recovery was only capable of inducing lung edema after AZD4547-mediated FGFR1 inhibition. There is a need for further study of alternative mechanisms of EXT1 induction, and how these mechanisms are impacted during sepsis. Our work specifically highlights the complexity of EXT1 regulation: the observed rise in protein expression before a statistically-significant rise in gene transcription suggests that rapid changes

in HS biosynthesis may occur at the post-translational level, potentially by prevention of EXT1 proteosomal degradation. Indeed, the *in vivo* regulation of HS synthesis and sulfation remains uncertain and is the focus of active investigation[235].

Consistent with the lungs' functional susceptibility to the consequences of ESL loss (e.g. hypoxia arising from pulmonary edema and inflammation), pulmonary ESL recovery after heparinase-III occurred much more rapidly (< 24 h) than cremasteric ESL recovery after heparinase-III (5 days[206]). Notably, even the slowed pace of pulmonary ESL recovery in CLP-treated mice (3 days, Fig 5.1f) was more rapid than that of the cremasteric ESL in healthy animals. Pulmonary ESL recovery is so highly prioritized that it is initiated prior to the resolution of systemic illness, as CLP-treated mice typically demonstrate continued signs of illness (lethargy, piloerection) at 48 h, a timepoint at which ESL reconstitution has already begun (Fig 5.2a). The mechanisms responsible for these organ-specific differences in the pace of ESL recovery require further investigation. While these may be partially explained by tissue-specific differences in FGFR signaling (as demonstrated by the differential expression of FGFR2 in pulmonary and systemic endothelium[220]), other influences such as organ-specific differences in vascular shear stress waveforms (with tidal variability occurring in the inflating/deflating lung) may contribute to the rapidity of pulmonary HS synthesis[236].

In the second study, we found that septic shock was associated with an early increase in urinary GAGs, predictive of ongoing/progressive renal dysfunction in the ensuing 72 h. Accordingly, urine HS and HA strongly (area under ROC curves > 0.87) were associated with in-hospital mortality in patients with septic shock. These associations strengthened after controlling for severity of illness. Comparable urinary GAG fragmentation was noted in ARDS patients with normal renal function at baseline who later developed AKI. These mass spectrometry-based measures could be largely replicated using an inexpensive, rapidly-performed colorimetric assay of sulfated glycosaminoglycans. As such, urinary

glycosaminoglycans are highly promising biomarkers with both diagnostic and prognostic implications in critical illness.

Our observation that urine HS correlated strongly with urine HS degradation activity in septic shock is consistent with septic induction of glomerular heparanase, as predicted by animal models of septic kidney injury[202]. These findings are compatible with a renal source of HS degradation (e.g. within the glomerular glycocalyx) and may not simply reflect circulating plasma HS (i.e., released from extra-renal injury). This potential renal selectivity of urine HS fragmentation is supported by the absence of association between urine HS and the etiology of septic shock (pulmonary *vs*. nonpulmonary), contrasting the significant associations we have previously observed between plasma HS and infection source during sepsis[31]. Interestingly, in patients with ARDS, baseline levels of urine HS were significantly elevated in comparison to our septic shock cohort (which was characterized by a low prevalence of ARDS). While we cannot exclude a "batch effect" of short-term (i.e. septic shock/trauma) vs. prolonged (ARDS) sample storage, we speculate that in ARDS, elevated levels of circulating HS fragments (reflecting pulmonary induction of heparanase[202]) may "spill" into the urine, obscuring the correlation of urinary HS with glomerular pathophysiology. Indeed, the presence of glycosaminoglycan "spilling" is supported by a strong trend of increased urine HS in ARDS patients with non-pulmonary sepsis, a pattern observed in the plasma of such patients[31].

While activation of glomerular heparanase can explain increased urine HS, this enzyme cannot directly account for the observed increases in HA and CS. These unexpected findings suggest the activation of additional GAG-degrading renal enzymes in septic shock. Elevated urinary CS has been previously observed in children with meningococcal sepsis[237], with roughly equivalent elevations of 4S- and 6S-CS, contrasting the 4S-predominance seen in our patients. Interestingly, 4S CS is commonly found within bikunin, a proteoglycan constituent of the urinary trypsin inhibitor IαI[238]. However, bikunin-associated CS is typically characterized by a 1:2 ratio of 4S:0S disaccharides[238], inconsistent with the pattern observed

in our patients with septic shock or ARDS. Accordingly, we found no association between urine CS and bikunin in patients with septic shock. The elevations of urine CS in septic shock contrast the relative stability of plasma CS in our previous study of sepsis-associated respiratory failure[31], again suggesting that urine GAG fragments primarily reflect localized renal degradation.

HA has been implicated in several renal diseases, including renal ischemia-reperfusion injury[239,240]. We observed that septic shock patients had a significant increase in urine HA, which was highly predictive of renal dysfunction and in-hospital mortality. Similarly, urine HA predicted mortality in patients with ARDS. Recent reports have highlighted the utility of urine HA as an early biomarker of kidney injury after intraoperative cardiopulmonary bypass[230]. We previously found no association between plasma HA and non-pulmonary sepsis in patients with respiratory failure[31], further supporting the conclusion that urinary HA fragments reflect renal HA degradation (and not systemic HA degradation) during septic shock.

The potential value of urine GAGs as a predictive biomarker may be limited by concerns about generalizability, given the high mortality in the septic shock and ARDS cohorts. However, we are reassured that the prognostic utility of urine GAGs remains even when expanding our prospectively-enrolled cohort to include the less-sick trauma population. Furthermore, this predictive value persists when controlling for severity of illness in septic shock. Of note, while APACHE-II contains indices of renal dysfunction, this potential collinearity would be expected to decrease the predictive ability of urinary GAGs. On the contrary, this ability was increased on multivariate analysis, meeting or exceeding previously-reported single or multiplexed plasma or urine biomarkers of kidney injury[241,242]. As individualized APACHE-II data were not available for the validation cohort of ARDS patients, we were unable to similarly control for severity of illness in the analysis of ARDS urine samples. However, these samples were collected from a parent study in which baseline (day 0) mean APACHE-III scores were identical between the ARDS group that developed AKI and that which maintained normal renal function[213].

The clinical impact of our findings is supported by the ability to largely replicate the predictive capabilities of our mass spectrometry findings by using DMMB, an inexpensive GAG assay that can be directly performed on urine. While mass spectrometry affords highly-sensitive analyses of GAG concentrations and patterns of disaccharide sulfation, such analyses are time-intensive and expensive, costing approximately $200 per sample in our study (not including the costs of mass spectrometry equipment purchase, maintenance, and data analysis). In contrast, the DMMB assay, which detects highly-sulfated GAGs including HS and CS, can be easily performed in minutes, at low cost ($2 per sample, not including the relatively-inexpensive and commonly-available colorimetric plate reader). The generalizability of this DMMB assay should be prospectively tested in a future multicenter study inclusive of lower-acuity sepsis cohorts and/or other systemic illnesses associated with kidney dysfunction (e.g., severe acute pancreatitis).

5.4. Conclusions and future directions

In summary, the data presented above details the first investigation of the endogenous mechanisms underlying homeostatic pulmonary ESL reconstitution. Furthermore, this report identifies that FGFR1 serves as a critical mediator of ESL repair and is suppressed during sepsis. Our work raises numerous additional mechanistic questions, the pursuit of which promises to provide greater insight into ESL physiology during health and disease. The second paper demonstrates an association between urinary glycosaminoglycan concentrations (measured early in the course of critical illness) and the later onset/progression of renal dysfunction and hospital mortality. These associations, derived from highly-sophisticated mass spectrometry approaches, can be replicated with a widely-applicable, inexpensive colorimetric assay, demonstrating practical relevance of urinary GAGs as predictive markers in septic shock and ARDS.

5.5. Materials and methods

5.5.1. Human subject plasma samples

As previously described[31,202], we prospectively obtained plasma samples from mechanically-ventilated patients with non-pulmonary sepsis or pneumonia within 72 h of admission to the Denver Health Medical Center Medical ICU (ClinicalTrials.gov NCT009380002). We obtained written, informed consent from patients' proxy decision makers prior to plasma collection. The Colorado Multiple Institutions Review Board approved all protocols.

5.5.2. Induction of murine sepsis

We induced sepsis in 8-12 week-old male C57BL/6 mice by cecal ligation and puncture (CLP), as previously described[202].

5.5.3. Measurement of pulmonary ESL thickness

As previously described[202,215], we measured pulmonary ESL thickness by dextran exclusion using closed-chest intravital microscopy of the mouse subpleural microvasculature. For determination of ESL recovery after non-septic degradation, we administered a one-time dose of intravenous heparinase-III (1 (Sigma) unit, Sigma Aldrich, St. Louis) or heat-inactivated heparinase-III (1 unit, boiled x 15 min) and measured ESL thickness via dextran exclusion 24 h later. For determination of ESL recovery after sepsis, we performed CLP and then performed intravital microscopy of the subpleural microcirculation 24, 48, or 72 h later.

5.5.4. Plasma heparan sulfate isolation and quantification

HS was isolated from the plasma of patients with nonpulmonary sepsis (pooled from 4 subjects) or pneumonia (5 subjects) as previously described[31], and disaccharide analyses were performed via liquid chromatography-tandem mass spectrometry (LC-MS/MS)[128]. Plasma HS fragment size was determined via polyacrylamide gel electrophoresis and Alcian blue/silver staining, as previously described[31].

5.5.5. Surface plasmon resonance

The binding of HS oligosaccharides to FGF2 was determined using surface plasmon resonance (SPR). FGF2-HS binding was measured by the ability of exogenous HS oligosaccharides (of various sizes, sulfation) to interfere with FGF2 binding to heparin immobilized on a SPR chip, as detailed in[99].

5.5.6. BaF3 signaling assay

We treated BaF3 cells expressing FGFR1c (the non-epithelial FGFR1 isoform[227]) with FGF2 (5 nmol/l), FGF1 (5 nmol/l), or HS oligosaccharides/fragments (various concentrations) and measured optical density to determine the impact of HS oligosaccharides on FGF2-FGFR1 signaling. Alternatively, we treated cells with FGF2 (5 nmol/l) and HS fragments isolated from pooled human plasma (1 μg/ml). As these cells are dependent on FGFR1c for survival, cell density directly reflects FGFR1c activity, as previously described[196].

5.5.7. Statistical analyses

Animals were randomized to treatment or control groups. Experimental replicates were performed on the same day as a matching control. Single comparisons were made using Student's two-tailed t-test. Multiple comparisons were made by ANOVA with Tukey's post-hoc analysis. Results were considered statistically significant if $p < 0.05$. All graphs demonstrate mean values with standard errors. Analyses were performed using Prism (GraphPad).

5.5.8. Prospective enrollment of human subjects

Between July 2013 and November 2014, we prospectively enrolled adult patients admitted to the Denver Health Medical Center (Denver, Colorado) Medical ICU with a diagnosis of sepsis shock, as defined in the supplementary methods (ClinicalTrials.gov NCT01900275). Patients were eligible for inclusion if the diagnosis of septic shock was made < 24 h before enrollment. As a relatively-healthy (yet

ICU-admitted) comparator group, we concurrently enrolled adult patients admitted within the previous 24 h to the Denver Health Medical Center Surgical ICU for severe trauma, as defined by an Injury Severity Score > 15. A subset of these surgical ICU samples have been previously used to optimize mass spectrometry measures of urine GAGs[202]. Exclusion criteria are included in the online supplement.

At enrollment, 5 ml of urine was collected from subjects' urinary collection devices, centrifuged, and aliquots frozen. Written, informed consent was obtained from the patient. If the patient lacked decisional capacity during the 24 h window of enrollment, urine was collected (and documented in the medical record), processed, and stored. Once the patient regained decisional capacity, written informed consent was obtained. If at that time the patient declined to participate in the trial, the stored urine was destroyed. If the patient expired prior to regaining decisional capacity, collected urine and data were kept for analysis, in accordance with Colorado Multiple Institutions Review Board (COMIRB) policies applying to minimal-risk protocols. All protocols were approved by the COMIRB (approval # 13-0425).

The primary outcome was the development of worsening renal function between 24 and 72 h of enrollment. We defined progressive renal dysfunction as the development of new Acute Kidney Injury Network (AKIN) stage 2 criteria: a 2 x increase in serum creatinine from admission values (or > 0.5 mg/dl absolute change if baseline Cr > 4.0 mg/dl) or decreased urine output (< 0.5 ml/kg/h x 12 h). We recorded in-hospital mortality as a secondary outcome. All bloodwork and urine output measurements were recorded as part of standard clinical care.

5.5.9. Validation cohort of ARDS urine samples

We obtained de-identified, remnant urine samples from a study of urine IL-18 in ARDS[213]. These samples had been collected from patients 0, 1, and 3 days after enrollment in the Acute Respiratory Distress Syndrome Network (ARDSNet) ARMA study[243]; the NHLBI provided permission for continued use

of these remnant samples. These samples included 70 ARDS patients with normal renal function at baseline; 22 patients ("cases") later developed acute kidney injury (AKI), while 48 patients ("controls") maintained normal renal function. COMIRB authorized the "exempt" use of these deidentified samples, as previously described[213] and confirmed prior to current analyses.

5.5.10. Urine analyses

Urine glycosaminoglycan content was determined using mass spectrometry, as previously described[202]. Measurement of urinary heparanase activity, urinary bikunin, urinary heparanase activity, were performed as previously described[202]. The dimethylmethylene blue (DMMB) colorimetric assay was used to measure urine sulfated GAG concentrations as previously described[202].

Bibliography

[1] Suflita, M., Fu, L., He, W., Koffas, M. & Linhardt, R. J. Heparin and related polysaccharides: synthesis using recombinant enzymes and metabolic engineering. *Appl. Microbiol. Biotechnol.* **99,** 7465–7479 (2015).

[2] Fu, L., Suflita, M. & Linhardt, R. J. Bioengineered heparins and heparan sulfates. *Adv. Drug Deliv. Rev.* **97,** 237–249 (2016).

[3] Salmivirta, M., Lidholt, K. & Lindahl, U. Heparan sulfate: a piece of information. *FASEB J* **10,** 1270–1279 (1996).

[4] Linhardt, R. J. Heparin: structure and activity. *J. Med. Chem.* **46,** 2551–2564 (2003).

[5] Murphy, K. J. *et al.* A new model for the domain structure of heparan sulfate based on the novel specificity of K5 lyase. *J. Biol. Chem.* **279,** 27239–27245 (2004).

[6] Turnbull, J. & Gallagher, J. Distribution of iduronate 2-sulphate residues in heparan sulphate. Evidence for an ordered polymeric structure. *Biochem. J.* **273,** 553–559 (1991).

[7] Mikami, T. & Kitagawa, H. Biosynthesis and function of chondroitin sulfate. Biochim. Biophys. Acta **1830**, 4719–4733 (2013).

[8] Esko, J. & Selleck, S. Order out of chaos: assembly of ligand binding sites in heparan sulfate. Annu. Rev. Biochem. **71**, 435–471 (2002).

[9] Duelli, A., Ronnberg, I., Waern, M., Ringvall, S. & Pejler, G. Mast cell differentiation and activation is closely linked to expression of genes coding for the serglycin proteoglycan core protein and a distinct set of chondroitin sulfate and heparin sulfotransferases. *J. Immunol.* **183,** 7073–7083 (2009).

[10] Kramer, K. & Yost, H. Heparan sulfate core proteins in cell-cell signaling. *Annu. Rev. Genet.* **37,** 461–484 (2003).

[11] Sheng, J., Liu, R., Xu, Y. & Liu, J. The dominating role of N-deacetylase/N-sulfotransferase 1 in forming domain structures in heparan sulfate. *J. Biol. Chem.* **286,** 19768–19776 (2011).

[12] Shi, X. & Zaia, J. Organ-specific heparan sulfate structural phenotypes. *J. Biol. Chem.* **284,** 11806–11814 (2009).

[13] Weyers, A. *et al.* A structural analysis of glycosaminoglycans from lethal and nonlethal breast cancer tissues: toward a novel class of theragnostics for personalized medicine in oncology. *OMICS* **16,** 79–89 (2012).

[14] Garcia, O. & Quiros, L. Multiple alterations of heparan sulphate in cancer. *OA Cancer* **1,** 1–7 (2013).

[15] Kamhi, E., Joo, E., Dordick, J. & Linhardt, R. Glycosaminoglycans in infectious disease. *Biol. Rev.* **88,** 928–943 (2013).

[16] Munoz, E. & Linhardt, R. Heparin-binding domains in vascular biology. *Arter. Thromb. Vasc. Biol.* **24,** 1549–1557 (2004).

[17] Mousa, S. & Fareed, J. Overview: from heparin to low molecular weight heparin: beyond anticoagulation. *Curr. Opin. Investig. Drugs* **2,** 1077–1080 (2001).

[18] Xiao, Z. *et al.* Heparin mapping using heparin lyases and the generation of a novel low molecular weight heparin. *J. Med. Chem.* **54,** 603–610 (2011).

[19] Linhardt, R. & Toida, T. Role of glycosaminoglycans in cellular communication. *Acc. Chem. Res.* **37,** 431–438 (2004).

[20] Nadanaka, S. & Kitagawa, H. Heparan sulphate biosynthesis and disease. *J. Biochem.* **144,** 7–14 (2008).

[21] Capila, I. & Linhardt, R. Heparin-protein interactions. *Angew. Chem. Int. Ed. Engl.* **41,** 391–412 (2002).

[22] Xu, D. & Esko, J. D. Demystifying heparan sulfate–protein interactions. *Annu. Rev. Biochem.* **83,** 129–157 (2014).

[23] Guimond, S. E. & Turnbull, J. E. Fibroblast growth factor receptor signaling is dictated by specific heparan sulphate saccharides. *Curr. Biol.* **9,** 1343–1346 (1999).

[24] Beenken, A. & Mohammadi, M. The FGF family: biology, pathophysiology and therapy. *Nat. Rev. Drug Discov.* **8,** 235 (2009).

[25] Schlessinger, J. *et al.* Crystal structure of a ternary FGF-FGFR-heparin complex reveals a dual role for heparin in FGFR binding and dimerization. *Mol. Cell* **6,** 743–750 (2000).

[26] Kim, S.-H., Turnbull, J. & Guimond, S. Extracellular matrix and cell signaling: the dynamic cooperation of integrin, proteoglycan and growth factor receptor. *J. Endocrinol.* **209,** 139–151 (2011).

[27] Zhang, B. *et al.* Heparan sulfate deficiency disrupts developmental angiogenesis and causes congenital diaphragmatic hernia. *J. Clin. Invest.* **124,** 209–221 (2014).

[28] Stringer, S. E. The role of heparan sulphate proteoglycans in angiogenesis. *Biochem. Soc. Trans.* **34,** 451 LP-453 (2006).

[29] Barash, U. *et al.* Proteoglycans in health and disease: New concepts for heparanase function in tumor progression and metastasis. *FEBS J.* **277,** 10.1111/j.1742-4658.2010.07799.x (2010).

[30] Bernfield, M. *et al.* Functions of cell surface heparan sulfate proteoglycans. *Annu. Rev. Biochem.* **68,** 729–777 (1999).

[31] Schmidt, E. P. *et al.* The circulating glycosaminoglycan signature of respiratory failure in critically ill adults. *J. Biol. Chem.* **289,** 8194–8202 (2014).

[32] Zcharia, E. *et al.* Heparanase accelerates wound angiogenesis and wound healing in mouse and rat models. *FASEB J.* **19,** 211–221 (2005).

[33] Elenius, K. *et al.* Induced expression of syndecan in healing wounds. *J. Cell Biol.* **114,** 585 LP-595 (1991).

[34] Shafti-Keramat, S. *et al.* Different heparan sulfate proteoglycans serve as cellular receptors for human papillomaviruses. *J. Virol.* **77,** 13125–13135 (2003).

[35] Liu, J. *et al.* Characterization of a heparan sulfate octasaccharide that binds to herpes simplex virus type 1 glycoprotein D. *J. Biol. Chem.* **277,** 33456–33467 (2002).

[36] Sinnis, P. *et al.* Mosquito heparan sulfate and its potential role in malaria infection and transmission. *J. Biol. Chem.* **282,** 25376–25384 (2007).

[37] Garcia, B., Fernandez-Vega, I., Garcia-Suarez, O., Castanon, S. & Quiros, L. M. The role of heparan sulfate proteoglycans in bacterial infections. *J. Med. Microbiol. Diagnosis* **3,** (2014).

[38] Hayashida, A., Amano, S. & Park, P. W. Syndecan-1 promotes *Staphylococcus aureus* corneal infection by counteracting neutrophil-mediated host defense. *J. Biol. Chem.* **286,** 3288–3297 (2011).

[39] Wang, L., Brown, J. R., Varki, A. & Esko, J. D. Heparin's anti-inflammatory effects require glucosamine 6-O-sulfation and are mediated by blockade of L- and P-selectins. *J. Clin. Invest.* **110,** 127–136 (2002).

[40] Nelson, R. M. *et al.* Heparin oligosaccharides bind L- and P-selectin and inhibit acute inflammation. *Blood* **82,** 3253–3258 (1993).

[41] Parish, C. R., Freeman, C. & Hulett, M. D. Heparanase: a key enzyme involved in cell invasion. *Biochim. Biophys. Acta* **1471,** M99-108 (2001).

[42] Takaoka, M. *et al.* Heparanase expression correlates with invasion and poor prognosis in gastric cancers. *Lab. Investig.* **83,** 613–622 (2003).

[43] Sato, T. *et al.* Heparanase expression in human colorectal cancer and its relationship to tumor angiogenesis, hematogenous metastasis, and prognosis. *J. Surg. Oncol.* **87,** 174–81 (2004).

[44] Vlodavsky, I. *et al.* Mammalian heparanase: gene cloning, expression and function in tumor progression and metastasis. *Nat. Med.* **5,** 793–802 (1999).

[45] Vlodavsky, I. & Friedmann, Y. Heparan sulfate proteoglycans: Molecular properties and involvement of heparanase in cancer metastasis and angiogenesis. *J. Clin. Investig.* **108,** 341–347 (2001).

[46] Ramani, V. C. *et al.* The heparanase/syndecan-1 axis in cancer: mechanisms and therapies. *FEBS* **280,** 2294–2306 (2013).

[47] Stevenson, J. L., Varki, A. & Borsig, L. Heparin attenuates metastasis mainly due to inhibition of P- and L-selectin, but non-anticoagulant heparins can have additional effects. *Thromb. Res.* **120,** 107–111 (2007).

[48] Li, J.-P. & Vlodavsky, I. Heparin, heparan sulfate and heparanase in inflammatory reactions. *Thromb. Haemost.* **102,** 823–8 (2009).

[49] Lazo-Langner, A., Goss, G. D., Spaans, J. N. & Rodger, M. A. The effect of low-molecular-weight heparin on cancer survival. A systematic review and meta-analysis of randomized trials. *J. Thromb. Haemost.* **5,** 729–737 (2007).

[50] Fath, M. A. *et al.* Interaction of secretory leukocyte protease inhibitor with heparin inhibits proteases involved in asthma. *J. Biol. Chem.* **273,** 13563–13569 (1998).

[51] Yu, G. *et al.* Preparation and anticoagulant activity of the phosphosulfomannan PI-88. *Eur. J. Med. Chem.* **37,** 783–791 (2002).

[52] Linhardt, R. J. Heparin: structure and activity. *J. Med. Chem.* **46,** 2551–2564 (2003).

[53] Guerrini, M. *et al.* Oversulfated chondroitin sulfate is a contaminant in heparin associated with adverse clinical events. *Nat. Biotechnol.* **26,** 669 (2008).

[54] Schonberger, L. New variant Creutzfeldt-Jakob disease and bovine spongiform encephalopathy. *Infect Dis. Clin. North Am.* **1**, 111–121 (1998).

[55] Evans T. D., Mozen M. M. Process for purifying heparin. US Pat. #3058884 (1962).

[56] Williams R. E., Process for the recovery of heparin. US Pat. #3337409 (1967).

[57] Okuyama T. *et al.* Method of separating and recovering mucopolysaccharides from connective tissues of animals. US Pat. #3862003 (1975).

[58] Vidic H-J. Process for the preparation of heparin. US patent #4283530 (1981).

[59] Linhardt, R. J. et al. Isolation and characterization of human heparin. *Biochemistry* **31**, 12441–12445 (1992).

[60] Van Gorp C. L., Vosburgh F., & Schubert R. L. Protein hydrolysate derived from mucosa tissue. US Pat. #5607840 (1997).

[61] Bhaskar, U. *et al.* Engineering of routes to heparin and related polysaccharides. *Appl. Microbiol. Biotechnol.* **93,** 1–16 (2012).

[62] Liu, H., Zhang, Z. & Linhardt, R. J. Lessons learned from the contamination of heparin. *Nat. Prod. Rep.* **26,** 313–321 (2009).

[63] Loganathan, D., Wang, H. M., Mallis, L. M. & Linhardt, R. J. Structural variation in the antithrombin III binding site region and its occurrence in heparin from different sources. *Biochemistry* **29,** 4362–4368 (1990).

[64] Fu, L. *et al.* Structural characterization of pharmaceutical heparins prepared from different animal tissues. *J. Pharm. Sci.* **102,** 1447–1457 (2013).

[65] Higashi, K. *et al.* Photochemical preparation of a novel low molecular weight heparin. *Carbohydr. Polym.* **67,** 1737–1743 (2012).

[66] Toschi, V. & Lettino, M. Fondaparinux: Pharmacology and clinical experience in cardiovascular medicine. *Mini-Rev. Med. Chem* **7,** (2007).

[67] Petitou, M. *et al.* Synthesis of heparin fragments. A chemical synthesis of the pentasaccharide O-(2-deoxy-2-sulfamido-6-O-sulfo-α-d-glucopyranosyl)-(1→4)-O-(β-d-glucopyranosyluronic acid)-(1→4)-O-(2-deoxy-2-sulfamido-3,6-di-O-sulfo-α-d-glucopyranosyl)-(1→4)-O-(2-O-sulfo-α-l-

idopyranosyluronic acid)-(1→4)-2-deoxy-2-sulfamido-6-O-sulfo-d-glucopyranose decasodium salt, a heparin fragment having high affinity for antithrombin III. *Carbohydr. Res.* **147,** 221–236 (1986).

[68] Bick, R. L., Frenkel, E. P., Walenga, J., Fareed, J. & Hoppensteadt, D. A. Unfractionated heparin, low molecular weight heparins, and pentasaccharide: Basic mechanism of actions, pharmacology, and clinical use. *Hematol. Clin.* **19,** 1–51 (2018).

[69] Viskov, C., Just, M., Laux, V., Mourier, P. & Lorenz, M. Description of the chemical and pharmacological characteristics of a new hemisynthetic ultra-low-molecular-weight heparin, AVE5026. *J. Thromb. Haemost.* **7,** 1143–1151 (2009).

[70] Lassen, M., Dahl, O., Mismetti, P., Destree, D. & Turpie, A. AVE5026, a new hemisynthetic ultra-low-molecular-weight heparin for the prevention of venous thromboembolism in patients after total knee replacement surgery – TREK: a dose-ranging study. *J. Thromb. Haemost.* **7,** 566–572 (2009).

[71] Gijsen, H. J. M., Qiao, L., Fitz, W. & Wong, C.-H. Recent advances in the chemoenzymatic synthesis of carbohydrates and carbohydrate mimetics. *Chem. Rev.* **96,** 443–474 (1996).

[72] Linhardt, R. & Karst, N. Recent chemical and enzymatic approaches to the synthesis of glycosaminoglycan oligosaccharides. *Curr. Med. Chem.* **10,** 1993–2031 (2003).

[73] Deangelis, P. L., Liu, J. & Linhardt, R. J. Chemoenzymatic synthesis of glycosaminoglycans: Re-creating, re-modeling and re-designing nature's longest or most complex carbohydrate chains. *Glycobiology* **23,** 764–777 (2013).

[74] Orellana, A., Hirschberg, C. B., Wei, Z., Swiedler, S. J. & Ishihara, M. Molecular cloning and expression of a glycosaminoglycan N-acetylglucosaminyl N-deacetylase/N-sulfotransferase from a heparin-producing cell line. *J. Biol. Chem.* **269,** 2270–2276 (1994).

[75] DeAngelis, P. L. & White, C. L. Identification and molecular cloning of a heparosan synthase from *Pasteurella multocida* type D. *J. Biol. Chem.* **277,** 7209–7213 (2002).

[76] Naggi, A. *et al.* Toward a biotechnological heparin through combined chemical and enzymatic modification of the *Escherichia coli* K5 polysaccharide. *Semin. Thromb. Hemost.* **27,** 437–444 (2001).

[77] Kuberan, B., Lech, M. Z., Beeler, D. L., Wu, Z. L. & Rosenberg, R. D. Enzymatic synthesis of antithrombin III–binding heparan sulfate pentasaccharide. *Nat. Biotechnol.* **21,** 1343 (2003).

[78] Liu, R. *et al.* Chemoenzymatic design of heparan sulfate oligosaccharides. *J. Biol. Chem.* **285,** 34240–9 (2010).

[79] Masuko, S. *et al.* Chemoenzymatic synthesis of uridine diphosphate-GlcNAc and uridine diphosphate-GalNAc analogs for the preparation of unnatural glycosaminoglycans. *J. Org. Chem.* **77,** 1449–1456 (2012).

[80] Xu, Y. *et al.* Homogeneous low-molecular-weight heparins with reversible anticoagulant activity. *Nat. Chem. Biol.* **10,** 248 (2014).

[81] Sugiura, N., Tawada, A., Sugimoto, K. & Watanabe, H. Molecular cloning and characterization of chondroitin polymerase from Escherichia coli strain K4. *J. Biol. Chem.* **277,** 21567–21575 (2002).

[82] Sismey-Ragatz, A. E. *et al.* Chemoenzymatic synthesis with distinct *Pasteurella* heparosan synthases: Monodisperse polymers and unnatural structures. *J. Biol. Chem.* **282,** 28321–28327 (2007).

[83] Chavaroche, A. a E., Van Den Broek, L. a M., Boeriu, C. & Eggink, G. Synthesis of heparosan oligosaccharides by *Pasteurella multocida* PmHS2 single-action transferases. *Appl. Microbiol. Biotechnol.* **95,** 1199–1210 (2012).

[84] Berninsone, P. & Hirschberg, C. Heparan sulfate/heparin N-deacetylase/N-sulfotransferase: The N-sulfotransferase activity domain is at the carboxyl half of the holoenzyme. *J. Biochem.* **273,** 25556–25559 (1998).

[85] Sheng, J., Liu, R., Xu, Y. & Liu, J. The dominating role of N-deacetylase/N-sulfotransferase 1 in forming domain structures in heparan sulfate. *J. Biol. Chem.* **286,** 19768–19776 (2011).

[86] Qin, Y. *et al.* Structural and functional study of D-glucuronyl C5-epimerase. *J. Biol. Chem.* **290,** 4620-4630 (2015).

[87] Liu, C. *et al.* Molecular mechanism of substrate specificity for heparan sulfate 2-O-sulfotransferase. *J. Biol. Chem.* **289,** 13407–13418 (2014).

[88] Moon, A. F. *et al.* Structural analysis of the sulfotransferase (3-O-sulfotransferase isoform 3) involved in the biosynthesis of an entry receptor for herpes simplex virus 1. *J. Biol. Chem.* **279,** 45185–45193 (2004).

[89] Moon, a. F. *et al.* Dissecting the substrate recognition of 3-O-sulfotransferase for the biosynthesis of anticoagulant heparin. *Proc. Natl. Acad. Sci.* **109,** 5265–5270 (2012).

[90] Kusche-Gullberg, M. & Kjellén, L. Sulfotransferases in glycosaminoglycan biosynthesis. *Curr. Opin. Struct. Biol.* **13,** 605–611 (2003).

[91] Sugiura, N. *et al.* Construction of a chondroitin sulfate library with defined structures and analysis of molecular interactions. *J. Biol. Chem.* **287,** 43390–43400 (2012).

[92] Silbert, J. E. & Sugumaran, G. Biosynthesis of chondroitin/dermatan sulfate. *IUBMB Life* **54,** 177–186 (2002).

[93] Pacheco, B., Maccarana, M., Goodlett, D. R., Malmström, A. & Malmström, L. Identification of the active site of DS-epimerase 1 and requirement of N-glycosylation for enzyme function. *J. Biol. Chem.* **284,** 1741–1747 (2009).

[94] Pacheco, B., Malmström, A. & Maccarana, M. Two dermatan sulfate epimerases form iduronic acid domains in dermatan sulfate. *J. Biol. Chem.* **284,** 9788–9795 (2009).

[95] Thelin, M. A. *et al.* Biological functions of iduronic acid in chondroitin/dermatan sulfate. *Febs J.* **280,** 2431–2446 (2013).

[96] Higashi, K. *et al.* Composition of Glycosaminoglycans in Elasmobranchs including Several Deep-Sea Sharks: Identification of Chondroitin/Dermatan Sulfate from the Dried Fins of Isurus oxyrinchus and Prionace glauca. *PLoS One* **10,** e0120860 (2015). https://doi.org/10.1371/journal.pone.0120860

[97] Burkart, M. D., Izumi, M., Chapman, E., Lin, C. H. & Wong, C. H. Regeneration of PAPS for the enzymatic synthesis of sulfated oligosaccharides. *J. Org. Chem.* **65,** 5565–74 (2000).

[98] Burkart, M. D. & Wong, C. H. A continuous assay for the spectrophotometric analysis of sulfotransferases using aryl sulfotransferase IV. *Anal. Biochem.* **274,** 131–7 (1999).

[99] Sterner, E. *et al.* Assays for determining heparan sulfate and heparin O-sulfotransferase activity and specificity. *Anal. Bioanal. Chem.* **406,** 525–536 (2014).

[100] Restaino, O. F. *et al.* High cell density cultivation of a recombinant E. coli strain expressing a key enzyme in bioengineered heparin production. *Appl. Microbiol. Biotechnol.* **97,** 3893–900 (2013).

[101] Zhang, J., *et al*. High cell density cultivation of a recombinant *Escherichia coli* strain expressing a 6-O-sulfotransferase for the production of bioengineered heparin. *Appl. Microbiol.* **97,** 3893–3900 (2014).

[102] Zhang, J., *et al*. High cell density cultivation of recombinant *Escherichia coli* strains expressing 2-O-sulfotransferase and C5-epimerase for the production of bioengineered heparin. *Appl. Biochem. Biotechnol.* **175,** 2986–2995 (2015).

[103] Xu, Y. *et al.* Chemoenzymatic synthesis of homogeneous ultralow molecular weight heparins. *Science* **334,** 498–501 (2011).

[104] Sheng, J., Xu, Y., Dulaney, S. B., Huang, X. & Liu, J. Uncovering biphasic catalytic mode of C5-epimerase in heparan sulfate biosynthesis. *J. Biol. Chem.* **287,** 20996–21002 (2012).

[105] Yi, C. *et al.* Tailored design and synthesis of heparan sulfate oligosaccharide analogues using sequential one-pot multienzyme systems. *Angew. Chemie Int. Ed.* **52,** 11852–11856 (2013).

[106] Fu, L. *et al.* Structure and activity of a new low-molecular-weight heparin produced by enzymatic ultrafiltration. *J. Pharm. Sci.* **103,** 1375–1383 (2014).

[107] Zhang, Z. *et al.* Solution structures of chemoenzymatically synthesized heparin and its precursors. *J. Am. Chem. Soc.* **130,** 12998–13007 (2008).

[108] Wang, Z. *et al.* Control of the heparosan N-deacetylation leads to an improved bioengineered heparin. *Appl. Microbiol. Biotechnol.* **91,** 91–99 (2011).

[109] Lindahl, U., Kusche-Gullberg, M. & Kjellen, L. Regulated diversity of heparan sulfate. *J. Biol. Chem.* **273,** 24979–24982 (1998).

[110] Linhardt, R. J. & Liu, J. Synthetic heparin. *Curr. Opin. Pharmacol.* **12,** 217–219 (2012).

[111] Zhou, X., Chandarajoti, K., Pham, T. Q., Liu, R. & Liu, J. Expression of heparan sulfate sulfotransferases in *Kluyveromyces lactis* and preparation of 3'-phosphoadenosine-5'-phosphosulfate. *Glycobiology* **21,** 771–780 (2011).

[112] Wang, W. *et al.* Expression of low endotoxin 3-o-sulfotransferase in *Bacillus subtilis* and *Bacillus megaterium*. *Appl. Biochem. Biotechnol.* **171,** 954–962 (2013).

[113] Xiong, J. *et al.* Immobilized enzymes to convert N-sulfo, N-acetyl heparosan to a critical intermediate in the production of bioengineered heparin. *J. Biotechnol.* **167,** 241–247 (2013).

[114] Clarke, B. R., Esumeh, F. & Roberts, I. S. Cloning, expression, and purification of the K5 capsular polysaccharide lyase (KflA) from coliphage K5A: Evidence for two distinct K5 lyase enzymes. *J. Bacteriol.* **182,** 3761–3766 (2000).

[115] Finke, A., Bronner, D., Nikolaev, A. V, Jann, B. & Jann, K. Biosynthesis of the *Escherichia coli* K5 polysaccharide, a representative of group II capsular polysaccharides: polymerization in vitro and characterization of the product. *J. Bacteriol.* **173,** 4088–4094 (1991).

[116] Fu, L. *et al.* Heparin stability by determining unsubstituted amino groups using hydrophilic interaction chromatography mass spectrometry. *Anal. Biochem.* **461,** 46–48 (2014).

[117] Bhaskar, U., *et al*. Combinatorial one-pot chemoenzymatic synthesis of heparin. *Carbohydr. Polym.* **122,** 399–407 (2014).

[118] Wang, Z. *et al.* E. coli K5 fermentation and the preparation of heparosan, a bioengineered heparin precursor. *Biotechnol. Bioeng.* **107,** 964–973 (2010).

[119] Chen, J. *et al.* Enzymatic redesigning of biologically active heparan sulfate. *J. Biol. Chem.* **280,** 42817–42825 (2005).

[120] Paul, P., Suwan, J., Liu, J., Dordick, J. S. & Linhardt, R. J. Recent advances in sulfotransferase enzyme activity assays. *Anal. Bioanal. Chem.* **403,** 1491–1500 (2012).

[121] Li, K., Bethea, H. N. & Liu, J. Using engineered 2-O-sulfotransferase to determine the activity of heparan sulfate C5-epimerase and its mutants. *J. Biol. Chem.* **285,** 11106–11113 (2010).

[122] Nakano, K., Rischke, M., Sato, S. & Markl, H. Influence of acetic acid on the growth of *Escherichia coli* K12 during high-cell-density cultivation in a dialysis reactor. *Appl. Microbiol. Biotechnol.* **48,** 597–601 (1997).

[123] Kwan, Y. S., Koo, K. W. & Hyun, P. T. Fed-batch operation of recombinant *Escherichia coli* containing trp promoter with controlled specific growth rate. *Biotechnol. Bioeng.* **43,** 995–999 (2004).

[124] Konstantin, K., Michimasa, K., Tatsuji, S. & Toshiomi, Y. A balanced DO-stat and its application to the control of acetic acid excretion by recombinant *Escherichia coli*. *Biotechnol. Bioeng.* **36,** 750–758 (2004).

[125] Jong-Am, S., Dae-Sung, L., Jin-Seung, P., Kyung-Yeon, H. & Jeewon, L. The N-domain of Escherichia coli phosphoglycerate kinase is a novel fusion partner to express aggregation-prone heterologous proteins. *Biotechnol. Bioeng.* **109,** 325–335 (2011).

[126] Dobson, C. M. Protein folding and misfolding. *Nature* **426,** 884 (2003).

[127] Muñoz, E. *et al.* Enzymatic synthesis of heparin related polysaccharides on sensor chips: Rapid screening of heparin–protein interactions. *Biochem. Biophys. Res. Commun.* **339,** 597–602 (2006).

[128] Yang, B., Chang, Y., Weyers, A. M., Sterner, E. & Linhardt, R. J. Disaccharide analysis of glycosaminoglycan mixtures by ultra-high-performance liquid chromatography–mass spectrometry. *J. Chromatogr. A* **1225,** 91–98 (2012).

[129] Cai, C., *et al*. Fluorous-assisted chemoenzymatic synthesis of heparan sulfate oligosaccharides. *Org. Lett.* **16,** 2240–3 (2014).

[130] Gandhi, N. S. & Mancera, R. L. Heparin/heparan sulphate-based drugs. *Drug Discov. Today* **15,** 1058–1069 (2010).

[131] Lindahl, U. & Kjellen, L. Heparin or heparan sulfate--what is the difference? *Thromb. Haemost.* **66,** 44–48 (1991).

[132] Casu, B. & Lindahl, U. in *Advances in Carbohydrate Chemistry and Biochemistry*. **57,** 159–206 (Academic Press, 2001).

[133] Bishop, J. R., Schuksz, M. & Esko, J. D. Heparan sulphate proteoglycans fine-tune mammalian physiology. *Nature* **446,** 1030 (2007).

[134] Gandhi, N. S. & Mancera, R. L. The Structure of glycosaminoglycans and their interactions with proteins. *Chem. Biol. Drug Des.* **72,** 455–482 (2008).

[135] Wang, Z. *et al.* A general strategy for the chemoenzymatic synthesis of asymmetrically branched N-glycans. *Science.* **341,** 379–383 (2013).

[136] Chen, Y. *et al.* Tailored design and synthesis of heparan sulfate oligosaccharide analogues using sequential one-pot multienzyme systems. *Angew. Chemie Int. Ed.* **52,** 11852–11856 (2013).

[137] Studer, A. *et al.* Fluorous synthesis: A fluorous-phase strategy for improving separation efficiency in organic synthesis. *Science.* **275,** 823 LP-8Fu26 (1997).

[138] Curran, D. P. Fluorous tags unstick messy chemical biology problems. *Science.* **321,** 1645 -1646 (2008).

[139] Brittain, S. M., Ficarro, S. B., Brock, A. & Peters, E. C. Enrichment and analysis of peptide subsets using fluorous affinity tags and mass spectrometry. *Nat. Biotechnol.* **23,** 463 (2005).

[140] Mizuno, M., Goto, K., Miura, T., Hosaka, D. & Inazu, T. A novel peptide synthesis using fluorous chemistry. *Chem. Comm.* **8,** 972-973 (2003).

[141] Ko, K.-S., Jaipuri, F. A. & Pohl, N. L. Fluorous-based carbohydrate microarrays. *J. Am. Chem. Soc.* **127,** 13162–13163 (2005).

[142] Zhang, W. & Lu, Y. Fluorous synthesis of hydantoins and thiohydantoins. *Org. Lett.* **5,** 2555–2558 (2003).

[143] Palmacci, E. R., Hewitt, M. C. & Seeberger, P. H. 'Cap-tag'—novel methods for the rapid purification of oligosaccharides prepared by automated solid-phase synthesis. *Angew. Chemie Int. Ed.* **40,** 4433–4437 (2001).

[144] Yang, B., Jing, Y. & Huang, X. Fluorous-assisted one-pot oligosaccharide synthesis. *European J. Org. Chem.* **2010,** 1290–1298 (2010).

[145] Jaipuri, F. A. & Pohl, N. L. Toward solution-phase automated iterative synthesis: fluorous-tag assisted solution-phase synthesis of linear and branched mannose oligomers. *Org. Biomol. Chem.* **6,** 2686–2691 (2008).

[146] Zong, C., Venot, A., Dhamale, O. & Boons, G.-J. Fluorous supported modular synthesis of heparan sulfate oligosaccharides. *Org. Lett.* **15,** 342–345 (2013).

[147] Linhardt, R. & Gunay, N. Production and chemical processing of low molecular weight heparins. *Semin. Thromb. Hemost.* **25,** 5–16 (1999).

[148] Wilesmith, J. W., Wells, G. A., Cranwell, M. P. & Ryan, J. B. Bovine spongiform encephalopathy: epidemiological studies. *Vet. Rec.* **123,** 638 LP-644 (1988).

[149] Hickey, A. M., Bhaskar, U., Linhardt, R. J. & Dordick, J. S. Effect of eliminase gene (elmA) deletion on heparosan production and shedding in *Escherichia coli* K5. *J. Biotechnol.* **165,** 175–177 (2013).

[150] Bethea, H., Xu, D., Liu, J. & Pedersen, L. Redirecting the substrate specificity of heparan sulfate 2-O-sulfotransferase by structurally guided mutagenesis. *PNAS* **105,** 18724–18729 (2008).

[151] Myette, J. R. *et al.* Expression in *Escherichia coli*, purification and kinetic characterization of human heparan sulfate 3-O-sulfotransferase-1. *Biochem. Biophys. Res. Commun.* **290,** 1206–1213 (2002).

[152] Polat, T. & Wong, C.-H. Anomeric reactivity-based one-pot synthesis of heparin-like oligosaccharides. *J. Am. Chem. Soc.* **129,** 12795–12800 (2007).

[153] Noti, C., de Paz, J., Polito, L. & Seeberger, P. Preparation and use of microarrays containing synthetic heparin oligosaccharides for the rapid analysis of heparin–protein interactions. *Chem. A Eur. J.* **12,** 8664–8686 (2006).

[154] Li, G. *et al.* Analysis of 3-O-sulfo group containing heparin tetrasaccharides in heparin by liquid chromatography-mass spectrometry. *Anal. Biochem.* **455,** 3–9 (2014).

[155] Zhang, F. *et al.* Structural characterization of heparins from different commercial sources. *Anal. Bioanal. Chem.* **401,** 2793–2803 (2011).

[156] Pinhal, M. A. S. *et al.* Enzyme interactions in heparan sulfate biosynthesis: Uronosyl 5-epimerase and 2-O-sulfotransferase interact *in vivo*. *Proc. Natl. Acad. Sci. U. S. A.* **98,** 12984–12989 (2001).

[157] Holmer, E., Kurachi, K. & Söderström, G. The molecular-weight dependence of the rate-enhancing effect of heparin on the inhibition of thrombin, factor Xa, factor IXa, factor XIa, factor XIIa and kallikrein by antithrombin. *Biochem. J.* **193,** 395–400 (1981).

[158] Mulloy, B. *et al.* USP compendial methods for analysis of heparin: chromatographic determination of molecular weight distributions for heparin sodium. *Anal. Bioanal. Chem.* **20,** 4815–4823 (2014).

[159] Chen, J., Jones, C. L. & Liu, J. Using an enzymatic combinatorial approach to identify anticoagulant heparan sulfate structures. *Chem. Biol.* **14,** 986–993 (2007).

[160] Higashi, K. *et al.* Controlled photochemical depolymerization of K5 heparosan, a bioengineered heparin precursor. *Carbohydr. Polym.* **86,** 1365–1370 (2011).

[161] Gallagher, J. T. Structure-activity relationship of heparan sulphate. *Biochem. Soc. Trans.* **25,** 1206–1209 (1997).

[162] Safaiyan, F., Lindahl, U. & Salmivirta, M. Structural diversity of N-sulfated heparan sulfate domains: Distinct modes of glucuronyl C5 epimerization, iduronic acid 2-O-sulfation, and glucosamine 6-O-sulfation. *Biochemistry* **39,** 10823–10830 (2000).

[163] Schultz, V. *et al.* Heparan sulfate domains required for fibroblast growth factor 1 and 2 signaling through fibroblast growth factor receptor 1c. *J. Biol. Chem.* **292,** 2495–2509 (2017).

[164] Jastrebova, N., Vanwildemeersch, M., Lindahl, U. & Spillmann, D. Heparan sulfate domain organization and sulfation modulate FGF-induced cell signaling. *J. Biol. Chem.* **285,** 26842–26851 (2010).

[165] Kusche-Gullberg, M., Nybakken, K., Perrimon, N. & Lindahl, U. Drosophila heparan sulfate, a novel design. *J. Biol. Chem.* **287,** 21950–21956 (2012).

[166] Smits, N. C. *et al.* The heparan sulfate motif (GlcNS6S-IdoA2S)3, common in heparin, has a strict topography and is involved in cell behavior and disease. *J. Biol. Chem.* **285,** 41143–41151 (2010).

[167] Lambaerts, K., Wilcox-Adelman, S. A. & Zimmermann, P. The signaling mechanisms of syndecan heparan sulfate proteoglycans. *Curr. Opin. Cell Biol.* **21,** 662–669 (2009).

[168] Lindahl, U. & Li, J. in *International Review of Cell and Molecular Biology* **276,** 105–159 (Academic Press, 2009).

[169] Kreuger, J., Spillmann, D., Li, J. & Lindahl, U. Interactions between heparan sulfate and proteins: the concept of specificity. *J. Cell Biol.* **174,** 323–327 (2006).

[170] Staples, G. O., Shi, X. & Zaia, J. Glycomics Analysis of mammalian heparan sulfates modified by the human extracellular sulfatase HSulf2. *PLoS One* **6,** e16689 (2011). https://doi.org/10.1371/journal.pone.0016689

[171] Ramani, V. C. *et al.* The heparanase/syndecan-1 axis in cancer: mechanisms and therapies. *FEBS* **280,** 2294–2306 (2013).

[172] Rosenberg, R. D., Armand, G. & Lam, L. Structure-function relationships of heparin species. *Proc. Natl. Acad. Sci. U. S. A.* **75,** 3065–3069 (1978).

[173] Gallagher, J. T., Turnbull, J. E. & Lyon, M. Patterns of sulphation in heparan sulphate: Polymorphism based on a common structural theme. *Int. J. Biochem.* **24,** 553–560 (1992).

[174] Puvirajesinghe, T. M. *et al.* Array-based functional screening of heparin glycans. *Chem. Biol.* **19,** 553–558 (2012).

[175] Pervin, A., Gallo, C., Jandik, K., Han, X. & Linhardt, R. Preparation and structural characterization of large heparin-derived oligosaccharides. *Glycobiology* **5,** 83–95 (1995).

[176] Hileman, R., Smith, A., Toida, T. & Linhardt, R. Preparation and structure of heparin lyase-derived heparan sulfate oligosaccharides. *Glycobiology* **7,** 231–239 (1997).

[177] Sterner, E. *et al.* Fibroblast growth factor-based signaling through synthetic heparan sulfate block copolymers studied using high-cell density 3D cell printing. *J. Biol. Chem.* **289**, 9754-9765 (2014).

[178] Williams, K. J., Halkes, K. M., Kamerling, J. P. & DeAngelis, P. L. Critical elements of oligosaccharide acceptor substrates for the *Pasteurella multocida* hyaluronan synthase. *J. Biol. Chem.* **281,** 5391–5397 (2006).

[179] Jing, W. & DeAngelis, P. L. Synchronized chemoenzymatic synthesis of monodisperse hyaluronan polymers. *J. Biol. Chem.* **279,** 42345–42349 (2004).

[180] Montesano, R., Vassalli, J. D., Baird, A., Guillemin, R. & Orci, L. Basic fibroblast growth factor induces angiogenesis *in vitro*. *Proc. Natl. Acad. Sci. U. S. A.* **83,** 7297–7301 (1986).

[181] Iwabu, A., Smith, K., Allen, F. D., Lauffenburger, D. A. & Wells, A. Epidermal growth factor induces fibroblast contractility and motility via a protein kinase C δ-dependent pathway. *J. Biol. Chem.* **279,** 14551–14560 (2004).

[182] Marie, P. J. Fibroblast growth factor signaling controlling osteoblast differentiation. *Gene* **316,** 23–32 (2003).

[183] Melder, R. J. *et al.* During angiogenesis, vascular endothelial growth factor regulate natural killer cell adhesion to tumor endothelium. *Nat. Med.* **2,** 992–997 (1996).

[184] Sanchez-Heras, E., Howell, F. V, Williams, G. & Doherty, P. The fibroblast growth factor receptor acid box is essential for interactions with N-cadherin and all of the major isoforms of neural cell adhesion molecule. *J. Biol. Chem.* **281,** 35208–35216 (2006).

[185] Ornitz, D. M. & Itoh, N. Fibroblast growth factors. *Genome Biol.* **2,** 1–12 (2001).

[186] Zhang, X. *et al.* Receptor specificity of the fibroblast growth factor family: The complete mammalian FGF family. *J. Biol. Chem.* **281,** 15694–15700 (2006).

[187] Mohammadi, M., Olsen, S. K. & Ibrahimi, O. a. Structural basis for fibroblast growth factor receptor activation. *Cytokine Growth Factor Rev.* **16,** 107–37 (2005).

[188] Ibrahimi, O. A., Zhang, F., Lang Hrstka, S. C., Mohammadi, M. & Linhardt, R. J. Kinetic model for FGF, FGFR, and proteoglycan signal transduction complex assembly. *Biochemistry* **43,** 4724–4730 (2004).

[189] Brown, A., Robinson, C. J., Gallagher, J. T. & Blundell, T. L. Cooperative heparin-mediated oligomerization of fibroblast growth factor-1 (FGF1) precedes recruitment of FGFR2 to ternary complexes. *Biophys. J.* **104,** 1720–1730 (2013).

[190] Jaye, M., Schlessinger, J. & Dionne, C. A. Fibroblast growth factor receptor tyrosine kinases: molecular analysis and signal transduction. *Biochim. Biophys. Acta* **1135,** 185–199 (1992).

[191] Ornitz, D. M. & Leder, P. Ligand specificity and heparin dependence of fibroblast growth factor receptors 1 and 3. *J. Biol. Chem.* **267,** 16305–16311 (1992).

[192] Naimy, H., Buczek-Thomas, J. A., Nugent, M. A., Leymarie, N. & Zaia, J. Highly sulfated nonreducing end-derived heparan sulfate domains bind fibroblast growth factor-2 with high affinity and are enriched in biologically active fractions. *J. Biol. Chem.* **286,** 19311–19319 (2011).

[193] Ibrahimi, O. A. *et al.* Analysis of mutations in fibroblast growth factor (FGF) and a pathogenic mutation in FGF receptor (FGFR) provides direct evidence for the symmetric two-end model for FGFR dimerization. *Mol. Cell. Biol.* **25,** 671–684 (2005).

[194] Faham, S., Linhardt, R. J. & Rees, D. C. Diversity does make a difference: fibroblast growth factor-heparin interactions. *Curr. Opin. Struct. Biol.* **8,** 578–586 (1998).

[195] Wu, Z. L. *et al.* The involvement of heparan sulfate (HS) in FGF1/HS/FGFR1 signaling complex. *J. Biol. Chem.* **278,** 17121–17129 (2003).

[196] Sterner, E., Meli, L., Kwon, S.-J., Dordick, J. S. & Linhardt, R. J. FGF–FGFR signaling mediated through glycosaminoglycans in microtiter plate and cell-based microarray platforms. *Biochemistry* **52,** 9009–9019 (2013).

[197] Nguyen, T. K. N., Raman, K., Trana, V. M. & Kuberan, B. Investigating the mechanism of the assembly of FGF1-binding heparan sulfate motifs. *FEBS Lett.* **585,** 2698–2702 (2011).

[198] Li, G. *et al.* N-sulfotestosteronan, a novel substrate for heparan sulfate 6-O-sulfotransferases and its analysis by oxidative degradation. *Biopolymers* **99,** 10.1002/bip.22263 (2013).

[199] Li, L., Zhang, F., Zaia, J. & Linhardt, R. J. Top-down approach for the direct characterization of low molecular weight heparins using LC-FT-MS. *Anal. Chem.* **84,** 8822–8829 (2012).

[200] Maruyama, T., Toida, T., Imanari, T., Yu, G. & Linhardt, R. J. Conformational changes and anticoagulant activity of chondroitin sulfate following its O-sulfonation. *Carbohydr. Res.* **306,** 35–43 (1998).

[201] Baik, J. Y. *et al.* Optimization of bioprocess conditions improves production of a CHO cell-derived, bioengineered heparin. *Biotechnol J* **10,** 1067–1081 (2015).

[202] Sun, X. *et al.* Analysis of total human urinary glycosaminoglycan disaccharides by liquid chromatography–tandem mass spectrometry. *Anal. Chem.* **87,** 6220–6227 (2015).

[200] Schmidt, E. P., Kuebler, W. M., Lee, W. & Downey, G. P. Adhesion molecules: Master controllers of the circulatory system. *Compr. Physiol.* **6,** 945–973 (2016).

[201] Haeger, S. M., Yang, Y. & Schmidt, E. P. Heparan sulfate in the developing, healthy, and injured lung. *Am. J. Respir. Cell Mol. Biol.* **55,** 5–11 (2016).

[202] Schmidt, E. P. *et al.* The pulmonary endothelial glycocalyx regulates neutrophil adhesion and lung injury during experimental sepsis. *Nat. Med.* **18,** 1–20 (2012).

[203] Yang, Y. *et al.* Fibroblast growth factor signaling mediates pulmonary endothelial glycocalyx reconstitution. *Am. J. Respir. Cell Mol. Biol.* **56,** 727–737 (2017).

[204] Schmidt, E. P. *et al.* Urinary glycosaminoglycans predict outcomes in septic shock and acute respiratory distress syndrome. *Am. J. Respir. Crit. Care Med.* **194,** 439–449 (2016).

[205] Lygizos, M. I. *et al.* Heparanase mediates renal dysfunction during early sepsis in mice. *Physiol. Rep.* **1,** e00153 (2013). https://dx.doi.org/10.1002%2Fphy2.153

[206] Potter, D. R., Jiang, J. & Damiano, E. R. The recovery time course of the endothelial-cell glycocalyx *in vivo* and its implications *in vitro*. *Circ. Res.* **104,** 1318–1325 (2009).

[207] Giantsos-Adams, K. M. *et al.* Heparan sulfate regrowth profiles under laminar shear flow following enzymatic degradation. *Cell. Mol. Bioeng.* **6,** 160–174 (2013).

[208] Liu, V. *et al*. Hospital deaths in patients with sepsis from 2 independent cohorts. *JAMA* **312,** 90–92 (2014).

[209] Vincent, J.L. *et al*. International study of the prevalence and outcomes of infection in intensive care units. *JAMA* **302,** 2323–2329 (2009).

[210] Vincent, J.L. *et al.* Assessment of the worldwide burden of critical illness: The Intensive Care Over Nations (ICON) audit. *Lancet Respir. Med.* **2,** 380–386 (2018).

[211] Martin, G. S., Mannino, D. M., Eaton, S. & Moss, M. The epidemiology of sepsis in the United States from 1979 through 2000. *N. Engl. J. Med.* **348,** 1546–1554 (2003).

[212] Salmon, A. H. J. *et al.* Loss of the endothelial glycocalyx links albuminuria and vascular dysfunction. *J. Am. Soc. Nephrol.* **23,** 1339–1350 (2012).

[213] Parikh, C. R., Abraham, E., Ancukiewicz, M., Edelstein, C. L. Urine IL-18 is an early diagnostic marker for acute kidney injury and predicts mortality in the intensive care unit. *J. Am. Soc. Nephrol.* **16,** 3046–3052 (2005).

[214] Chappell, D. *et al.* Heparinase selectively sheds heparan sulphate from the endothelial glycocalyx. *Biol. Chem.* **389,** 79–82 (2007).

[215] Yang, Y., Yang, G. & Schmidt, E. P. *In vivo* measurement of the mouse pulmonary endothelial surface layer. *J. Vis. Exp.* **72,** 50322 (2013).

[216] Sarrazin, S., Lamanna, W. C. & Esko, J. D. Heparan sulfate proteoglycans. *Cold Spring Harb. Perspect. Biol.* **3,** a004952 (2011). https://dx.doi.org/10.1101%2Fcshperspect.a004952

[217] Nigro, J. *et al.* Regulation of heparan sulfate and chondroitin sulfate glycosaminoglycan biosynthesis by 4-fluoro-glucosamine in murine airway smooth muscle cells. *J. Biol. Chem.* **284,** 16832–16839 (2009).

[218] Cedeno-Laurent, F. *et al.* Metabolic inhibition of galectin-1-binding carbohydrates accentuates anti-tumor immunity. *J. Invest. Dermatol.* **132,** 410–420 (2012).

[219] Okada, M., Nadanaka, S., Shoji, N., Tamura, J. & Kitagawa, H. Biosynthesis of heparan sulfate in *EXT1* deficient cells. *Biochem. J.* **428,** 463–471 (2010).

[220] Oladipupo, S. S. *et al.* Endothelial cell FGF signaling is required for injury response but not for vascular homeostasis. *Proc. Natl. Acad. Sci. U. S. A.* **111,** 13379–13384 (2014).

[221] Zhang, L. Q. *et al.* RNA-seq reveals novel transcriptome of genes and their isoforms in human pulmonary microvascular endothelial cells treated with thrombin. *PLoS One* **7,** e31229 (2012). https://doi.org/10.1371/journal.pone.0031229

[222] Gavine, P. R. *et al.* AZD4547: An orally bioavailable, potent, and selective inhibitor of the fibroblast growth factor receptor tyrosine kinase family. *Cancer Res.* **72,** 2045–2056 (2012).

[223] Chamorro-Jorganes, A. *et al.* MicroRNA-16 and MicroRNA-424 regulate cell-autonomous angiogenic functions in endothelial cells via targeting VEGFR2 and FGFR1. *Arterioscler. Thromb. Vasc. Biol.* **31,** 2595–2606 (2011).

[224] Wang, H. *et al.* Evidence for serum miR-15a and miR-16 levels as biomarkers that distinguish sepsis from systemic inflammatory response syndrome in human subjects. *Clin. Chem. Lab. Med.* **50,** 1423–1428 (2012).

[225] Wu, S.-C. *et al.* Profiling circulating microRNA expression in experimental sepsis using cecal ligation and puncture. *PLoS One* **8,** e77936 (2013). https://doi.org/10.1371/journal.pone.0077936

[226] Colbert, J. F. & Schmidt, E. P. Endothelial and microcirculatory function and dysfunction in sepsis. *Clin. Chest Med.* **37,** 263–275 (2016).

[227] Goetz, R. & Mohammadi, M. Exploring mechanisms of FGF signaling through the lens of structural biology. *Nat. Rev. Mol. Cell Biol.* **14,** 166–180 (2013).

[228] Guzy, R. D., Stoilov, I., Elton, T. J., Mecham, R. P. & Ornitz, D. M. Fibroblast growth factor 2 is required for epithelial recovery, but not for pulmonary fibrosis, in response to bleomycin. *Am. J. Respir. Cell Mol. Biol.* **52,** 116–128 (2015).

[229] Krump-Konvalinkova, V. *et al.* Generation of human pulmonary microvascular endothelial cell lines. *Lab. Investig.* **81,** 1717–1727 (2001).

[230] Zarbock, A., Meersch, M., Van Aken, H., Görlich, D. & Singbartl, K. Urinary hyaluronic acid as an early predictor of acute kidney injury after cardiac surgery. *J. Am. Coll. Cardiol.* **64,** 737–738 (2014).

[231] Ginsberg, J. M., Chang, B. S., Matarese, R. A. & Garella, S. Use of single voided urine samples to estimate quantitative proteinuria. *N. Engl. J. Med.* **309,** 1543–1546 (1983).

[232] Kato, M. *et al.* Physiological degradation converts the soluble syndecan-1 ectodomain from an inhibitor to a potent activator of FGF-2. *Nat. Med.* **4,** 691–697 (1998).

[233] Yang, Y. & Schmidt, E. P. The endothelial glycocalyx: An important regulator of the pulmonary vascular barrier. *Tissue Barriers* **1,** e23494 (2013). https://dx.doi.org/10.4161%2Ftisb.23494

[234] Wang, H. *et al.* Serum microRNA signatures identified by Solexa sequencing predict sepsis patients' mortality: A prospective observational study. *PLoS One* **7,** e38885 (2012). https://doi.org/10.1371/journal.pone.0038885

[235] Zhang, X., Wang, F. & Sheng, J. 'Coding' and 'Decoding': hypothesis for the regulatory mechanism involved in heparan sulfate biosynthesis. *Carbohydr. Res.* **428,** 1–7 (2016).

[236] Koo, A., Dewey, C. F. & García-Cardeña, G. Hemodynamic shear stress characteristic of atherosclerosis-resistant regions promotes glycocalyx formation in cultured endothelial cells. *Am. J. Physiol. - Cell Physiol.* **304,** C137–C146 (2013).

[237] Oragui, E. E., Nadel, S., Kyd, P. & Levin, M. Increased excretion of urinary glycosaminoglycans in meningococcal septicemia and their relationship to proteinuria. *Crit. Care Med.* **28,** 3002–3008 (2000).

[238] Ly, M. *et al.* The proteoglycan bikunin has a defined sequence. *Nat. Chem. Biol.* **7,** 827–833 (2011).

[239] Declèves, A.-E. *et al.* Synthesis and fragmentation of hyaluronan in renal ischaemia. *Nephrol. Dial. Transplant.* **27,** 3771–3781 (2012).

[240] Göransson, V. *et al.* Renal hyaluronan accumulation and hyaluronan synthase expression after ischaemia-reperfusion injury in the rat. *Nephrol. Dial. Transplant.* **19,** 823–830 (2004).

[241] Dai, X. *et al.* Diagnostic value of neutrophil gelatinase-associated lipocalin, cystatin C, and soluble triggering receptor expressed on myeloid cells-1 in critically ill patients with sepsis-associated acute kidney injury. *Crit. Care* **19,** 223 (2015).

[242] Prucha, M., Bellingan, G. & Zazula, R. Sepsis biomarkers. *Clin. Chim. Acta* **440,** 97–103 (2015).

[243] The Acute Respiratory Distress Syndrome Network. Ventilation with lower tidal volumes as compared with traditional tidal volumes for acute lung injury and the acute respiratory distress syndrome. *N. Engl. J. Med.* **342,** 1301–1308 (2000).